

University of Strathclyde

Bioengineering Unit

Investigation of Oxygen Transfer in Novel Medical Devices

by

Ewan A Dougall, MSci

A thesis presented in part-fulfilment of the requirements for the degree of Doctor of
Engineering in Medical Devices

August, 2011

Copyright Statement

This thesis is the result of the author's original research. It has been composed by the author and has not been previously submitted for examination which has led to the award of a degree.

The copyright of this thesis belongs to the author under the terms of the United Kingdom Copyright Acts as qualified by University of Strathclyde Regulation 3.50. Due acknowledgement must always be made of the use of any material contained in, or derived from, this thesis.

Signed:

Date:

Acknowledgements

Like every thesis before, and presumably every one after, this one is not just the work of its author. There is a small army of people that helped bring this project to completion and I'd like to take a few moments to thank the most pertinent ones.

Firstly, I extend my thanks and overwhelming gratitude to Dr. John D S Gaylor. Your door has always been open to me and your words have always been kind. I don't know if you've got any idea how supportive you've been, but believe me, I wouldn't be sitting here now if it wasn't for that. Thanks, John. Enjoy your retirement.

Next, Prof. Nigel J Mottram deserves an award for putting up with me, but alas I can only say "thank you". Like John, Nigel's suffered a lot of headaches because of me, but never once did he turn me away. It can't have been easy coaxing an engineer to do some mathematical work, and I may not have taken to it as readily as he'd hoped, but we got there in the end. Thanks, Nigel.

My third supervisor, Prof. Sean McKee should definitely be mentioned. He took me under his wing, providing many an anecdote that may or may not have been work related. Sean took his role as my editor in chief very seriously – I doubt he looked at the actual content of any reports I wrote; he always took at least two drafts to sort my grammar out. Thanks, Sean. Again, I hope you enjoy retirement.

Every engineering student is adopted by a technician, and I'm lucky that it was Liz Smith that got landed with me. She knew when to give me encouragement, knew when I needed some serious motivation, and pretty much kept the entire experimental side of my project running on a daily basis. Thanks, Liz. You're another that should be off enjoying retirement.

Now we come to the others that managed to keep me vaguely sane throughout the project. First of all, John Burns; we met on this EngD course complete strangers; we left it just after I was best man at your wedding. I'd say thank you to you, but I already have. Next, Dave Constable; you've been my friend since we were children. To say thanks would not do the support you've given me any justice, but it's about all I can do here. Lastly, Andy Apsley, Ewan Bennett, Dylan Dowd and Tony Herbert; morning coffee was a great time and shall be mourned. Thanks guys, for all the wisdom, for all the help, for all the laughs. I hope we're all EngDs and PhDs at some point soon.

This wouldn't be an acknowledgements section if I failed to mention my mum, Kathryn, my gran, Ella, and my aunt, Isobel. All three of you have shown me encouragement my entire life; you've kept me going when I would rather just have given up. You've made sure I knew what I was doing, even if you didn't. I can't even begin to put in words the thanks you richly deserve. But thanks all the same.

Finally, Janet Bell. I really don't know how thank you for getting me through this. You're the one that's put up with every high and every single low that I've been through. Yet you've remained my constant companion and source of strength. Thank you for everything.

Contents

COPYRIGHT STATEMENT	I
ACKNOWLEDGEMENTS	II
CONTENTS	V
LIST OF FIGURES	IX
LIST OF TABLES	XVI
ABSTRACT	- 1 -
CHAPTER 1 – INTRODUCTION	- 3 -
1.1 NATURAL RESPIRATION	- 3 -
1.2 CARDIOPULMONARY BYPASS	- 6 -
1.3 EXTRACORPOREAL OXYGENATION	- 9 -
1.4 OVERVIEW	- 11 -
CHAPTER 2 – HISTORY OF EXTRACORPOREAL OXYGENATION	- 12 -
2.1 THE FIRST DEVICES	- 12 -
2.2 TECHNOLOGICAL ADVANCES	- 19 -
2.3 SECONDARY MIXING TECHNIQUES	- 24 -
2.3.1 <i>Helical static mixers</i>	- 27 -
2.4 THEORETICAL WORK	- 29 -
2.5 THE CURRENT WORK	- 31 -

CHAPTER 3 – MATHEMATICAL MODEL	- 32 -
3.1 ASSUMPTIONS	- 32 -
3.2 GOVERNING EQUATIONS	- 33 -
CHAPTER 4 – PRELIMINARY WATER EXPERIMENTS	- 46 -
4.1 MATERIALS AND METHODOLOGY	- 46 -
4.1.1 <i>Oxygenator construction</i>	- 48 -
4.1.2 <i>Experimental method</i>	- 52 -
4.2 RESULTS	- 56 -
4.2.1 <i>PDMS oxygenators</i>	- 56 -
4.2.2 <i>Sherwood Number</i>	- 58 -
4.2.3 <i>Celgard 2500 Oxygenators</i>	- 60 -
4.3 DISCUSSION	- 70 -
CHAPTER 5 – MATHEMATICAL SIMULATIONS OF OXYGENATION OF WATER	- 75 -
5.1 BOUNDARY AND INITIAL CONDITIONS	- 75 -
5.1.1 <i>Boundary conditions</i>	- 75 -
5.1.2 <i>Inlet conditions</i>	- 77 -
5.1.3 <i>Model parameters</i>	- 78 -
5.2 MATERIALS AND METHODOLOGY	- 80 -
5.3 RESULTS	- 82 -
5.3.1 <i>Water flow in a three-dimensional non-mixing oxygenator</i>	- 82 -
5.3.2 <i>Water flow in a three-dimensional mixing oxygenator</i>	- 88 -
5.4 DISCUSSION	- 98 -

5.4.1 Non-mixing hollow fibre simulations _____	- 99 -
5.4.2 Mixing hollow fibre simulations _____	- 102 -
CHAPTER 6 – BLOOD EXPERIMENTS _____	- 110 -
6.1 MATERIALS AND METHODOLOGY _____	- 110 -
6.2 RESULTS _____	- 112 -
6.3 DISCUSSION _____	- 118 -
CHAPTER 7 – BLOOD SIMULATIONS _____	- 127 -
7.1 BOUNDARY AND INITIAL CONDITIONS _____	- 127 -
7.1.1 Boundary conditions _____	- 127 -
7.1.2 Inlet conditions _____	- 127 -
7.2 MATERIALS AND METHODOLOGY _____	- 129 -
7.3 RESULTS _____	- 132 -
7.4 DISCUSSION _____	- 140 -
CHAPTER 8 – A COMPARISON OF FINDINGS _____	- 146 -
8.1 COMPARISON OF WATER EXPERIMENTS _____	- 146 -
8.1.1 Practical _____	- 146 -
8.1.2 Theory _____	- 149 -
8.2 COMPARISON OF BLOOD EXPERIMENTS _____	- 152 -
8.2.1 Practical _____	- 152 -
8.2.2 Theory _____	- 154 -
8.3 EVALUATION OF STATIC MIXER _____	- 155 -
8.4 LIMITATIONS OF THE STUDY _____	- 157 -
8.4.1 Practical limitations _____	- 157 -

8.4.2 <i>Theoretical limitations</i>	- 159 -
8.5 CONCLUSIONS	- 160 -
8.6 FUTURE WORK	- 162 -
REFERENCES	- 164 -

List of Figures

FIGURE 1.1 – THE BRONCHIAL TREE _____	- 4 -
FIGURE 1.2 - GAS EXCHANGE IN THE LUNGS _____	- 5 -
FIGURE 1.3 - A SCHEMATIC OF CARDIOPULMONARY BYPASS _____	- 7 -
FIGURE 2.1 - HOOKER'S ROTATING DISK OXYGENATOR FROM 1915 _____	- 14 -
FIGURE 2.2 - GIBBON'S ROTATING DISK OXYGENATOR _____	- 15 -
FIGURE 2.3 - A BUBBLE OXYGENATOR _____	- 17 -
FIGURE 2.4 - GIBBON'S VERTICAL SCREEN OXYGENATOR _____	- 18 -
FIGURE 2.5 - BLOOD FLOW WITHIN A HOLLOW FIBRE. BLUE DENOTES AREAS OF LOW OXYGENATION; RED SHOWS AREAS OF HIGH OXYGENATION. _____	- 21 -
FIGURE 2.6 - (A) INTRA-LUMINAL FLOW AND (B) EXTRA-LUMINAL FLOW TAKEN WITH PERMISSION FROM GAYLOR (1988) _____	- 22 -
FIGURE 2.7 - VORTICES IN A HOLLOW FIBRE: (A) VORTICES ARE FORMED AS THE BLOOD FLOWS PAST THE HOLLOW REGIONS; (B) AS THE FLOW IS STOPPED, THE VORTICES ARE ESTABLISHED IN THE HOLLOW REGIONS AND FILL INTO THE CENTRAL REGION; (C) THE FLOW IS REVERSED, BUT THE VORTICES BLOCK THE CENTRAL REGION, CHANNELLING THE FLOW ALONG THE SURFACE, PUSHING THE VORTICES FURTHER INTO THE CENTRAL REGION _____	- 25 -
FIGURE 2.8 – (A) THE PLAN OF A DIMPLED MEMBRANE; (B) THE CROSS-SECTION OF THE BLOOD CHANNEL; (C) THE PLAN OF THE SUPPORT PLATE _____	- 26 -

FIGURE 2.9 - THE EFFECT A KENICS MOTIONLESS MIXER HAS ON TWO FLUIDS (ONE
 DEPICTED IN RED AND THE OTHER IN BLUE. BY THE END OF THE CHANNEL, THEY
 HAVE BEEN MIXED TOGETHER TO FORM A SINGLE FLUID (SHOWN IN GREEN). - 28 -

FIGURE 3.1 - THREE-DIMENSIONAL SCHEMATIC REPRESENTATIONS OF TWO
 GEOMETRIES: (A) DEOXYGENATED BLOOD FLOWS INTO A CYLINDER, OXYGEN IS
 PUMPED INTO THE CYLINDER THROUGH THE CYLINDER WALLS MADE FROM A
 SEMI-PERMEABLE MATERIAL, AND THEN THE OXYGENATED BLOOD EXITS; (B) A
 SINGLE BLADED REPRESENTATION OF A HELICAL STATIC MIXER HAS BEEN
 INCLUDED IN THE DEVICE TO ENHANCE THE DIFFUSION OF THE OXYGEN. - 35 -

FIGURE 3.2 – OXYGEN DISSOCIATION CURVE. - 41 -

FIGURE 3.3 – SLOPE OF OXYGEN DISSOCIATION CURVE. - 42 -

FIGURE 4.1 – TWO DIFFERENT HELICAL STATIC MIXERS; IN THE BACKGROUND, THE
 LARGER MIXER MEASURES 3.18 *MM* IN DIAMETER AND 3.30 *CM* IN LENGTH; THE
 FOREGROUND ELEMENT IS 2.36 *MM* IN DIAMETER AND 2.95 *CM* IN LENGTH. - 47 -

FIGURE 4.2 – A COMPLETED TEST HOUSING UNIT, WITH INLET AND OUTLET HOLES
 VISIBLE. - 49 -

FIGURE 4.3 – CELGARD 2500 TUBULAR MEMBRANE WITH CONNECTORS - 50 -

FIGURE 4.4 – CELGARD 2500 TUBE POSITIONED WITHIN TEST HOUSING, HELD IN PLACE
 WITH SILICONE RUBBER ADHESIVE. - 51 -

FIGURE 4.5 – FINISHED CELGARD 2500 OXYGENATOR - 52 -

FIGURE 4.6 – EXPERIMENTAL SETUP - 54 -

FIGURE 4.7 – INLET AND OUTLET P_{O_2} FOR PDMS OXYGENATORS AS A FUNCTION OF
 EXPERIMENTAL TIME – EFFECT OF STATIC MIXER. DISTILLED WATER AT 2 *ML MIN*⁻¹, AIR VENTILATION - 57 -

FIGURE 4.8 – P_{O_2} INCREASE ACROSS PDMS OXYGENATORS – EFFECT OF STATIC MIXER	- 57 -
FIGURE 4.9 – SHERWOOD NUMBER DEPENDENCY ON PDMS MEMBRANE THICKNESS	- 60 -
FIGURE 4.10 – INLET AND OUTLET P_{O_2} FOR CELGARD 2500 OXYGENATORS AS A FUNCTION OF EXPERIMENTAL TIME – EFFECT OF STATIC MIXER. DISTILLED WATER AT 2 ML MIN^{-1} , AIR VENTILATION	- 61 -
FIGURE 4.11 – P_{O_2} INCREASE ACROSS CELGARD 2500 OXYGENATOR – EFFECT OF STATIC MIXER. DISTILLED WATER AT 2 ML MIN^{-1} , AIR VENTILATION	- 62 -
FIGURE 4.12 - COMPARISON OF MATERIALS	- 63 -
FIGURE 4.13 – INLET AND OUTLET P_{O_2} FOR CELGARD 2500 OXYGENATORS. DISTILLED WATER AT 1 ML MIN^{-1} , 100% O_2 VENTILATION	- 65 -
FIGURE 4.14 – OXYGEN TRANSFER RATES IN MIXING AND NON-MIXING OXYGENATORS. DISTILLED WATER AT 1 ML MIN^{-1} , 100% O_2 VENTILATION	- 65 -
FIGURE 4.15 - INLET AND OUTLET P_{O_2} FOR CELGARD 2500 OXYGENATORS. DISTILLED WATER AT 2 ML MIN^{-1} , 100% O_2 VENTILATION	- 66 -
FIGURE 4.16 – OXYGEN TRANSFER RATES IN MIXING AND NON-MIXING OXYGENATORS. DISTILLED WATER AT 2 ML MIN^{-1} , 100% O_2 VENTILATION	- 66 -
FIGURE 4.17 - INLET AND OUTLET P_{O_2} FOR CELGARD 2500 OXYGENATORS. DISTILLED WATER AT 3 ML MIN^{-1} , 100% O_2 VENTILATION	- 67 -
FIGURE 4.18 – OXYGEN TRANSFER RATES IN MIXING AND NON-MIXING OXYGENATORS. DISTILLED WATER AT 3 ML MIN^{-1} , 100% O_2 VENTILATION	- 67 -

FIGURE 4.19 - INLET AND OUTLET P_{O_2} FOR CELGARD 2500 OXYGENATORS. DISTILLED WATER AT 4 $ML\ MIN^{-1}$, 100% O_2 VENTILATION _____	- 68 -
FIGURE 4.20 – OXYGEN TRANSFER RATES IN MIXING AND NON-MIXING OXYGENATORS. DISTILLED WATER AT 4 $ML\ MIN^{-1}$, 100% O_2 VENTILATION _____	- 68 -
FIGURE 4.21 – OVERALL CHANGES IN P_{O_2} AGAINST WATER FLOW RATE (CELGARD 2500 OXYGENATORS) _____	- 69 -
FIGURE 4.22 – O_2 TRANSFER RATES FOR THREE PAIRS OF CELGARD 2500 OXYGENATORS _____	- 69 -
FIGURE 5.1 – COMSOL MULTIPHYSICS REPRESENTATION OF (A) NON-MIXING UNIT, (B) THREE-BLADE MIXING UNIT, AND (C) SIX-BLADE MIXING UNIT. NOTE: THE MIXING BLADES IN (B) AND (C) ARE NOT TO SCALE; THE TUBES ARE SET TO 9 CM LONG AND THE BLADES ARE 2.39 MM LONG. _____	- 81 -
FIGURE 5.2 – CHANGES IN P_{O_2} WITH WATER FLOW RATE (NON-MIXING UNITS) _____	- 83 -
FIGURE 5.3 – CHANGES IN J_{O_2} WITH WATER FLOW RATE (NON-MIXING FIBRES) _____	- 83 -
FIGURE 5.4 – PAIR 1: THEORETICAL VS. EXPERIMENTAL P_{O_2} WITH WATER FLOW RATE _____	- 85 -
FIGURE 5.5 – PAIR 1: THEORETICAL VS. EXPERIMENTAL J_{O_2} WITH WATER FLOW RATE _____	- 85 -
FIGURE 5.6 – PAIR 2: THEORETICAL VS. EXPERIMENTAL P_{O_2} WITH WATER FLOW RATE _____	- 86 -
FIGURE 5.7 – PAIR 2: THEORETICAL VS. EXPERIMENTAL J_{O_2} WITH WATER FLOW RATE _____	- 86 -

FIGURE 5.8 – PAIR 3: THEORETICAL VS. EXPERIMENTAL P_{O_2} WITH WATER FLOW RATE	- 87 -
FIGURE 5.9 – PAIR 3: THEORETICAL VS. EXPERIMENTAL J_{O_2} WITH WATER FLOW RATE	- 87 -
FIGURE 5.10 - COLLECTION OF THEORETICAL AND EXPERIMENTAL FINDINGS FOR PAIRS 1 TO 3	- 88 -
FIGURE 5.11 – CHANGES IN OUTLET P_{O_2} WITH WATER FLOW RATE (3 BLADE MIXER)	- 90 -
FIGURE 5.12 – CHANGES IN J_{O_2} WITH WATER FLOW RATE (3 BLADE MIXER)	- 90 -
FIGURE 5.13 – CHANGES IN ABSOLUTE P_{O_2} WITH FLOW RATE (6 BLADE MIXER)	- 92 -
FIGURE 5.14 – CHANGES IN J_{O_2} WITH FLOW RATE (6-BLADE MIXER)	- 92 -
FIGURE 5.15 – PAIR 1: THEORETICAL VS. EXPERIMENTAL P_{O_2} WITH WATER FLOW RATE (3- AND 6-BLADE MIXERS)	- 94 -
FIGURE 5.16 – PAIR 1: THEORETICAL VS. EXPERIMENTAL J_{O_2} WITH WATER FLOW RATE (3- AND 6-BLADE MIXERS)	- 94 -
FIGURE 5.17 – PAIR 2: THEORETICAL VS. EXPERIMENTAL P_{O_2} WITH WATER FLOW RATE (3- AND 6-BLADE MIXERS)	- 95 -
FIGURE 5.18 – PAIR 2: THEORETICAL VS. EXPERIMENTAL J_{O_2} WITH WATER FLOW RATE (3- AND 6-BLADE MIXERS)	- 95 -
FIGURE 5.19 – PAIR 3: THEORETICAL VS. EXPERIMENTAL P_{O_2} WITH WATER FLOW RATE (3- AND 6-BLADE MIXERS)	- 96 -

FIGURE 5.20 – PAIR 3: THEORETICAL VS. EXPERIMENTAL J_{O_2} WITH WATER FLOW RATE (3- AND 6-BLADE MIXERS)	- 96 -
FIGURE 5.21 - COLLECTION OF THEORETICAL AND EXPERIMENTAL FINDINGS FOR PAIRS 1 TO 3	- 97 -
FIGURE 6.1 - EXPERIMENTAL SETUP	- 111 -
FIGURE 6.2 - BOXPLOT SHOWING SCATTERING IN RESULTS RECORDED IN BOVINE BLOOD	- 113 -
FIGURE 6.3 – O_2 TRANSFER RATE FOR CELGARD 2500 OXYGENATORS – BOVINE BLOOD AT 1 $ML\ MIN^{-1}$ AND 100% O_2 VENTILATION	- 114 -
FIGURE 6.4 – O_2 TRANSFER RATE FOR CELGARD 2500 OXYGENATORS – BOVINE BLOOD AT 2 $ML\ MIN^{-1}$ AND 100% O_2 VENTILATION	- 115 -
FIGURE 6.5 – O_2 TRANSFER RATE FOR CELGARD 2500 OXYGENATORS – BOVINE BLOOD AT 3 $ML\ MIN^{-1}$ AND 100% O_2 VENTILATION	- 115 -
FIGURE 6.6 – O_2 TRANSFER RATE FOR CELGARD 2500 OXYGENATORS – BOVINE BLOOD AT 4 $ML\ MIN^{-1}$ AND 100% O_2 VENTILATION	- 116 -
FIGURE 6.7 – AVERAGE O_2 TRANSFER RATES AS A FUNCTION OF BLOOD FLOW IN CELGARD 2500 OXYGENATORS – BOVINE BLOOD AND 100% O_2 VENTILATION	- 117 -
FIGURE 6.8 - OUTLET O_2 SATURATION WITH VARYING BLOOD FLOW RATE IN CELGARD 2500 OXYGENATORS – BOVINE BLOOD AND 100% O_2 VENTILATION	- 117 -
FIGURE 6.9 – INCREASE IN S ACROSS DEVICES WITH BLOOD FLOW RATE IN CELGARD 2500 OXYGENATORS – BOVINE BLOOD AND 100% O_2 VENTILATION	- 118 -
FIGURE 6.10 - RESIDENCE TIME SHOWN ON FIGURE 6.8	- 123 -

FIGURE 7.1 – O ₂ SATURATION, S, MEASURED AT THE OUTLET OF A NON-MIXING OXYGENATOR. THE LEGEND SHOWS THE VARYING LEVELS OF HAEMOGLOBIN CONCENTRATION (KG M ⁻³).	- 133 -
FIGURE 7.2 – O ₂ SATURATION, S, MEASURED AT DIFFERENT AXIAL POSITIONS ALONG A NON-MIXING OXYGENATOR. THE LEGEND SHOWS THE VARYING LEVELS OF HAEMOGLOBIN CONCENTRATION (KG M ⁻³).	- 134 -
FIGURE 7.3 – RADIAL PROFILE OF P _{O₂} AT THE NON-MIXING DEVICE OUTLET. THE LEGEND SHOWS THE VARYING LEVELS OF HAEMOGLOBIN CONCENTRATION (KG M ⁻³).	- 135 -
FIGURE 7.4 – RADIAL PROFILE OF P _{O₂} MEASURED AT DIFFERENT AXIAL POSITIONS ALONG NON-MIXING DEVICE. THE LEGEND SHOWS THE VARYING LEVELS OF HAEMOGLOBIN CONCENTRATION (KG M ⁻³).	- 136 -
FIGURE 7.5 - φ PREDICTED AT NON-MIXING DEVICE OUTLET. THE LEGEND SHOWS THE VARYING LEVELS OF HAEMOGLOBIN CONCENTRATION (KG M ⁻³).	- 137 -
FIGURE 7.6 - φ PREDICTED AT DIFFERENT AXIAL POSITIONS ALONG THE NON-MIXING DEVICE. THE LEGEND SHOWS THE VARYING LEVELS OF HAEMOGLOBIN CONCENTRATION (KG M ⁻³).	- 138 -
FIGURE 7.7 – C _B DEPENDENCE ON C _{HB} : EXAMPLE ONE	- 139 -
FIGURE 7.8 – C _B DEPENDENCE ON C _{HB} : EXAMPLE TWO	- 139 -
FIGURE 7.9 – THE MIXING AND NON-MIXING TWO-DIMENSIONAL MODELS SHARED A GEOMETRY SHAPE. TO SIMULATE THE EFFECT OF THE MIXER WITHIN THE FIBRE, THE MIXING MODEL HAD RADIAL VELOCITY, WHEREAS THE NON-MIXING MODEL DID NOT.	- 141 -

List of Tables

TABLE 4.1 - PARAMETERS USED TO CALCULATE SHERWOOD NUMBER _____	- 59 -
TABLE 4.2 - COMPARISON OF MATERIALS _____	- 70 -
TABLE 4.3 - COMPARISON OF WATER FLOW RATES _____	- 71 -
TABLE 5.1 – AVERAGE INLET PARTIAL PRESSURES FOR USE IN THE MATHEMATICAL MODELS _____	- 77 -
TABLE 5.2 - MATHEMATICAL MODEL DIMENSIONS _____	- 78 -
TABLE 5.3 - CONVECTION-DIFFUSION CONSTANTS _____	- 79 -
TABLE 6.1 - HAEMATOCRIT VALUES MEASURED BEFORE PROCEDURE _____	- 112 -
TABLE 6.2 - OXYGEN TRANSFER RATE FOR MIXING AND NON-MIXING UNITS AT VARYING BLOOD FLOW RATES (VALUES SHOWN AS MEAN \pm SD) _____	- 119 -
TABLE 6.3 - COMPARISON OF OXYGEN TRANSFER RATES BETWEEN BOVINE BLOOD AND DISTILLED WATER _____	- 120 -
TABLE 7.1 - CONVECTION-DIFFUSION CONSTANTS _____	- 128 -
TABLE 8.1 - WATER EXPERIMENTAL RESULTS (O ₂ PARTIAL PRESSURE) WITH VALUES = MEAN \pm SD _____	- 147 -
TABLE 8.2 - WATER EXPERIMENTAL RESULTS (OXYGEN TRANSFER) WITH VALUES = MEAN \pm SD _____	- 148 -
TABLE 8.3 – BOVINE BLOOD EXPERIMENTAL RESULTS (OXYGEN TRANSFER) WITH VALUES = MEAN \pm SD _____	- 152 -

Abstract

Historically, membrane oxygenating devices have been constructed in two distinct formats: intra-luminal flow, where blood is contained within a hollow fibre lumen and gas transfer is through diffusion only; and extra-luminal flow, where blood flows around a series of oxygenated hollow fibres, leading to convection playing a greater role in blood oxygenation. From the convective transport of gas, extra-luminal flow has been found to be more efficient at gas exchange than intra-luminal flow, which is dependent upon gas diffusion alone for oxygenation.

This study is an investigation of a method of improving the oxygen transfer in an intra-luminal flow device. This was achieved by the insertion of a series of passive mixing elements within a tubular membrane lumen, introducing convection within the unit. Prototype modules, each containing a single tube were constructed. The membrane tubes were made from Celgard 2400 polypropylene and were 9 *cm* in length and 2.39 *mm* in internal diameter, with an area of 675 *mm*² each. The modules were of similar length, with an internal diameter of 1 *cm*. Bovine blood was used in experimentation.

The helical static mixing elements were available commercially and measured 2.39 *mm* in diameter and 2.95 *cm* in length. This allowed two mixing elements to be used in each unit. It was noted that the oxygen transfer in bovine blood was greatly enhanced with the inclusion of the mixing elements over empty membrane tubes of

comparable dimensions. This was found to be most obvious at a flow rate of 3 ml min^{-1} , where a 241% increase in oxygen transfer was observed.

A series of two- and three-dimensional mathematical models were created to simulate the oxygen transfer. Initially simulating the oxygenation of distilled water, the theoretical findings closely match the experimental results. Simulating bovine blood proved to be problematic, resulting in the breakdown of the numerical code.

Chapter 1 – Introduction

This thesis will begin with a brief introduction to the biological function of the lungs and their importance. Following this, in Section 1.2 there will be a discussion of cardiopulmonary bypass, a surgical procedure that requires the patient to be supported by artificial means. Section 1.3 will detail the concept of extracorporeal oxygenation and establish context for this current investigation.

1.1 Natural respiration

Respiration is one of the most important functions of the human body. Without it, life could not be sustained. Respiration begins with the inhalation of air, which is transported into the lungs via the bronchial tree to the alveoli at the base. This structure is shown in Figure 1.1¹.

Bronchi, Bronchial Tree, and Lungs

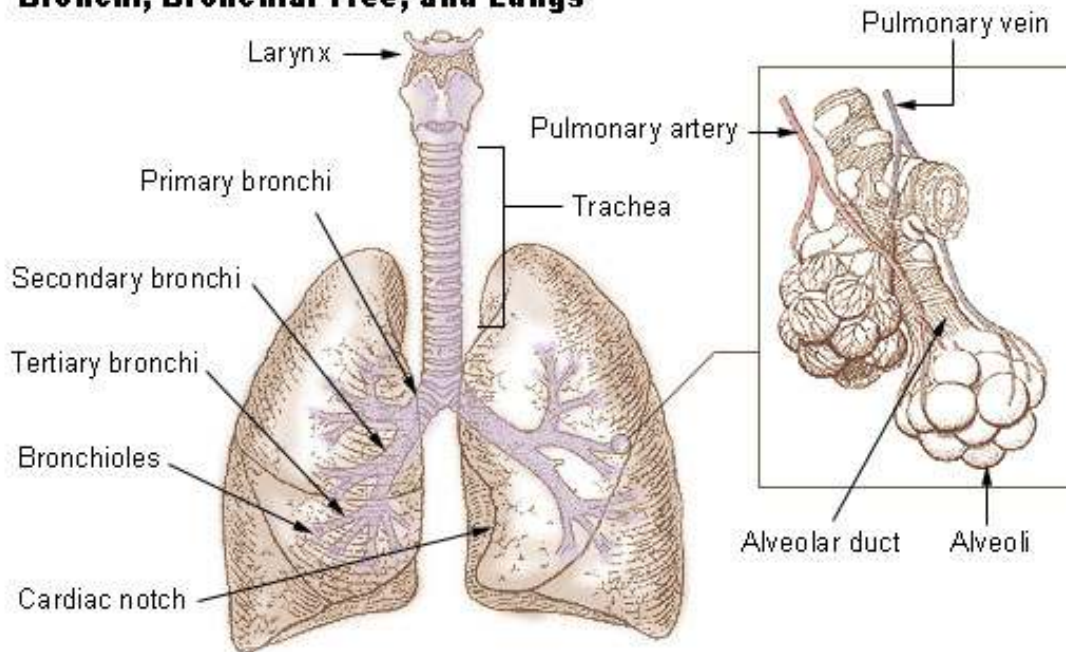


Figure 1.1 – The bronchial tree¹

The alveoli are spherical in shape, with an average diameter of 200 to 300 μm . There are approximately 300 million alveoli in an adult human lung and have a total surface area of 70 m^2 . The exchange of gas to and from the blood can occur more efficiently in the alveoli than anywhere else within the body as the blood and gas are separated by only 1 μm . A closer examination of this process is shown in Figure 1.2².

Oxygen diffusing from the alveoli is bound to haemoglobin within red blood cells, giving the blood a brighter red colour. The oxygenated blood follows the pulmonary vein to the heart where it is then transported around the body, delivering the oxygen to the cells where it is required. Carbon dioxide is released in the tissues and

transported, by the red blood cells, to the alveoli for removal from the body. This system is known collectively as the pulmonary system.

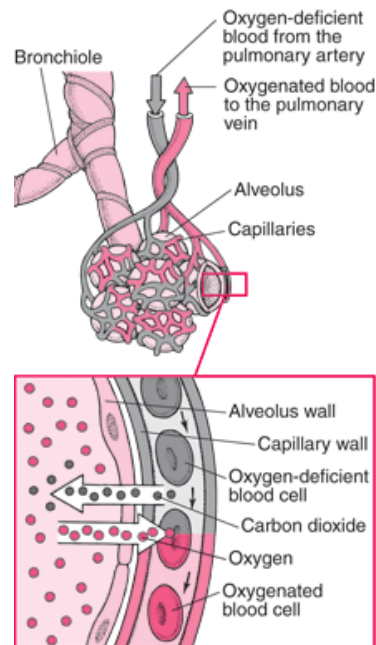


Figure 1.2 - Gas exchange in the lungs²

In summary, oxygen is transported from the air to red blood cells via the lungs. The oxygen is taken to the cells within the body. Carbon dioxide is generated by these cells and is transported via red blood cells back to the lungs for removal.

1.2 Cardiopulmonary bypass

In the United Kingdom, an individual is more likely to die from some form of cardiovascular disease (CVD), such as coronary heart disease (CHD), than anything else. CHD is, at its simplest, caused by insufficient blood flow to the cardiac muscle, which can be caused by a build up of atherosclerotic plaques in the arteries supplying the heart. This type of CHD is referred to as coronary artery disease (CAD).

In 2007³, 34% of all deaths in the UK were attributed to CVD, with almost half of those caused specifically by CHD. When considering Europe as a whole, 49% (4.35 million) of all deaths were caused by CVD; as with the UK, CHD was responsible for almost half of those.

In order to perform surgery on a patient suffering from CHD, as well as other heart conditions such as cardiac valve repair or replacement⁴, the patient's heart must be stopped. This makes surgery on the heart easier, as the organ is not moving and can be manipulated in such a manner that the right side of the heart can be accessed. This technique is known as cardiopulmonary bypass (CPB).

In CPB, the patient's heart must be stopped to allow a stable surface on which to perform the surgery. Blood is removed from the body by a cannula placed in the vena cava or the right atrium of the heart. This blood is directed through an extracorporeal circuit containing a mechanical pump and a blood/gas exchanger,

commonly known as a blood oxygenator. The oxygenated blood is returned to the body via a second cannula placed either in the aorta or the femoral artery. A schematic representation of CPB is shown in Figure 1.3.

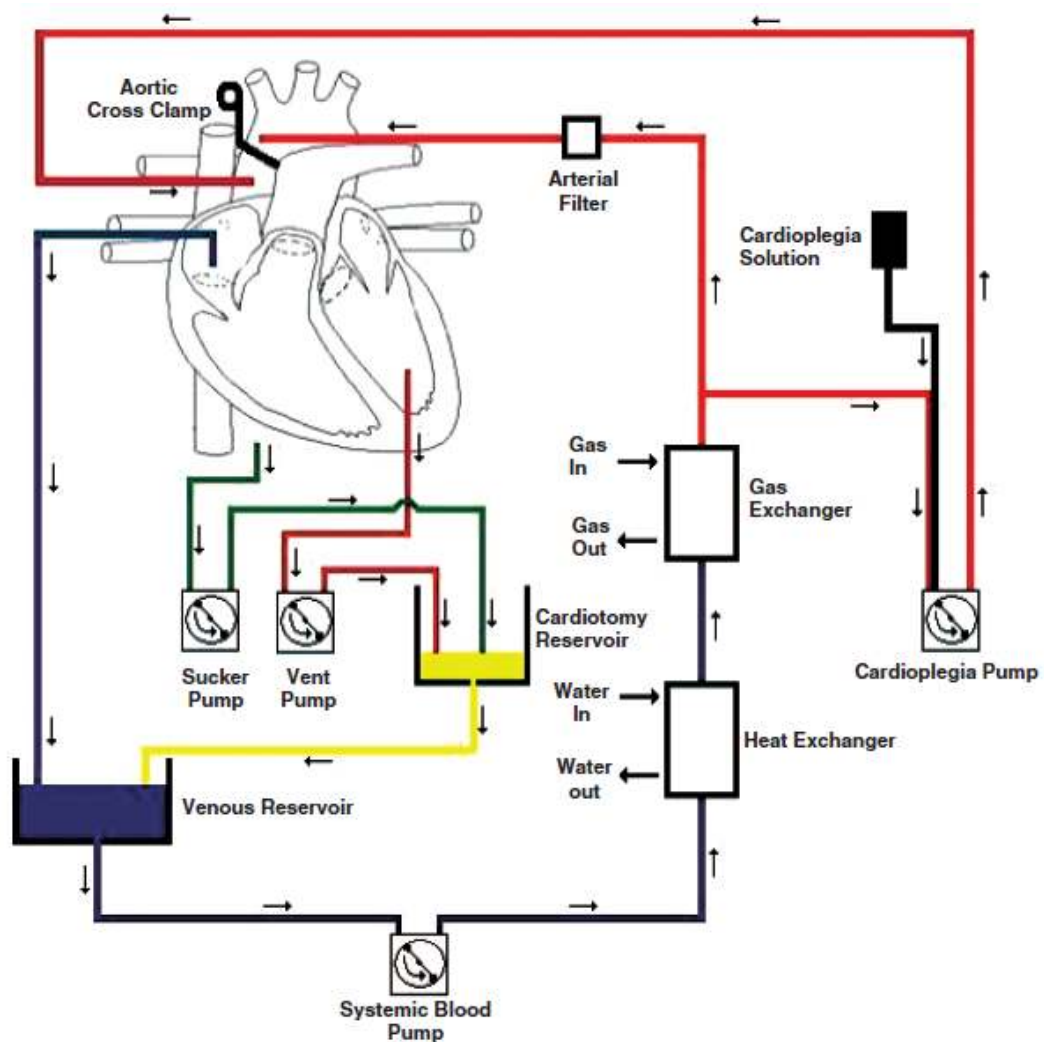


Figure 1.3 - A schematic of cardiopulmonary bypass⁵

In Figure 1.3, blood is removed from the heart into a reservoir containing deoxygenated venous blood. From there, it is passed through a heat exchanger and into the blood oxygenator. Once the blood has been oxygenated, it is returned to the

aorta to be distributed around the body, having bypassed the cardiopulmonary system.

A method of cardiac surgery for CHD that does not require the use of CPB is that of “off-pump surgery”⁶. In this technique, the patient’s heart is not stopped; the movement of the cardiac surface is arrested by mechanical stabilisers so that vessel grafting can be performed. One of the primary benefits for using this procedure over traditional CPB is that incidents of post-operative stroke and cognitive impairment are reduced⁷.

1.3 Extracorporeal oxygenation

During CPB, the blood oxygenator in the extracorporeal circuit provides total respiratory support for the patient. Most oxygenator designs are based on an array of gas permeable hollow fibres over which the blood is passed. The hollow fibres must be hydrophobic to avoid plasma infiltration from the blood phase of the device into the gas side. Ventilating gas, mainly oxygen, is circulated through the fibre lumen; oxygen and carbon dioxide exchange with the blood occurs across the hollow fibre wall. In most modern devices, the hollow fibres are constructed from microporous, silicone or polypropylene materials⁸.

One of the first designs involving hollow fibres involved the blood flowing down the fibre lumen with oxygen diffusing in from outside. This type of oxygenator was found to be less efficient than the modern configuration as the oxygenation process is wholly dependent upon the diffusivity of oxygen (the passive transport of oxygen molecules from a region of high concentration to a region of low concentration) into the fibre lumen; in the extra-luminal flow used in modern devices uses the convection of the blood (the transport of oxygen molecules caused by the fluid motion) around the fibre array to aid the gas exchange.

In recent years, there has been a drive to reduce the size of the CPB apparatus⁹. This is an attempt to reduce the inflammatory response in patients undergoing CPB. Since the introduction of CPB, a number of adverse effects have been noted,

including cell activation on contact with non-biological surfaces¹⁰ and hypotension¹¹. Some devices currently available have a membrane surface area of only 1.1 m², and are commercially available¹². The inflammatory response to traditional CPB in the patients is seen as harmful, and may lead to post-operative complications¹³; the reduction in membrane area in mini-CPB devices has been shown to reduce this inflammatory response and thus is less likely to induce post-operative injury¹⁴.

This study returns to the concept of intra-luminal flow. Using a commercially available helical static mixer, convective terms can be added to the oxygen transfer process. The primary aim of this study is to investigate the oxygen transfer within a hollow fibre with the inclusion of a static mixing element compared to a simple hollow fibre of comparable dimensions.

1.4 Overview

Chapter 2 provides a more in-depth exploration of the history of the extracorporeal oxygenator and will end with a statement of the objectives of this study. Chapter 3 details the governing equations of the theoretical investigation that was undertaken as part of the project. Chapter 4 discusses the preliminary experimental work performed with distilled water. The theoretical work based upon the practical experiments is documented in Chapter 5. Chapter 6 and Chapter 7 detail the experimental work done with bovine blood and the theoretical simulations based upon the same work, respectively. In Chapter 8 there is a direct comparison between the theoretical and experimental findings and the limitations of the work will be discussed. At the end of this chapter, conclusions on the work are drawn, before recommending areas of further research.

Chapter 2 – History of Extracorporeal Oxygenation

Before discussing the work carried out in this study, some historical context must be given. The following chapter shall be a brief discussion about the creation, development and subsequent refinement of blood oxygenators, from 1667 through to modern day. Section 2.1 will concentrate on the bubble and film oxygenators; Section 2.2 will document the rise of the membrane oxygenator and the later advances into hollow fibre technology; Section 2.3 will discuss secondary mixing techniques used in some devices. Once this framework has been established, Section 2.4 will provide the aims of this study.

2.1 The first devices

The concept of artificial respiration has existed for several centuries. Robert Hooke proposed in the mid-17th century that the mechanical movement of the natural lungs was not required for successful oxygenation of the blood^{15,16}. This idea was investigated during the 18th and 19th centuries, but these studies were primarily concerned with the oxygenation of individual organs^{17,18,19}.

By the end of the 19th century, two different methods for organ perfusion had been developed. Von Schröder designed a “bubble” oxygenator in 1882²⁰, whereby oxygen was fed directly into a reservoir filled with venous blood. The gas would

bubble through the blood, oxygenating it, and the oxygenated blood would be transported to the isolated organ. However, this method of oxygenation resulted the blood foaming. Von Frey and Gruber developed a rotating disc oxygenator in 1885²¹ in which venous blood was placed on a rotating disc, creating a thin film of blood across the disc, and exposed to an oxygen-rich environment. Hooker later used both methods in his experiments in 1910²² and 1915²³ (see Figure 2.1).

In 1926, Brukhonenko and Tchetchuline began work toward whole body perfusion²⁴. The method proposed involved mechanically inflating a donor set of lungs to act as the oxygenator. During the procedure, the heart and lungs of the test animal were bypassed entirely. The venous blood was pumped from the body to the donor lungs and a second pump returned the blood after being oxygenated. The first successful trial resulted in a canine subject being kept alive for two hours by extracorporeal circulation, before the animal's mammary artery haemorrhaged^{25,26}.

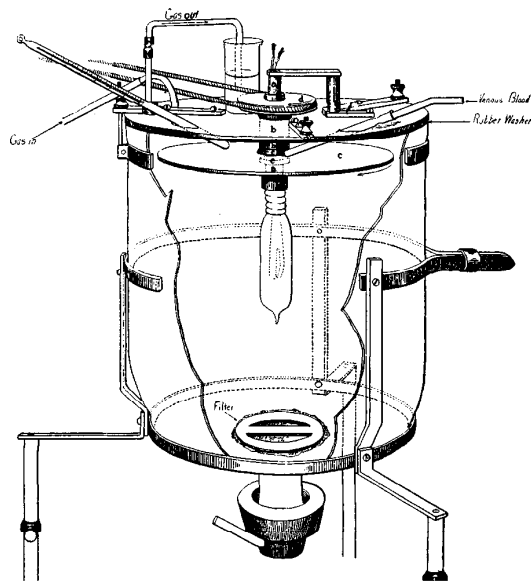


Figure 2.1 - Hooker's rotating disc oxygenator from 1915²³

The exclusion of the natural heart and lungs was viewed as a massive advantage when combating certain types of cardiothoracic problems. In 1930, J.H. Gibbon wrote of a patient suffering from a pulmonary embolism “helplessly watching the patient struggle for life as her blood became darker and her veins more distended, the idea naturally occurred to me that if it were possible to remove continuously some of the blue blood from the patient’s swollen veins, put oxygen into that blood and allow carbon dioxide to escape from it, and then to inject continuously the now-red blood back into the patient’s arteries, we might have saved her life...we would have bypassed the obstructing embolus and performed part of the work of the patient’s heart and lungs outside the body”^{27, 28}.

During the 1930s, Gibbon worked on the rotating disc oxygenator. However, his modifications were insufficient to sustain anything larger than a cat²⁹. The principle behind the rotating disc oxygenator was to create a large surface area of blood spread onto an array of rotating discs that would be exposed to the oxygen-rich environment. Having spent the majority of the early 1940s in the army, Gibbon returned to work on the rotating disc oxygenator. By 1950, Gibbon began to investigate creating a film oxygenator with no rotating mechanism^{30,31}.

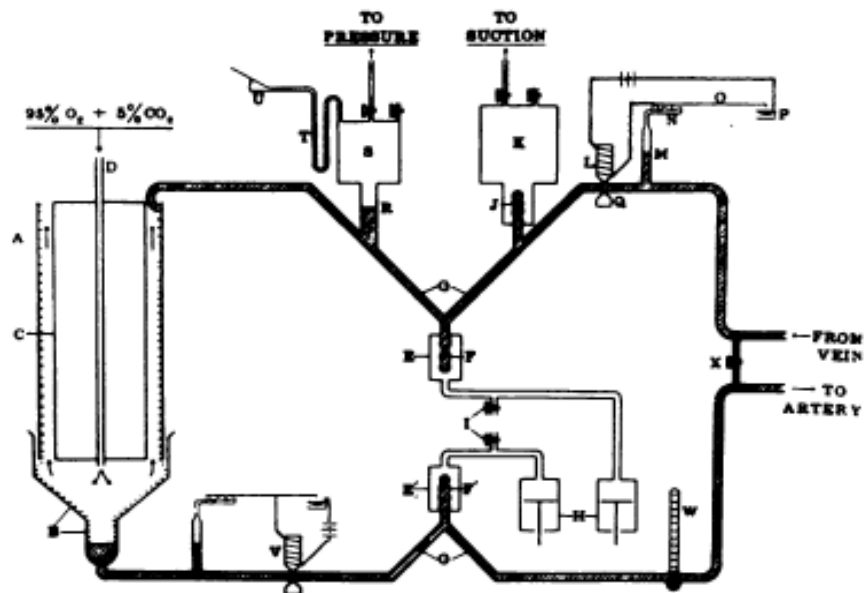


Figure 2.2 - Gibbon's Rotating Disk Oxygenator³²

Gibbon's vertical screen oxygenator operated by channelling blood down six mesh screens, creating thin films of blood (see Figure 2.4). Oxygen was directed onto the blood films. This device was used in the first successful clinical cardiopulmonary bypass procedure on an 18-year old girl on the 16th May 1953³³. Thanks to Gibbon's

pioneering work, she survived into the late 1980s; Gibbon stated after the operation that the successful use of his technique was “an event I hardly dreamed of in 1931”³⁴.

Kirklín and associates at the Mayo Clinic refined the “Gibbon-type” oxygenator, using it in human trials in 1956³⁵. The device was used in 8 procedures; there was 50% success rate, although 3 of the 4 patients that died were due to biological complications, not failures in the equipment²⁸.

Despite the alterations that were made to the various oxygenators, the direct contact between the blood and oxygen remained. In the case of the disc oxygenators, due to the rotating parts, the blood cells were damaged and the machines could only be used for a maximum of four hours³⁶. With the advent of anti-foaming agents, bubble oxygenators (see Figure 2.3) became widely used, partly because the machines had disposable components, but blood damage was still noted; bubble oxygenators were used for perfusions not exceeding three hours. In both types of oxygenator, film and bubble, damage was further inflicted upon the blood by biocompatibility issues. In addition to that, continued direct contact with the gas phase was found to cause protein denaturation³⁷.

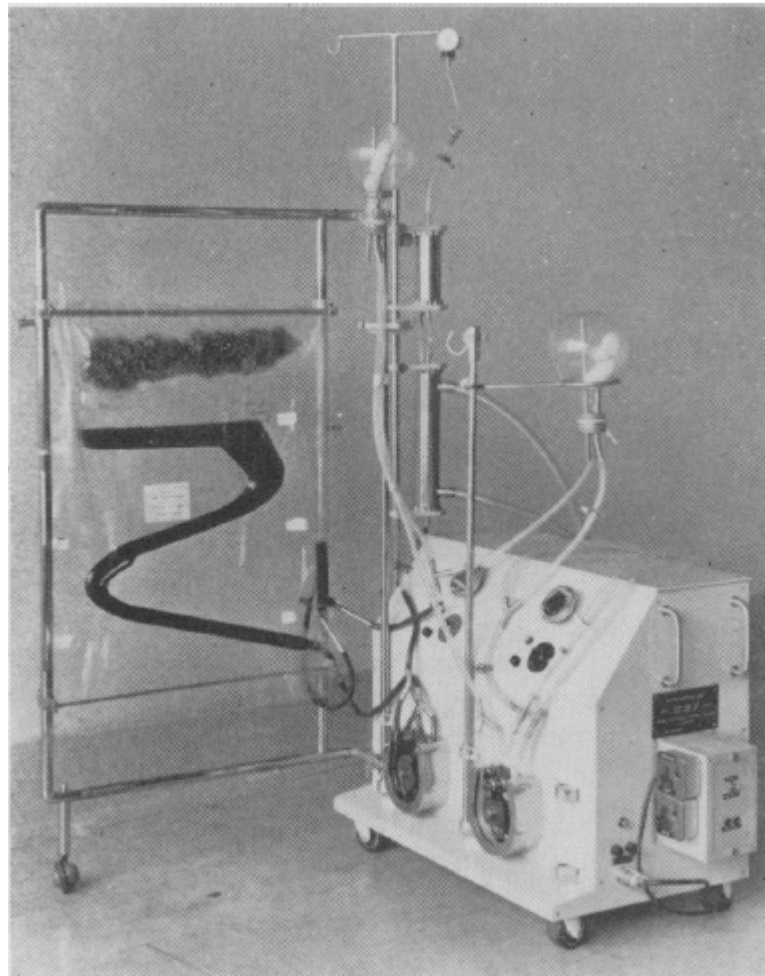


Figure 2.3 - A bubble oxygenator³⁶

Between 1954 and 1955, Lillehei and his team used a different approach; rather than using an artificial device to provide oxygenation of a patient's blood, a cross-circulation method was devised. In the first instance, where the patient was an 11 year old boy, the child's father served as the oxygenator³⁸. This technique did not come into general use due to the perceived risk to the patient serving as the oxygenator.

Throughout the late 1950s, the decision on which oxygenator to use seemed to be based upon personal preference. However, all were in agreement that the direct contact between the gas and blood phases was not conducive to prolonged use surgically. To counter this problem, several groups began investigating the use of a membrane^{39,40,41} separating the blood and gas phases.

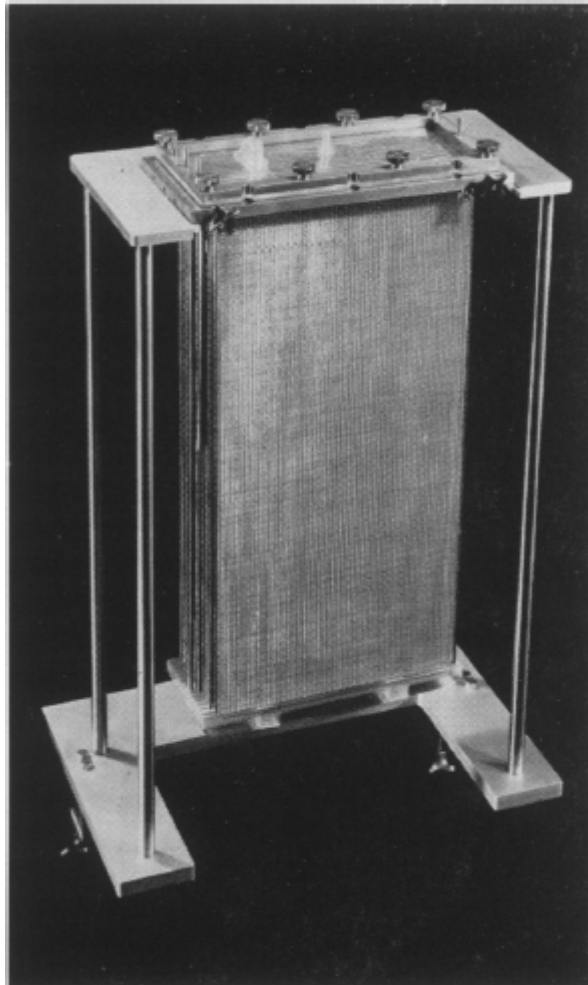


Figure 2.4 - Gibbon's vertical screen oxygenator³⁵

2.2 Technological advances

The initial attempts to design a membrane oxygenator were based upon observations made during haemodialysis in 1944^{18,42}. Kolff and Berk recorded that the oxygen levels in a patient's blood equalised with those of the dialysate through diffusion across the membrane surface.

The drive to improve upon the membrane oxygenator continued, with a focus on the material used in such a device. Poor gas permeability and inadequate mechanical properties resulted in the membrane oxygenators requiring a significant amount of material surface area. Even when polyethylene, one of the more gas permeable materials, was employed the membrane oxygenator required approximately 25 m^2 of material⁴³.

In an attempt to combat blood forming into viscous rivulets, the membrane was supported by ridged plates that directed the blood to flow down parallel channels. This meant that the early membrane oxygenators were bulky to accommodate the plates as well as the membrane.

With the advent of polydimethylsiloxane (silicone rubber) membranes in the late 1950s to early 1960s, the membrane area of oxygenating devices could be greatly reduced. Silicone rubber membranes were found to have a higher permeability for oxygen and carbon dioxide than any materials used previously⁴⁴. This development

meant that the oxygenating devices were not limited in performance by diffusion across the membrane, but instead by diffusion of oxygen and carbon dioxide within the blood.

However, silicone rubber was not without problems of its own. It had poor mechanical strength and was prone to the formation of minute holes when stretched into a thin film⁴⁵. These problems were overcome by Burns⁴⁶. A technique was developed by Burns that allowed a continuous membrane to be formed, rather than the semi-continuous ones produced earlier⁴⁷.

Using a shell and tube configuration⁴¹, membrane oxygenators could be adapted to mimic the capillaries in the natural lungs. In the lungs, the pulmonary capillaries are only large enough to allow red blood cells to flow in single file. However, in the membrane oxygenators the channels are of much larger dimensions and it is this difference that reduces the gas exchange. When blood flows down the fibre lumen, with oxygen diffusing from the sides, the cells closest to the fibre wall rapidly become oxygenated⁴⁸. Those cells flowing closer to the centre of the fibre will not be exposed to the oxygen until it has diffused through the outer-most layers. This is shown in Figure 2.5. This configuration of blood and gas phases was termed intraluminal flow.

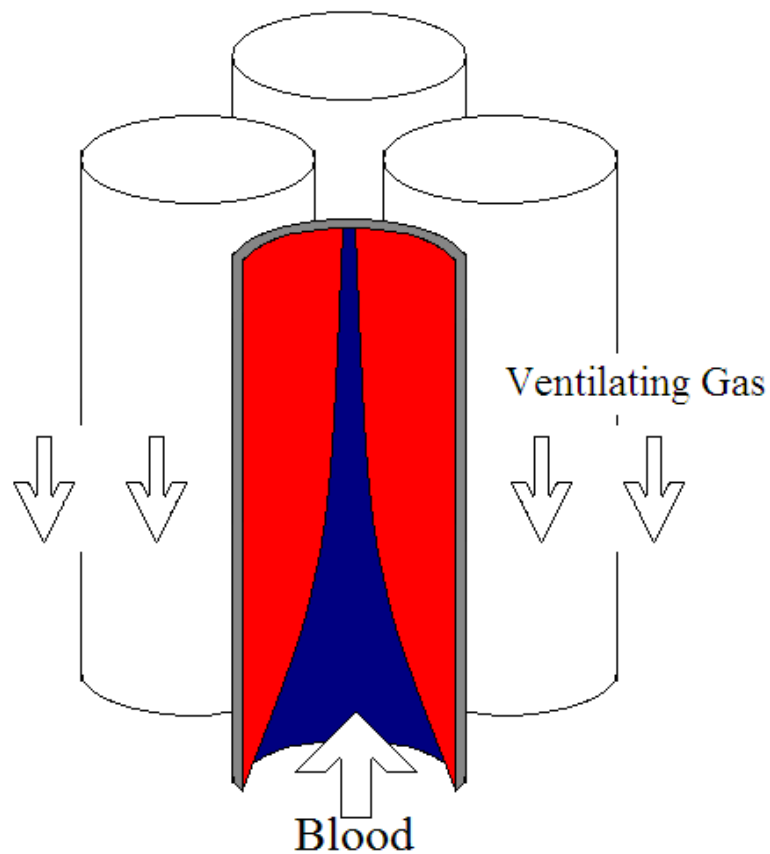


Figure 2.5 - Blood flow within a hollow fibre. Blue denotes areas of low oxygenation; red shows areas of high oxygenation.

In an attempt to better understand the blood-gas interactions within the fibre lumen, several studies used mathematical models to describe the transfer. Section 2.4 discusses these in more detail.

Due to the surface area required in the intra-luminal flow devices, the patient's inflammatory response is activated. Various adverse effects have been noted^{49,50,51}. From this, a drive to reduce the membrane area was instigated.

A different configuration of the hollow fibre arrangement, having blood flowing on the outside of the fibres with the oxygen contained within, was tested^{52,53,54}. This was termed extra-luminal flow. This use of the hollow fibres was found to have several advantages over the intra-luminal flow: the principal of these was enhanced gas transfer caused by passive mixing of the blood as it flowed around the fibre arrangement. Both configurations are shown in Figure 2.6.

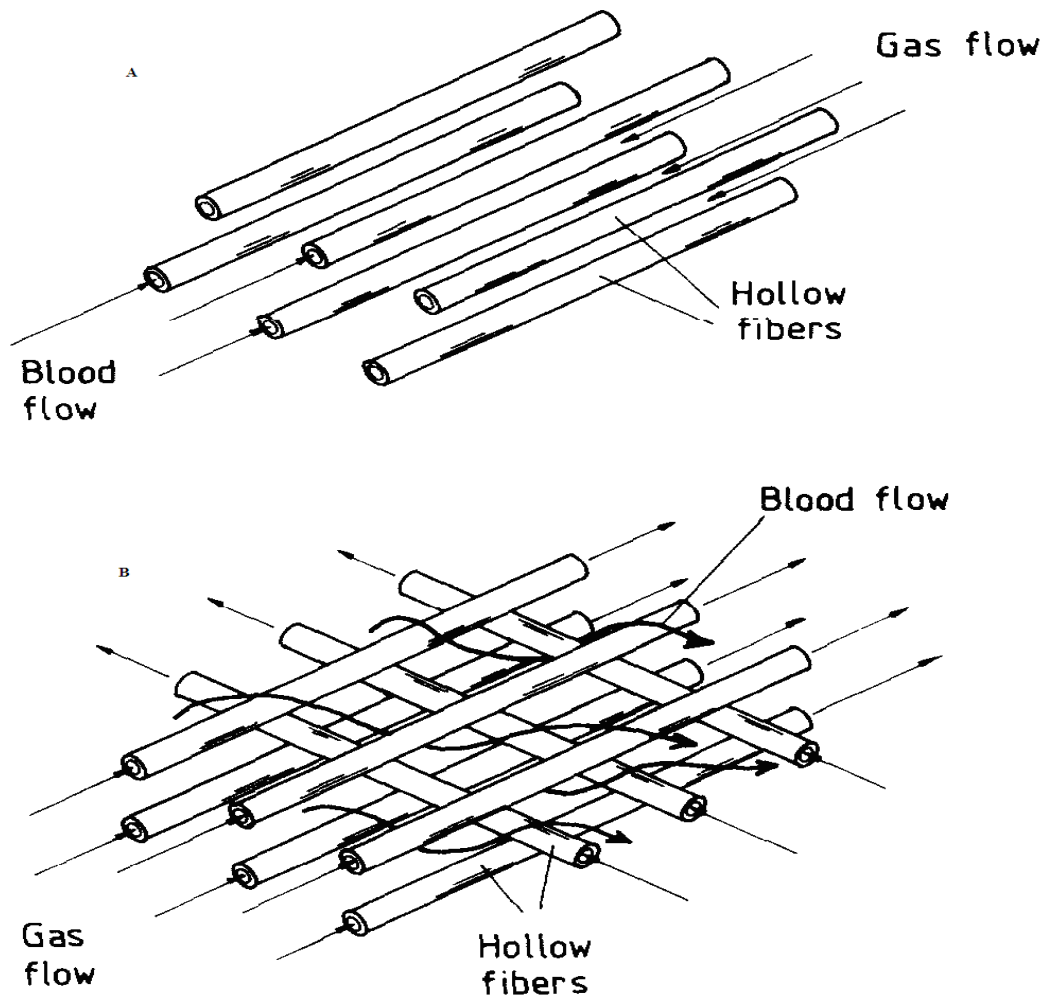


Figure 2.6 - (A) Intra-luminal flow and (B) Extra-luminal flow taken with permission from Gaylor (1988)⁵³

With the extra-luminal flow configuration, membrane areas were reduced by a factor of 2 to 2.5 over the intra-luminal flow devices. Other forms of mixing have been investigated, predominantly in the 1970s. These will be looked at in closer detail in Section 2.3.

Microporous membranes have been used in blood oxygenators since their creation due to their higher permeability compared to homogenous membranes⁵⁵. However, they are unsuitable for prolonged, long-term. This limitation stems from the pores in the material surface becoming clogged as well as plasma leaking from the blood phase to the gas phase of the device⁵⁶.

Recently, there has been a drive towards the creation of microchannel oxygenating devices⁵⁷. This type of device comprises of a series of channels between 12 μm and 25 μm in diameter, decreasing the distance gas must diffuse across, more closely mimicking the pulmonary capillaries than the traditional microporous hollow fibres. Concurrent studies investigated closed⁵⁸ and open⁵⁹ 40 μm -wide rectangular channels. The primary limitation in this form of device is ensuring that the blood flow is evenly distributed throughout the channels.

2.3 Secondary mixing techniques

Two general forms of mixing were studied; passive mixing and active mixing. In passive mixing devices, the mixing was induced by blood flowing either in a circuitous path or by the inclusion of obstacles in the blood channels. Active mixing is created by using energetic mechanisms to impart convective mass transfer to the blood. Examples of both types of device are examined below.

A variety of techniques were devised in order to create mixing within blood oxygenating fibres. Dorson *et al*⁶⁰ proposed having blood flow in spirally wound membrane tubes with gas flow perpendicular to the blood flow in order to create vortices within the channels. This combination of helical fibres and gas flow led to the oxygen transfer doubling⁶¹.

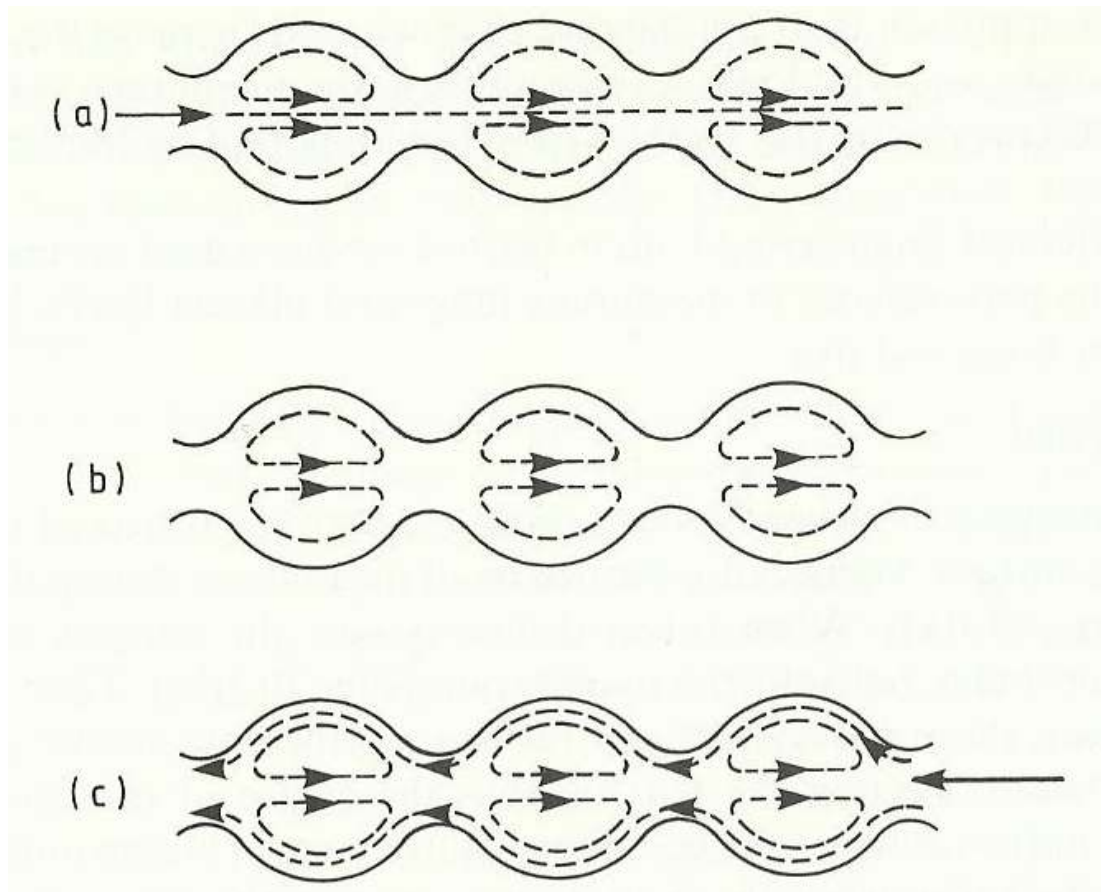


Figure 2.7 - Vortices in a furrowed membrane channel: (a) Vortices are formed as the blood flows past the hollow regions; (b) as the flow is stopped, the vortices are established in the hollow regions and fill into the central region; (c) the flow is reversed, but the vortices block the central region, channelling the flow along the surface, pushing the vortices further into the central region⁶²

Pierce and Dibelius⁶³ were able to cause passive mixing by having blood flow down a dimpled membrane surface; at the parts of the membrane where the flows met, mixing occurred.

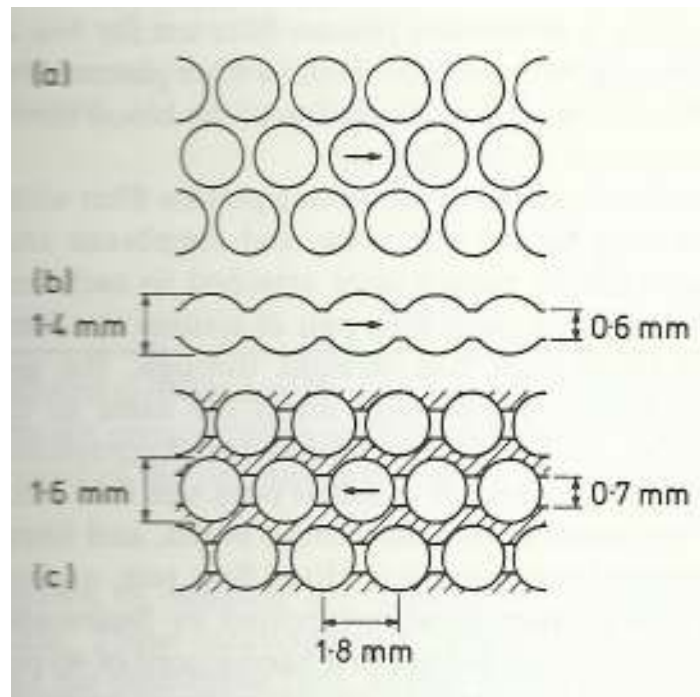


Figure 2.8 – (a) The plan of a dimpled membrane; (b) the cross-section of the blood channel; (c) the plan of the support plate⁶²

Other studies were concerned with a more active form of mixing. Kolobow and Bowman⁶⁴ ensured that the blood within their device was constantly moving despite having no net flow by periodical changes of the gas phase. Using this technique, the gas transfer recorded was greater than the diffusion limit calculated for the material used. However, this form of mixing was not used clinically.

Drinker *et al*⁶⁵ were able to enhance the gas transfer by rotating membrane chambers containing blood. Bellhouse worked on pulsatile mixing system in 1973⁶⁶ and in 1981⁶⁷. In this system, shown in Figure 2.7, blood is pulsed down blood channels which have perpendicular furrows at set intervals. Mixing vortices are created within these furrows as the blood flows past. When compared with a standard intra-luminal

flow oxygenator, this type of mixing reduced the membrane area required for oxygenation by a factor of six. This device became the Interpulse membrane oxygenator. A later design of the furrowed membrane device is shown in Figure 2.8.

However, despite the advantages that active mixing has over passive, only a few of the device designs were mass-produced. The simple reason for this is that these active mixing devices are more complex and more expensive than the simple passive mixing ones⁶⁸.

2.3.1 Helical static mixers

In 1965, Armeniades *et al*⁶⁹ created a simple device that could be used to mix two fluids, or a fluid and a gas, and had applications in synthetic resin manufacturing. Eventually, the Kenics Corporation licensed the device under the trading name Kenics Motionless Mixer. Figure 2.9 shows the mixer used with two fluids.

The device is inserted into the fluid channel and remains static throughout the process. Two or more components that require mixing are passed down the channel and across the mixer. The helical design of the Kenics Motionless Mixer aids mixing in the radial direction and the offset nature of the individual blades causes the flow to separate, encouraging further mixing.

Currently, there are many other suppliers of helical static mixers and the devices are used in a range of applications. Large scale versions of the mixers are used in the oil industry to desalt crude oil as it is processed⁷⁰

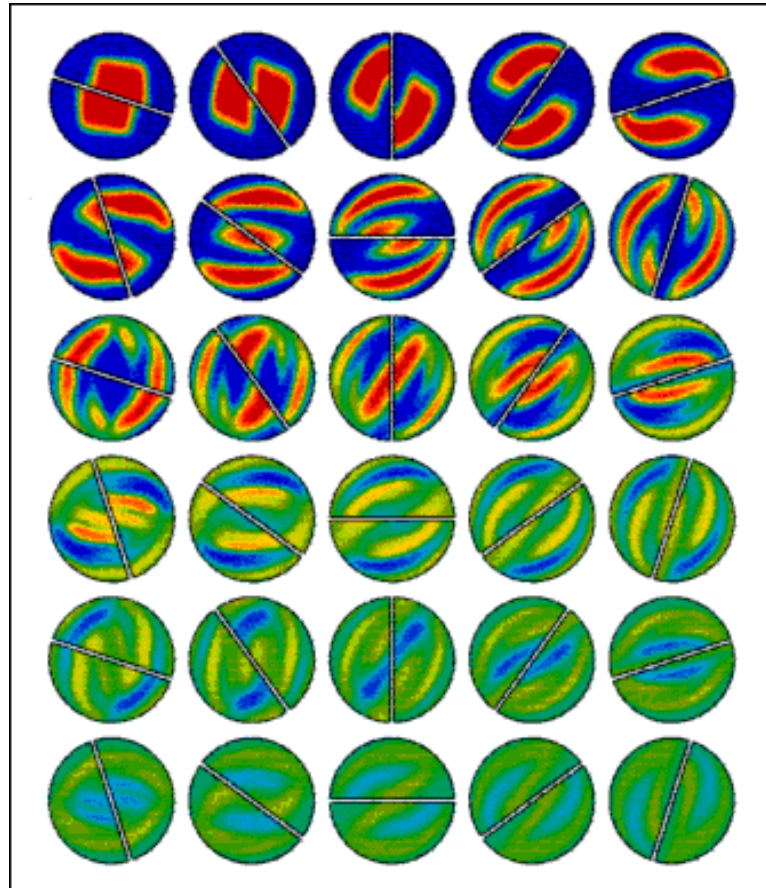


Figure 2.9 - The effect a Kenics Motionless Mixer has on two fluids (one depicted in red and the other in blue. By the end of the channel, they have been mixed together to form a single fluid (shown in green)⁷¹.

In 1995, Bellhouse and Najarian⁷² used a helical static insert in order to separate the red blood cells from the plasma. Work involving the helical static mixer in other

microfluidic situations is ongoing^{73,74}. As yet, there appears to be no work conducted on using a helical static mixer in a blood oxygenating setting.

2.4 Theoretical work

In 1967, Weissman and Mockros⁷⁵ devised a theoretical model that attempted to define the behaviour of oxygen transfer into blood flowing in a hollow fibre. Using bovine blood, they were able to match their theoretical model to reality. Despite solving the equations for the model numerically, the pair was unable to set down an analytical solution due to the non-linear behaviour of the oxygen dissociation curve. As well as setting down the series of equations that would be used, in some capacity, in most theoretical oxygen transfer studies, they drew the conclusion that oxygen transfer within a hollow fibre is independent of fibre diameter.

Lightfoot continued this work, producing a simplified version of Weissmann and Mockros' model⁴⁸. This work was followed up by Weissmann and Mockros in a second study in 1969⁷⁶ in which they considered the effects turbulent mixing and helical coiling would have on the oxygenation of blood. The primary conclusion of this theoretical work was that if the coils were made tighter, then the oxygenation transfer rate would increase. Dindorf *et al*⁷⁷ adapted the Weissman/Mockros model to give a general solution to the oxygenation process.

Colton and Drake⁷⁸ used the Dindorf *et al* model to investigate the effect the oxygen saturation region and direction of transfer had upon the oxygen transfer rate. This study found that differences between the inlet oxygen partial pressure and the external gas pressure altered the dependence the total oxygen concentration has upon the axial length of the fibre. Spaeth quoted some of Colton and Drake's findings in his own review⁷⁹ in which he noted the need for theoretical models to be used in the design process of extracorporeal oxygenators. Different analytical techniques have been employed in an attempt to more accurately simulate specific devices and flow settings^{80,81,82}. It was assumed in the development of the mathematical models that blood behaved in a Newtonian manner.⁸³

2.5 The Current Work

This current study intends to investigate, through both theoretical and experimental means, a novel perspective on previously established technologies. Earlier works have examined various forms of passive and active mixing, but none have documented the use of a helical static mixer as the method of this mixing.

This study also seeks to combine a mathematical model with experimentally derived results. The purpose of this is to provide a useful optimisation tool when designing a membrane oxygenator, and reduce the time spent required in experimentally testing such a device.

Chapter 3 – Mathematical Model

This chapter outlines the details for the theoretical model developed during this project. The governing equations for the model are set out and explained in Section 3.2. These are discussed separately from the boundary and initial conditions, which will be detailed fully in Chapter 5, as the experimental procedure will also make use of the governing equations.

3.1 Assumptions

In previous theoretical studies^{84,85}, although blood is a non-Newtonian fluid at low shear rates ($< 100 \text{ s}^{-1}$) it has been treated as a Newtonian one. The reasoning for this is that for practical operation of oxygenating devices, the wall shear rates are greater than 100 s^{-1} . In addition, blood behaves as a Newtonian fluid in sufficiently large channels, such as those found in an oxygenator, as particle interactions in blood are negligible. This study shall also make these assumptions.

Many models^{82,75} of such a system assume that the flow in the radial direction is small, i.e. close to the boundary, $u_x = u_y = 0$. It is often assumed that the diffusion in the z -direction is small compared to other mechanisms, such as convection in the z -direction. This study will maintain these assumptions.

For the purposes of this model, to simulate oxygen binding to haemoglobin, it will also be assumed that bound oxygen cannot diffuse in the system.

Given the complex geometry of a helical static mixer, the Cartesian coordinate system will be used in this study.

3.2 Governing equations

For a Newtonian fluid, the velocity profile in a cylinder can be found by solving Navier-Stokes equations with the appropriate boundary conditions. These take the general form:

$$\nabla \cdot \vec{u} = 0 \quad (3.1)$$

$$\rho \left(\frac{\partial \vec{u}}{\partial t} + \vec{u} \cdot \nabla \vec{u} \right) = -\nabla P + \mu \nabla^2 \vec{u} + \vec{F}, \quad (3.2)$$

where ρ is the constant fluid density, \vec{u} is the fluid velocity, t is time, P is fluid pressure, μ is the dynamic viscosity and F represents other body forces acting upon the fluid. Equation (3.1) is derived from the principle of conservation of mass, assuming the density to be constant, while Equation (3.2) is derived from the conservation of linear momentum. If only steady flow is considered then $\frac{\partial \vec{u}}{\partial t} = 0$.

Additionally, the other forces, i.e. gravitational, experienced by the fluid are assumed to be negligible and therefore $\vec{F}=0$.

Thus, Equation (3.2) becomes:

$$\rho(\vec{u} \cdot \nabla \vec{u}) = -\nabla P + \mu \nabla^2 \vec{u}. \quad (3.3)$$

In the setup shown in Figure 3.1 (a), where the fluid flows up a cylindrical tube, the velocity may be determined analytically; in this case the Poiseuille flow solution:

$$u_x = u_y = 0, \quad (3.4)$$

$$u_z = 2\bar{u} \left(1 - \left(\left(\frac{x}{R} \right)^2 + \left(\frac{y}{R} \right)^2 \right) \right), \quad (3.5)$$

where \bar{u} is the average velocity, and R is the radius of the hollow fibre. A Cartesian co-ordinate system, rather than a cylindrical co-ordinate system, is adopted to allow comparison between an empty tubular membrane and one with a helical static mixer in the lumen – describing the exact geometry of the mixer would be unnecessarily complex in cylindrical co-ordinates.

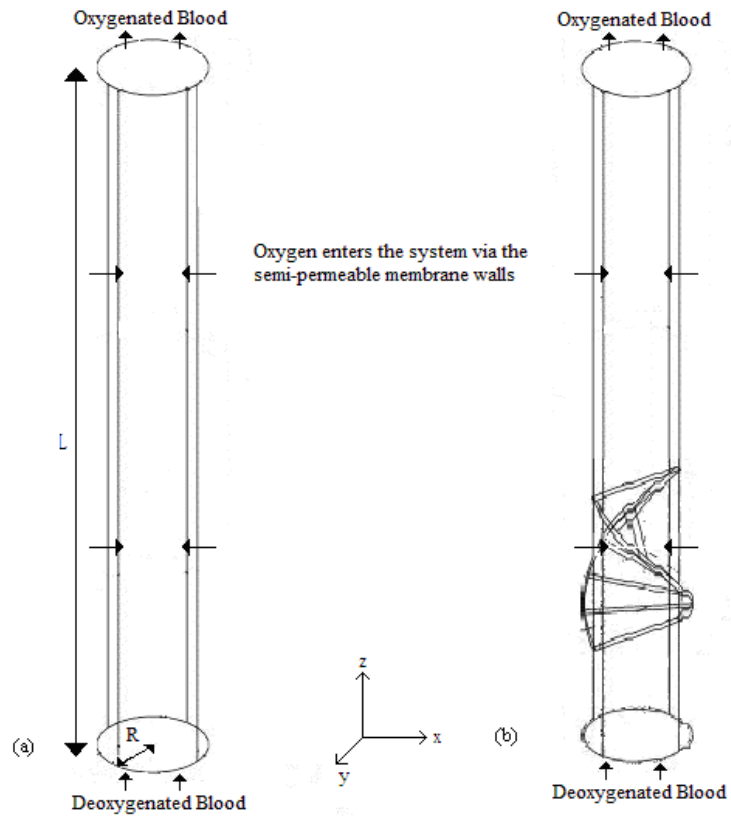


Figure 3.1 - Three-dimensional schematic representations of two geometries: (a) deoxygenated blood flows into a cylinder, oxygen is pumped into the cylinder through the cylinder walls made from a semi-permeable material, and then the oxygenated blood exits; (b) a single bladed representation of a helical static mixer has been included in the device to enhance the diffusion of the oxygen.

In the current study, in addition to the fluid velocity, there are two coupled concentrations to be modelled. In general, the steady-state convection-diffusion-reaction of a concentration of material can be modelled using:

$$\nabla \cdot (-D \nabla C) = -\vec{u} \cdot \nabla C + f(C), \quad (3.6)$$

where D is the diffusion coefficient, C is the concentration, and $f(C)$ is the reaction rate. The reaction function $f(C)$ contains terms which model the introduction and removal of the material being simulated. The velocity dependent term of Equation (3.6) is the convection of material caused by the fluid flow.

When modelling oxygen within blood flow, there are two different concentrations to be considered: C_b is the concentration of oxygen bound to haemoglobin; C_d is the concentration of dissolved oxygen in the system. Therefore, there are two concentration equations that are coupled through the reaction function $f(C)$, which now becomes $f(C_b, C_d)$. This function models the reaction between oxygen and haemoglobin, producing oxygen bound to haemoglobin, as well as the reverse reaction where bound oxygen reverts to dissolved oxygen. The reaction function will be discussed in more detail below. The two concentration equations can be written as:

$$\nabla \cdot (-D_b \nabla C_b) = -\vec{u} \cdot \nabla C_b + f(C_b, C_d), \quad (3.7)$$

and

$$\nabla \cdot (-D_d \nabla C_d) = -\vec{u} \cdot \nabla C_d - f(C_b, C_d). \quad (3.8)$$

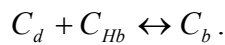
In Cartesian co-ordinates, Equations (3.7) and (3.8) may be written as:

$$D_b \left(\frac{\partial^2 C_b}{\partial x^2} + \frac{\partial^2 C_b}{\partial y^2} + \frac{\partial^2 C_b}{\partial z^2} \right) = u_x \frac{\partial C_b}{\partial x} + u_y \frac{\partial C_b}{\partial y} + u_z \frac{\partial C_b}{\partial z} - f(C_b, C_d), \quad (3.9)$$

and

$$D_d \left(\frac{\partial^2 C_d}{\partial x^2} + \frac{\partial^2 C_d}{\partial y^2} + \frac{\partial^2 C_d}{\partial z^2} \right) = u_x \frac{\partial C_d}{\partial x} + u_y \frac{\partial C_d}{\partial y} + u_z \frac{\partial C_d}{\partial z} + f(C_b, C_d). \quad (3.10)$$

The reaction term is of the opposite sign in the two equations because oxygen is never lost nor created during a reaction; rather oxygen either changes from dissolved to bound or the reverse. The reaction may be written as



Clearly, the total oxygen concentration within the system is the sum of the bound and dissolved concentrations:

$$C_{O_2} = C_d + C_b. \quad (3.11)$$

Recalling the assumptions that flow in the radial direction is negligible, that diffusion in the axial direction is negligible and that bound oxygen is convected within the fluid, then

$$D_b = 0.$$

It is more common in the literature to consider the partial pressure of the dissolved oxygen, P_{O_2} , rather than the concentration C_d ^{68,84}. This convention will be maintained in this study, and C_d can be replaced by the partial pressure using the following relationship:

$$C_d = \alpha_{O_2} P_{O_2}, \quad (3.12)$$

where α_{O_2} is the solubility of oxygen in blood. With these assumptions, Equations (3.9) and (3.10) become:

$$u_z \frac{\partial C_b}{\partial z} = \frac{1}{\alpha_{O_2}} f(C_b, P_{O_2}), \quad (3.13)$$

and

$$D_d \alpha_{O_2} \left(\frac{\partial^2 P_{O_2}}{\partial x^2} + \frac{\partial^2 P_{O_2}}{\partial y^2} \right) = u_z \alpha_{O_2} \frac{\partial P_{O_2}}{\partial z} + \frac{1}{\alpha_{O_2}} f(C_b, P_{O_2}). \quad (3.14)$$

Combining Equations (3.13) and (3.14), and simplifying gives:

$$D_d \left(\frac{\partial^2 P_{O_2}}{\partial x^2} + \frac{\partial^2 P_{O_2}}{\partial y^2} \right) = u_z \frac{\partial P_{O_2}}{\partial z} + \frac{u_z}{\alpha_{O_2}} \frac{\partial C_b}{\partial z}. \quad (3.15)$$

If a maximum of four molecules of dissolved oxygen can combine with a single molecule of haemoglobin to form a single molecule of oxygenated haemoglobin, then the steady state expression for the amount of bound oxygen can be calculated as,

$$C_b = C_{\max} \left(\frac{P_{O_2}^n}{P_{O_2}^n + P_{0.5}^n} \right), \quad (3.16)$$

where $P_{0.5}$ is the partial pressure when half of the haemoglobin is saturated. The empirically derived value, stated as $n = 2.8$, is a stochastic average of the many intermediary reactions. In deriving this expression, it is assumed that the haemoglobin can become saturated, and thus a maximum amount of bound oxygen, C_{\max} , can be measured where,

$$C_{\max} = \beta_{O_2} C_{Hb}, \quad (3.17)$$

where β_{O_2} is the oxygen carrying capacity of haemoglobin and C_{Hb} is the concentration of haemoglobin present in the blood. Equation (3.16) is known as the Hill formula⁸⁶ and n can either be assumed as a model variable or found empirically. In a single reaction, the number of molecules of oxygen binding to the haemoglobin may be between one and four.

An alternative to the Hill formula is the Margaria equation⁸⁷, and is such that,

$$C_b = C_{\max} \left[\frac{\left(\frac{1 + KP_{O_2}}{KP_{O_2}} \right)^3 + m}{\left(\frac{1 + KP_{O_2}}{KP_{O_2}} \right)^4 + m} \right], \quad (3.18)$$

where K and m are experimentally derived constants. K is dependent upon the pH of the blood: $K = 6.47 \times 10^{-5} Pa^{-1}$ for pH of 7.0; $K = 7.83 \times 10^{-5} Pa^{-1}$ for pH of 7.2; $K = 9.59 \times 10^{-5} Pa^{-1}$ for normal human blood at pH of 7.4; and $K = 1.20 \times 10^{-4} Pa^{-1}$ for pH of 7.6. The constant $m = 124$. Equation (3.18) has the shape shown in Figure 3.2.

The fractional saturation may then be defined as:

$$S = \frac{C_b}{C_{\max}} = \frac{C_b}{\beta_{O_2} C_{Hb}}. \quad (3.19)$$

Substituting Equation (3.19) into Equation (3.15) results in:

$$D\left(\frac{\partial^2 P_{O_2}}{\partial x^2} + \frac{\partial^2 P_{O_2}}{\partial y^2}\right) = u_z \frac{\partial P_{O_2}}{\partial z} + \frac{u_z \beta_{O_2} C_{Hb}}{\alpha_{O_2}} \frac{\partial S}{\partial z}. \quad (3.20)$$

Simplifying further, Equation (3.20) becomes,

$$D\left(\frac{\partial^2 P_{O_2}}{\partial x^2} + \frac{\partial^2 P_{O_2}}{\partial y^2}\right) = u_z \frac{\partial P_{O_2}}{\partial z} \left(1 + \frac{\beta_{O_2} C_{Hb}}{\alpha_{O_2}} \frac{\partial S}{\partial P_{O_2}}\right), \quad (3.21)$$

where $\frac{\partial S}{\partial P_{O_2}}$ has the shape shown in Figure 3.3 when the Margaria equation is used.

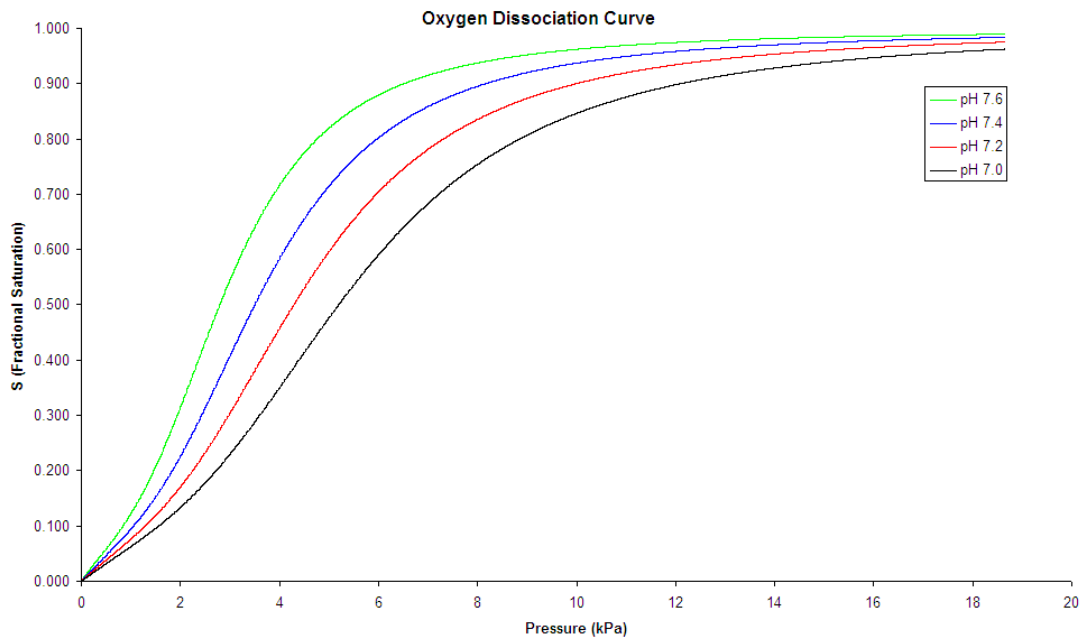


Figure 3.2 – Oxygen dissociation curve⁸⁷.

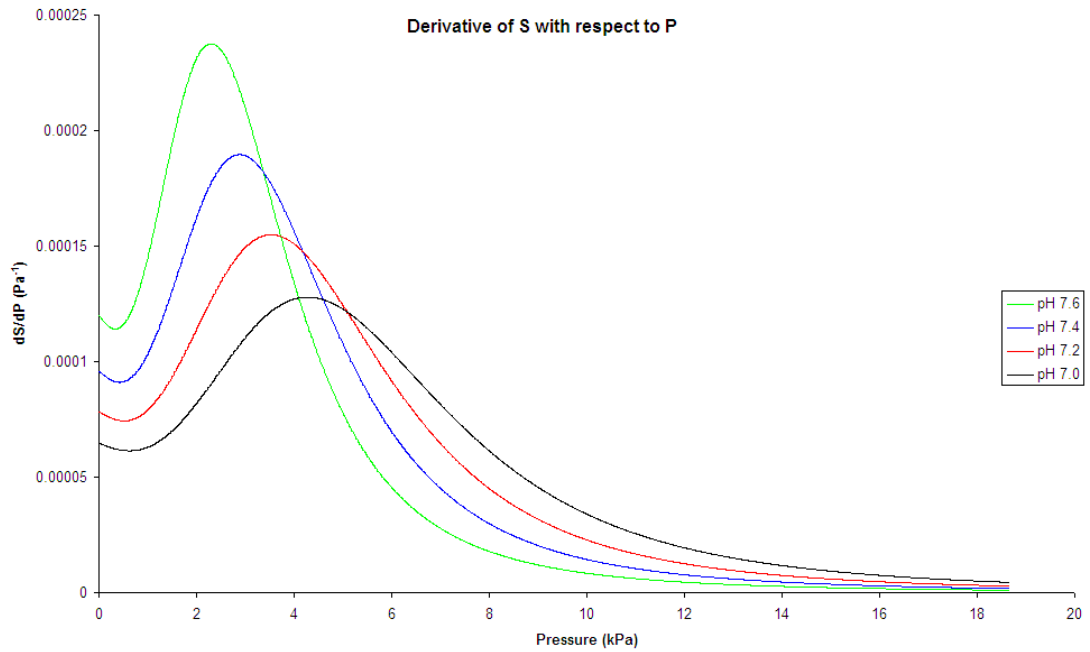


Figure 3.3 – Slope of oxygen dissociation curve⁸⁷.

For a continuous membrane boundary, found in polydimethylsilicone (PDMS) tubing, oxygen diffusing through the membrane will be subject to Fick's first law, such that:

$$J_{O_2} = \frac{D_m \alpha_m}{R \cdot \ln\left(\frac{R+t_m}{R}\right)} \cdot (P_{O_2}|_w - P_g), \quad (3.22)$$

where D_m is the diffusion coefficient for oxygen in the membrane, α_m is the solubility of oxygen in the membrane, t_m is the thickness of the membrane, $P_{O_2}|_w$ is

the partial pressure of oxygen at the membrane wall, and P_g is the partial pressure of oxygen outside the membrane.

For a microporous membrane, such as Celgard 2500, Equation (3.22) becomes:

$$J_{O_2} = G(P_{O_2}|_w - P_g), \quad (3.23)$$

where G is the gas transfer rate.

Equally, oxygen diffusing through the media is defined as,

$$J_{O_2} = -D_d \alpha_{O_2} \cdot \nabla P_{O_2}, \quad (3.24)$$

To solve for oxygen diffusing in the radial direction, at the membrane, Equations (3.22) and (3.24) are combined to give,

$$n \cdot \nabla P_{O_2} = \frac{D_m \alpha_m}{D_d \alpha_{O_2} R \ln\left(\frac{R+t_m}{R}\right)} (P_g - P_{O_2}), \quad (3.25)$$

where n is normal to the membrane. The dimensionless Sherwood number is defined as:

$$Sh_w(PDMS) = \frac{2D_m \alpha_m}{D_d \alpha_{O_2} \ln\left(\frac{R+t_m}{R}\right)}, \quad (3.26)$$

or

$$Sh_w(\text{Microporous}) = \frac{2GR}{D_d \alpha_{O_2}}, \quad (3.27)$$

Thus, Equation (3.25) may be rewritten as,

$$n \cdot \nabla P_{O_2} = \frac{Sh_w}{2R} (P_g - P_{O_2}). \quad (3.28)$$

The total oxygen transferred to the fluid can be measured using,

$$J_{mol} = \int (V_o C_o - V_i C_i) dA, \quad (3.29)$$

where C_o and C_i are the outlet and inlet concentrations of C_{O_2} and V_o and V_i are the outlet and inlet fluid flow velocities and A is the cross-sectional area of the outlet. If the velocity is assumed constant, Equation (3.29) becomes,

$$J_{O_2} = Q \left[(C_{b_o} + C_{d_o}) - (C_{b_i} + C_{d_i}) \right], \quad (3.30)$$

where Q is the flow rate. If the fluid in question is water, then as there is no haemoglobin to bind oxygen molecules, Equation (3.11) is simply $C_{O_2} = C_d$.

Equation (3.29) may be rewritten as,

$$J_{O_2} = Q \alpha_{O_2} (P_o - P_i). \quad (3.31)$$

Together with the Navier-Stokes Equations solving for u_z , these are the equations that govern the mathematical model.

Chapter 4 – Preliminary Water Experiments

This chapter documents the experiments carried out with distilled deoxygenated water, flowing in tubular membrane oxygenators. These studies provided the initial test of the mathematical model which is presented in Chapter 5. Section 4.1 details the construction of the oxygenator modules as well as the experimental setup. The results of the distilled water experiments are recorded in Section 4.2. Finally, Section 4.3 provides a discussion on the results.

4.1 Materials and methodology

Two materials were used to for the tubular membrane oxygenators. Initial devices utilised Dow Corning polydimethylsiloxane (PDMS) which was already in the form of a hollow cylinder as it was supplied as tubing. Later devices used Celgard 2500⁸⁸, a thin microporous polypropylene sheet membrane that needed to be constructed into a cylindrical structure. The reason for the change in oxygenation membrane will be given in Section 4.2.2, with further discussion in Section 4.3.

In current clinical hollow fibre oxygenators, the fibre internal diameter is approximately 0.2 *mm*. Due to the diameter of the static mixer units, the internal diameter of any device constructed to accommodate them would need to be increased from what is used in current devices. The acetal static mixers that were inserted into

the tubular membrane lumens were purchased from Nordson EFD⁸⁹. Two static mixer sizes, shown in Figure 4.1, were selected for consideration. The smaller of the two mixers, measuring 2.36 *mm* in diameter and 2.95 *cm* in length, was selected as it was a better fit for the PDMS tubing. Both static mixers were supplied in units of twelve mixing blades.

According to Weissman and Mockros⁷⁵, for the blood flowing inside a tubular membrane the change in diameter should not impact upon the amount of oxygen transferred within the fibre as “oxygen saturation of blood is dependent upon flow rate, the tube length and the diffusion coefficient and independent of the tube diameter.” The increase in diffusion path length with increasing diameter is offset by an increase in the transfer area; however, the transfer efficiency (transfer per unit area) is dependent upon the diameter, leading to a larger membrane tube being less efficient than one of smaller diameter.

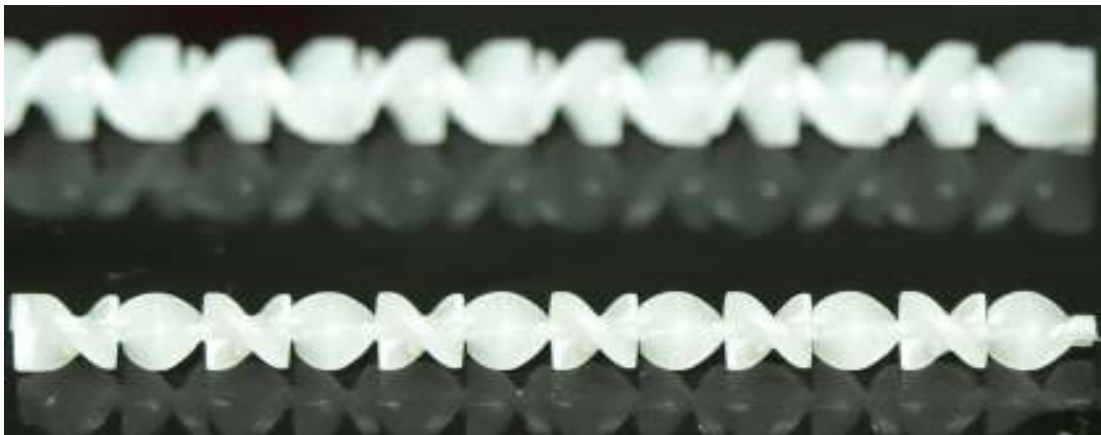


Figure 4.1 – Two different helical static mixers; in the background, the larger mixer measures 3.18 *mm* in diameter and 3.30 *cm* in length; the foreground element is 2.36 *mm* in diameter and 2.95 *cm* in length.

4.1.1 Oxygenator construction

The oxygenator consisted of a single PDMS or Celgard 2500 tube housed inside a Perspex® jacket. Perspex® tubing, 10 mm bore and 5 mm wall, was cut into sections measuring 9 cm in length. Two holes, 4 mm diameter, were drilled 1 cm from the top and bottom of the housing and fitted with male luer connectors to act as a gas inlet and outlet respectively. Figure 4.2 shows a finished test housing.



Figure 4.2 – A completed test housing unit, with inlet and outlet holes visible.

4.1.1.1 Celgard 2500 Oxygenator

A total of ten oxygenators were constructed from Celgard 2500. Five of these devices contained two static mixing elements, numbering twenty-four mixing blades in total. Two mixing elements were chosen to ensure thorough mixing down the

membrane tube's length. The other five were used as control modules, with no static mixers included.

The Celgard sheet membrane⁸⁸ was cut into sections of the same length as the housings and 7.5 mm wide, slightly wider than the circumference of the static mixers. The membrane was then folded loosely and heat sealed along the open boundary to create a tube. For the oxygenators with mixers, two static mixing units (each 2.95 mm in length with 12 mixing blades) were placed in series in the lumen.

Polypropylene female luer connectors⁹⁰ (purchased from Altec Products Ltd.) were positioned at the open ends of the tubes and held in place with a small amount of silicone sealant⁹¹. Figure 4.3 shows the device construction at this stage.

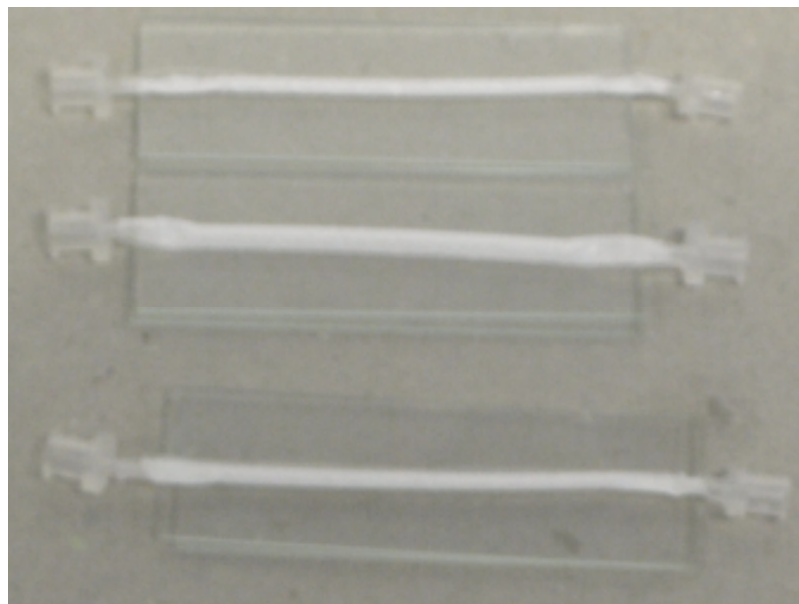


Figure 4.3 – Celgard 2500 tubular membrane with connectors

The tube was positioned inside the housing and, using the silicone sealant, sealed at both ends. The adhesive was allowed to cure for at least eight hours at room temperature. Figure 4.4 shows a device during the curing process.



Figure 4.4 – Celgard 2500 tube positioned within test housing, held in place with silicone rubber adhesive.

Once the silicone sealant had set, Araldite® epoxy adhesive⁹² was injected via the housing side holes to give the membrane tube more structural stability at the tube/housing seal region. The device assembly was completed with the fitting of male luer connectors in the side holes to form gas inlet and outlet ports. Figure 4.5 shows a complete Celgard membrane in the housing, ready for testing.



Figure 4.5 – Finished Celgard 2500 oxygenator

The total time taken to construct one module was approximately 3 days. The majority of this time was taken by the curing process required by the epoxy resin.

4.1.1.2 PDMS Oxygenator

Six oxygenators containing the PDMS tubular membrane were constructed. Three of these contained two static mixer elements, so that each tubular membrane had twenty-four individual mixing blades. The remaining three PDMS oxygenators were left as empty tubes and acted as controls. The construction procedure was similar to that described above for the Celgard 2500 oxygenators.

4.1.2 Experimental method

The test circuit for the water experiments is shown in

Figure 4.6. Approximately 500 ml of distilled water was added to a conical flask and heated to 37 °C by placing the flask in a water bath. The distilled water was

deoxygenated by sparging with oxygen-free nitrogen. The oxygen partial pressure (P_{O_2}) of the water was measured periodically until it was found to be approximately between 2.5 *kPa* and 5 *kPa*.

Once this partial pressure range had been obtained, the water was taken into a 60 *ml* syringe and, using a JMS SP-100 syringe pump, driven through the tubular membrane. Water samples were taken at tubular membrane entry and exits via three-way taps and P_{O_2} levels were determined. All P_{O_2} measurements were made using a Siemens RAPIDLab 248 blood/gas analyser.

Modern blood oxygenators consist of thousands of hollow fibres; to replicate the possible fluid flow rates in a single tube, the water flow rate was varied over the range 1 to 4 *ml min⁻¹*. The oxygenator was ventilated with room air (via an air pump) or with 100% oxygen from a gas cylinder. The gas cylinder flow rate was set at 30 *ml min⁻¹*.

Each experiment began with a pre-oxygenation sample being tested from the syringe pump. This was proceeded by between one and three post-oxygenation samples (dependent upon flow rate). Another pre-oxygenation sample was taken to ensure the base level had not changed. Another set of post-oxygenation samples were measured followed by a final pre-oxygenation sample. The pre-oxygenation samples were used to show that the oxygen partial pressure in the syringe did not change over

module was tested on the same day as a module with static mixer. Modules tested on the same day in this manner were titled Pair 1 to Pair 3.

4.1.2.2 Celgard 2500 oxygenators

After a review of the gas exchange performance of the PDMS tubular membranes, the Celgard 2500 oxygenators were constructed. Literature data on the oxygen permeability of Celgard 2500 indicated that this material would have a higher Sherwood number and therefore would allow oxygen to diffuse more readily through the membrane wall⁹³.

Of the ten constructed from Celgard 2500, six were selected for a repeat of the experiment described in Section 4.1.2.1; three of these units contained static mixers; three did not. A more detailed evaluation of the Celgard devices was conducted using 100% oxygen ventilating gas and a range of water flow rates were selected in order to assess the optimum oxygenating conditions. The flow rates ranged from 1 $ml\ min^{-1}$ to 4 $ml\ min^{-1}$ in increments of 1 $ml\ min^{-1}$.

The inlet values of P_{O_2} for the Celgard units were used as the initial conditions of the mathematical model describing the water experiments.

4.2 Results

In all figures presented in this section, solid lines represent the mean value observed; broken lines represent plus and minus one standard deviation of that mean.

4.2.1 PDMS oxygenators

In Figure 4.7, the inlet and outlet values of P_{O_2} are shown as a function of experimental time for all tests with PDMS oxygenators. The lower spread of data points (diamonds) were taken at the inlet of the fibre, before the water had been oxygenated. The middle group of points (triangles) represent the outlet P_{O_2} when no mixer is present within the tube lumen. The upper data group (squares) indicates the outlet P_{O_2} with the static mixer present.

To calculate the improvement in the increase of P_{O_2} , the pre-oxygenation oxygen levels must be subtracted from the outlet values of oxygenation. The mean inlet partial pressure was calculated and subtracted from the outlet pressures. Figure 4.8 shows the oxygenation values after this adjustment.

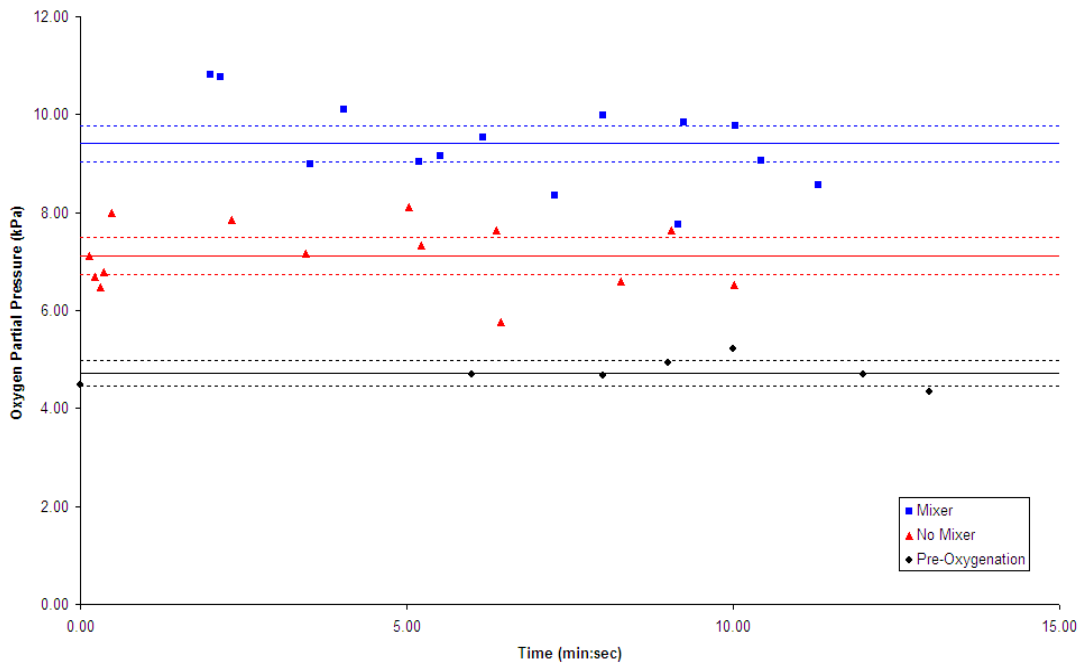


Figure 4.7 – Inlet and outlet P_{O_2} for PDMS oxygenators as a function of experimental time – effect of static mixer. Distilled water at 2 ml min^{-1} , air ventilation

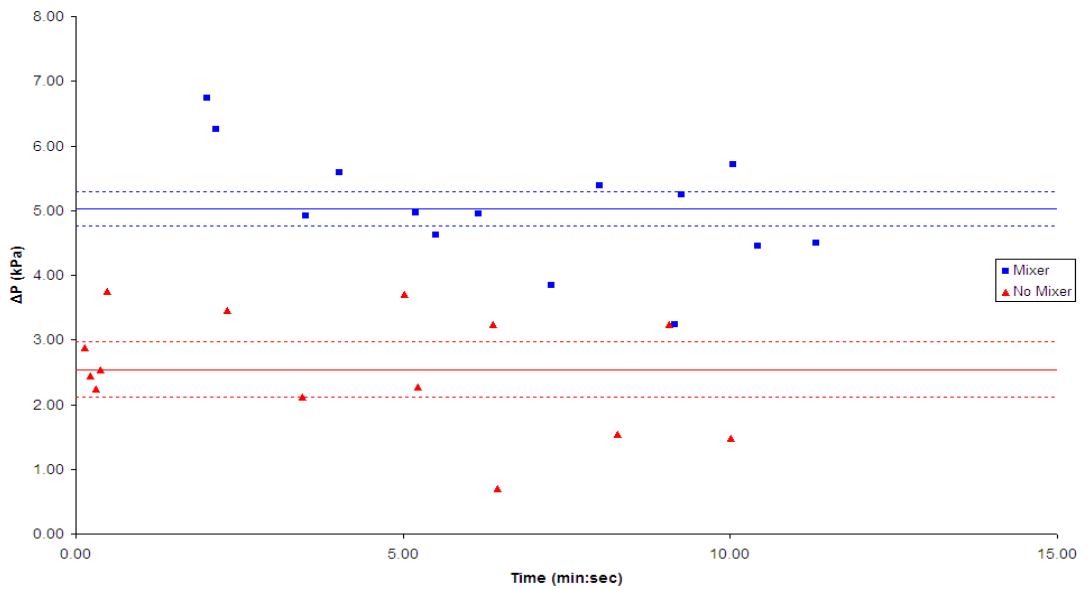


Figure 4.8 – P_{O_2} increase across PDMS oxygenators – effect of static mixer

Using the mean values for inlet and outlet P_{O_2} in conjunction with Equation (3.31),

$$J_{O_2} = Q\alpha_{O_2}(P_o - P_i),$$

the oxygen transfer rate of both the mixing and non-mixing units can be calculated. The solubility of oxygen in water at 37°C was taken to be, $\alpha_{O_2} = 2.07 \times 10^{-6} \text{ mol.m}^{-3} \cdot \text{Pa}^{-1} \text{ }^{94}$. For the non-mixing oxygenators, the mean \pm one standard deviation was $J_{O_2} = 1.79 \times 10^{-10} \text{ mol.s}^{-1} \pm 2.95 \times 10^{-11}$. The oxygenators with mixer in place had a total molar transfer rate of $J_{O_2} = 3.44 \times 10^{-10} \text{ mol.s}^{-1} \pm 1.85 \times 10^{-11}$. These results are judged to be significantly different when compared using a two sample t-test ($t(24) = 7.69, p \gg 0.05$).

4.2.2 Sherwood Number

Recalling Equations (3.26), (3.27) and (3.28),

$$Sh_w(PDMS) = \frac{2D_m\alpha_m}{D_d\alpha_{O_2} \ln\left(\frac{R+t_m}{R}\right)}, \quad (3.26)$$

$$Sh_w(Microporous) = \frac{2GR}{D_d\alpha_{O_2}}, \quad (3.27)$$

$$n \cdot \nabla P_{O_2} = \frac{Sh_w}{2R} (P_g - P_{O_2}). \quad (3.28)$$

Table 4.1 shows the values used in solving (3.26).

Table 4.1 - Parameters used to calculate Sherwood Number

Parameter	Symbol	Value	Unit
Diffusion in membrane ⁷⁸	D_m	9.90×10^{-6}	$m^2 s^{-1}$
Solubility in membrane ⁷⁸	α_m	1.54×10^{-9}	$mol m^{-3} Pa^{-1}$
Radius of tube	R	1.2×10^{-3}	M
Diffusion in water ⁹⁴	D_d	3.24×10^{-9}	$m^2 s^{-1}$
Solubility in water at 37 °C ⁹⁴	α_{O_2}	2.07×10^{-6}	$mol m^{-3} Pa^{-1}$
Gas transfer rate ⁹⁵	G	3.01×10^{-8}	$mol m^{-2} Pa^{-1} s^{-1}$

It is apparent that the change of gas pressure across the fibre wall is dependent upon the wall Sherwood Number, which is in turn dependent upon the membrane wall thickness for PDMS membranes. Figure 4.9 shows the relation between Sherwood Number and membrane thickness for the PDMS material used in this study.

Based on the nominal PDMS tubing size, the wall thickness was calculated to be 420 μm . The Sherwood Number calculated from this is 10.7, which is the lowest value shown in Figure 4.9.

For the microporous membrane Celgard 2500, the Sherwood Number is calculated to be 10771.2. For PDMS tubing of similar thickness to the microporous membrane ($25\ \mu\text{m}$), the Sherwood Number would only be 145.5.

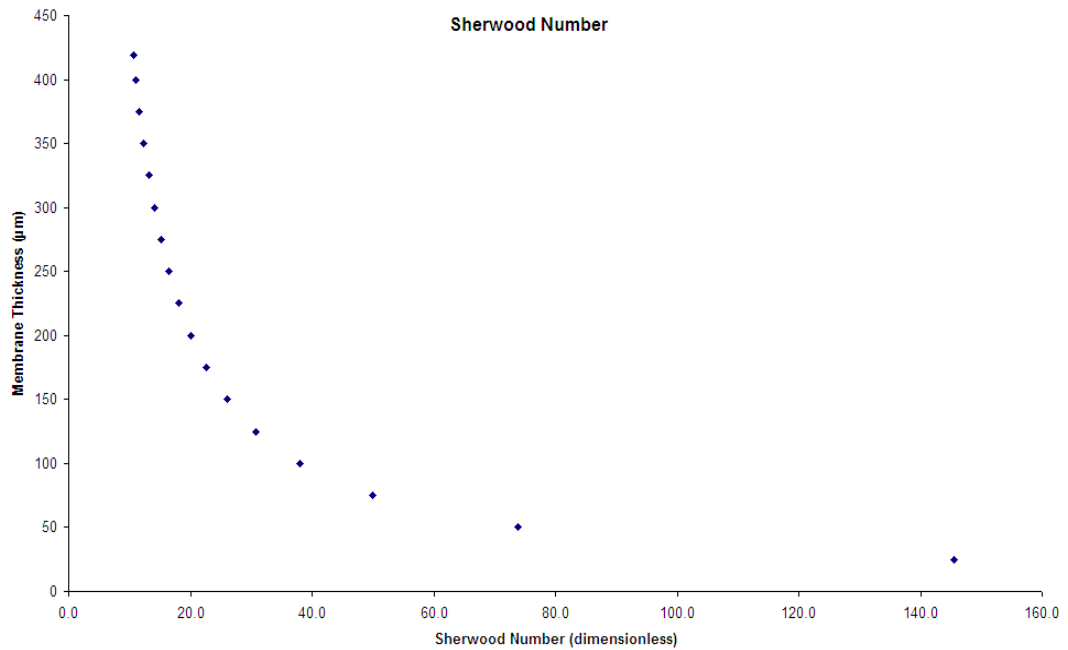


Figure 4.9 – Sherwood number dependency on PDMS membrane thickness

4.2.3 Celgard 2500 Oxygenators

Figure 4.10 shows the inlet and outlet P_{O_2} data for the Celgard 2500 oxygenators with and without the static mixing elements. To allow for direct comparison between membrane types, the experimental conditions were the same as those previously reported for the PDMS oxygenators, with a water flow rate of $2\ \text{ml}\ \text{min}^{-1}$ and room air ventilation.

Figure 4.11 shows the improvement in partial pressure increase across the fibres after the same adjustment as was performed for Figure 4.8. The average inlet partial pressure was calculated and subtracted from the outlet pressures of the mixing and non-mixing units.

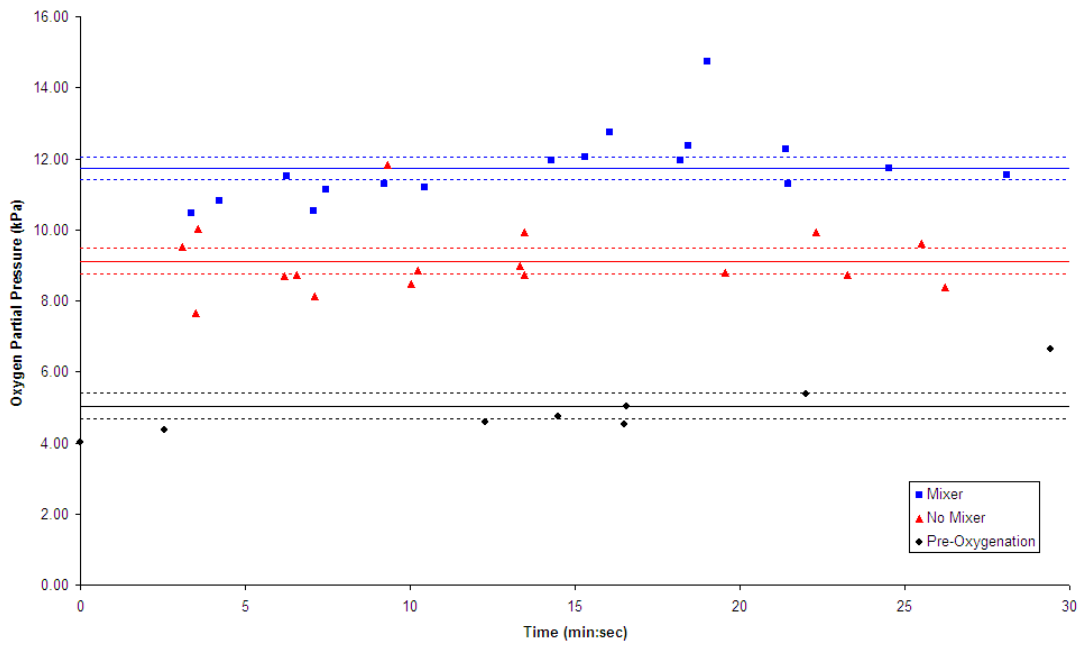


Figure 4.10 – Inlet and outlet P_{O_2} for Celgard 2500 oxygenators as a function of experimental time – effect of static mixer. Distilled water at 2 ml min^{-1} , air ventilation

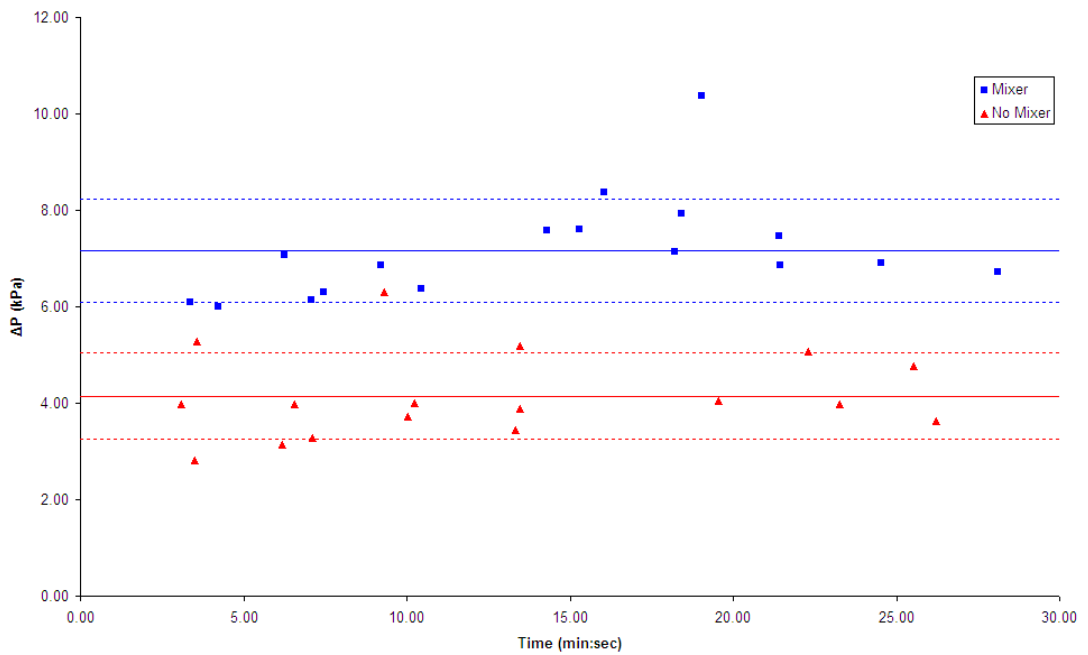


Figure 4.11 – P_{O_2} increase across Celgard 2500 oxygenator – effect of static mixer. Distilled water at 2 ml min^{-1} , air ventilation

Again, using the mean values \pm one standard deviation for inlet and outlet P_{O_2} , the total molar transfer rates for non-mixing and mixing oxygenators were $J_{O_2} = 2.86 \times 10^{-10} \text{ mol.s}^{-1} \pm 6.20 \times 10^{-11}$ and $J_{O_2} = 4.98 \times 10^{-10} \text{ mol.s}^{-1} \pm 7.33 \times 10^{-11}$ respectively. Analysing these values using a two sample t-test, $t(32) = 7.78$, $p \gg 0.05$, meaning there is significant difference between the mixing and non-mixing units.

The PDMS units were prone to leaking after approximately fifteen minutes; this explains why none of these units were tested beyond this time period.

When the differences between the two materials used to construct the membrane tubes were examined in detail, the Celgard 2500 membrane was found to have higher oxygen transfer rates than the PDMS tubing. This comparison is shown in Figure 4.12.

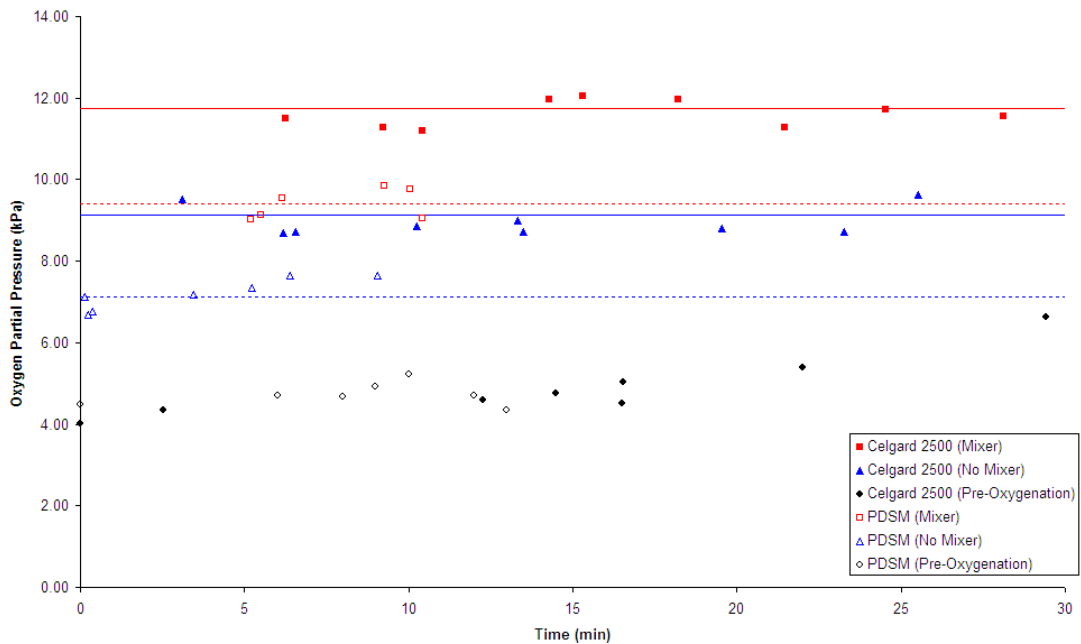


Figure 4.12 - Comparison of materials

The difference in materials was found to be significant (for mixing, $t(29) = 6.82, p \gg 0.05$; for non-mixing, $t(29) = 6.52, p \gg 0.05$). As such, the decision to continue using only the Celgard 2500 tubes was made. The remainder of this section will detail the results gathered for this material. To maximise its performance, the ventilating gas was changed from air to 100% oxygen.

Figures 4.13, 4.15, 4.17, and 4.19 show the all inlet and outlet P_{O_2} data for the three mixing and non-mixing unit pairs tested with water at flow rates 1, 2, 3 and 4 $ml\ min^{-1}$ respectively. The broken lines above and below the average values represent the average value plus or minus one standard deviation.

Figures 4.14, 4.16, 4.18, and 4.20 show the oxygen transfer rates corresponding to the data given in Figures 4.13, 4.15, 4.17, and 4.19 respectively. Plotted with the individual data points are the average values determined for each data set. The broken lines above and below the average values represent the average value plus or minus one standard deviation.

The average outlet P_{O_2} is shown as a function of water flow rate in Figure 4.21. Oxygen transfer rates based on the average ΔP_{O_2} values is shown in Figure 4.22 as a function of water flow rate.

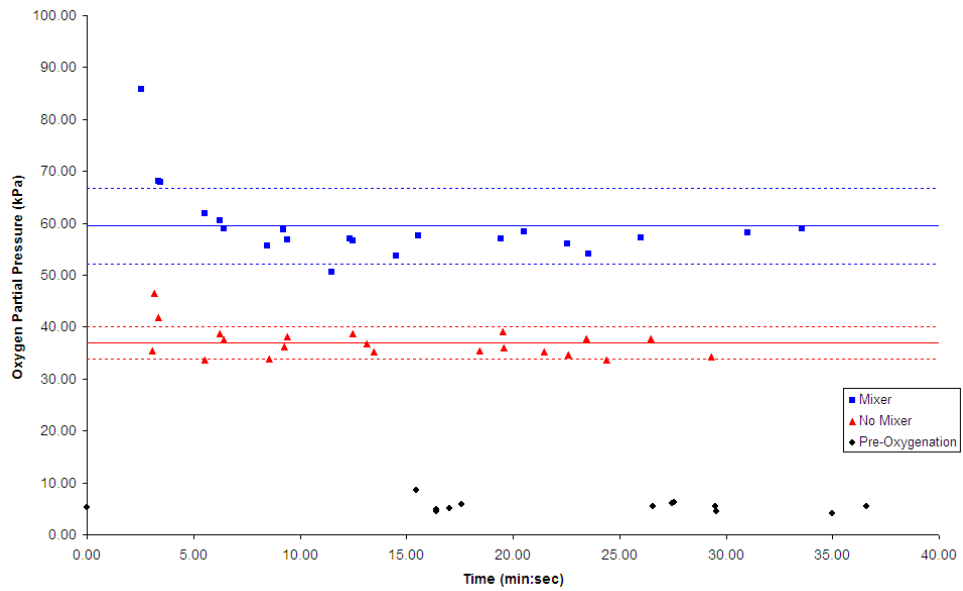


Figure 4.13 – Inlet and outlet P_{O_2} for Celgard 2500 oxygenators. Distilled water at 1 ml min^{-1} , 100% O_2 ventilation

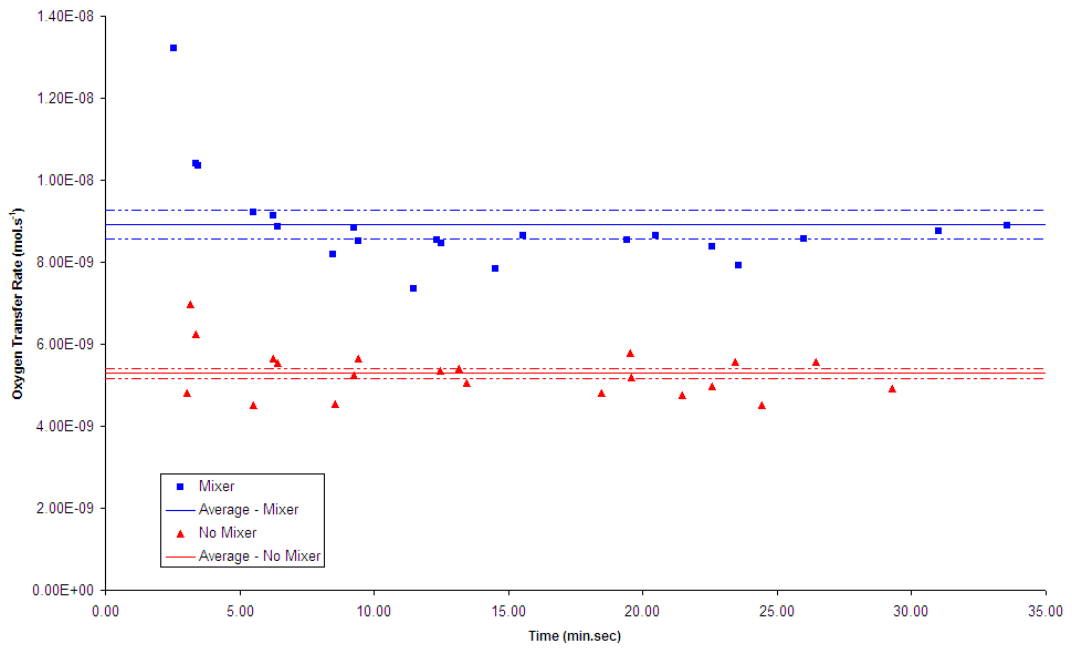


Figure 4.14 – Oxygen transfer rates in mixing and non-mixing oxygenators. Distilled water at 1 ml min^{-1} , 100% O_2 ventilation

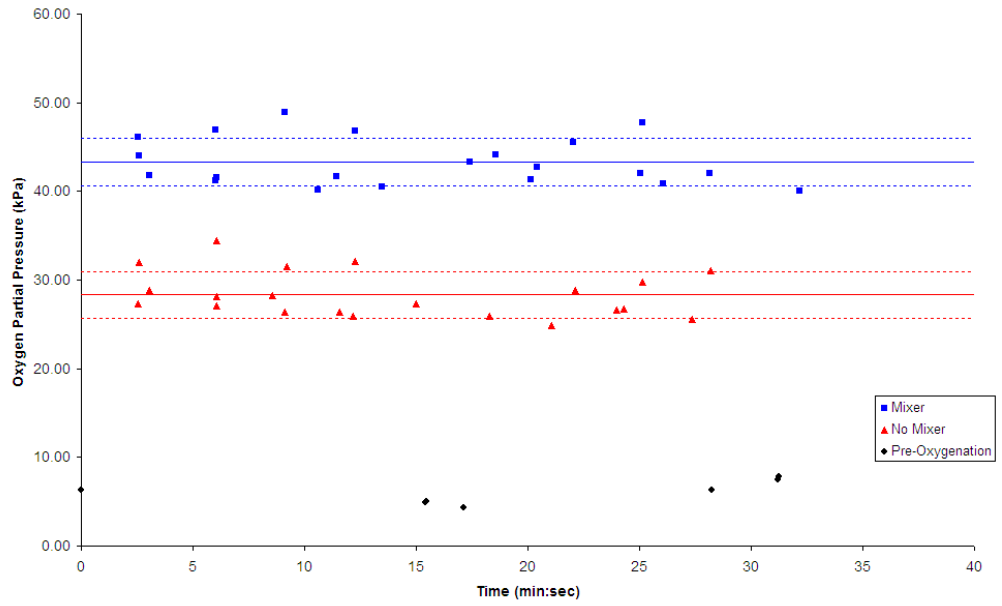


Figure 4.15 - Inlet and outlet P_{O_2} for Celgard 2500 oxygenators. Distilled water at 2 ml min^{-1} , 100% O_2 ventilation

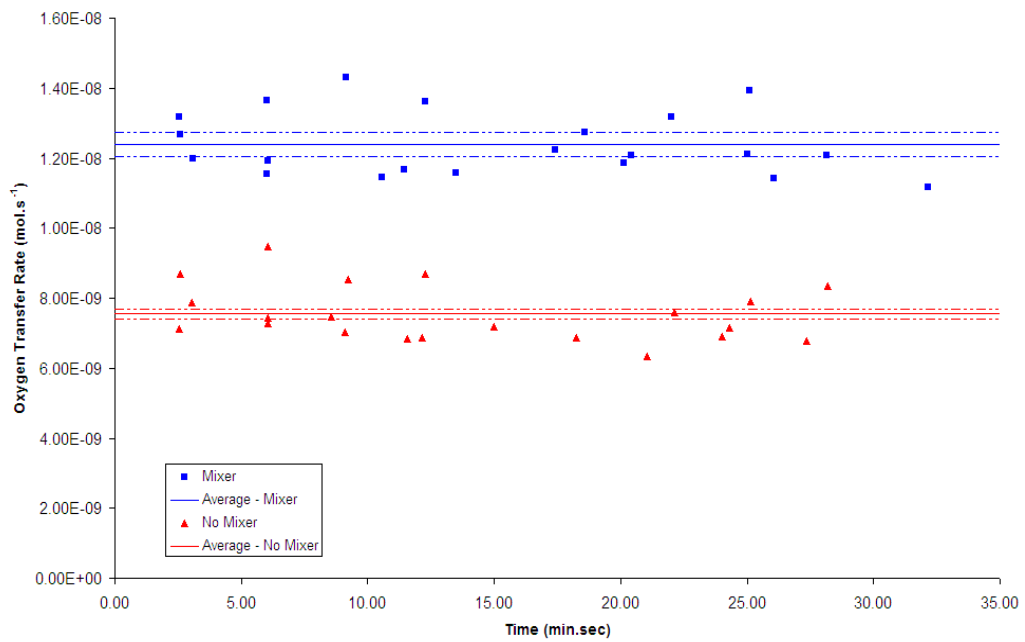


Figure 4.16 – Oxygen transfer rates in mixing and non-mixing oxygenators. Distilled water at 2 ml min^{-1} , 100% O_2 ventilation

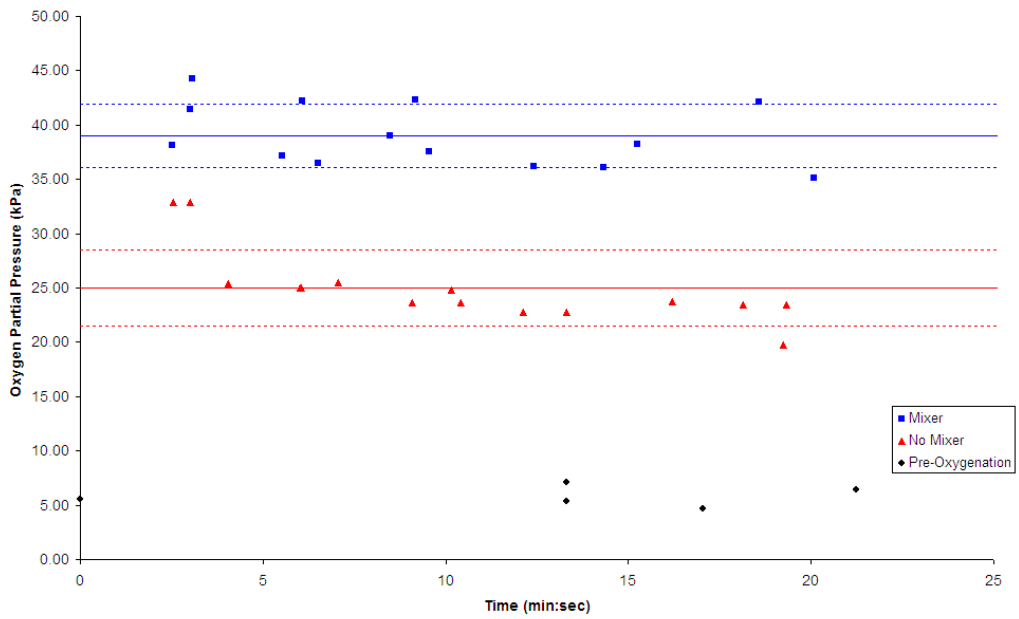


Figure 4.17 - Inlet and outlet P_{O_2} for Celgard 2500 oxygenators. Distilled water at 3 ml min^{-1} , 100% O_2 ventilation

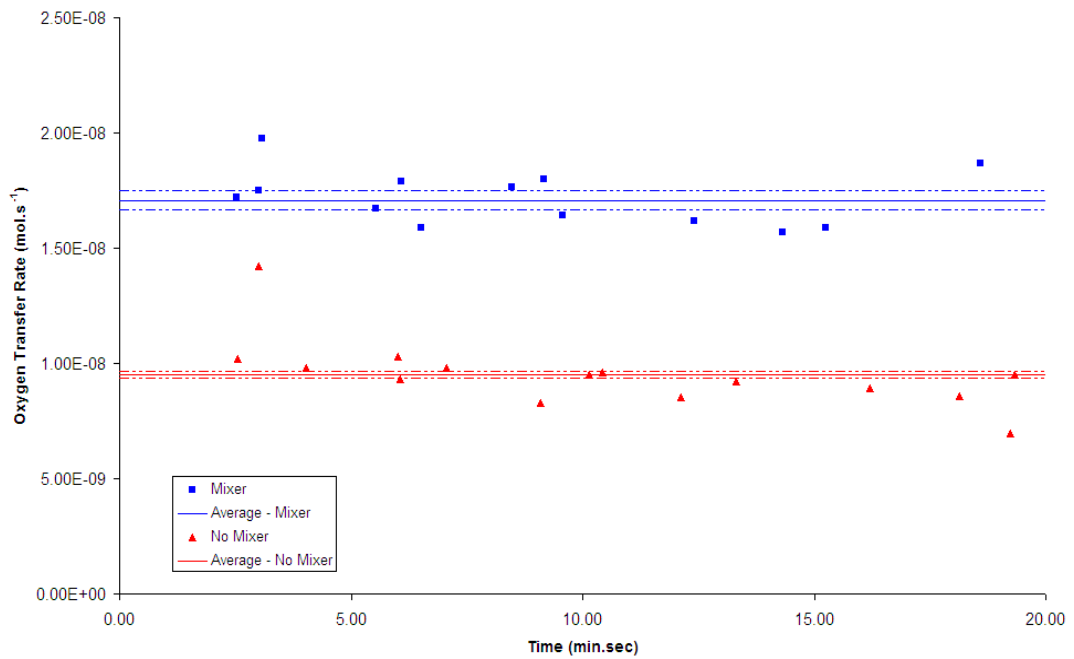


Figure 4.18 – Oxygen transfer rates in mixing and non-mixing oxygenators. Distilled water at 3 ml min^{-1} , 100% O_2 ventilation

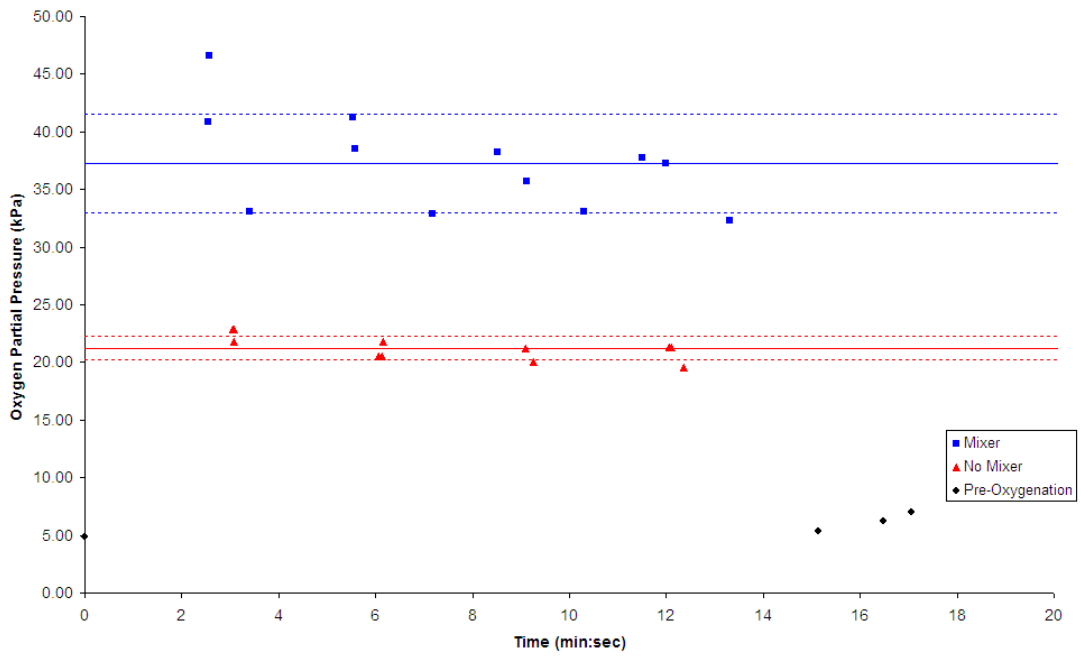


Figure 4.19 - Inlet and outlet P_{O_2} for Celgard 2500 oxygenators. Distilled water at 4 ml min^{-1} , 100% O_2 ventilation

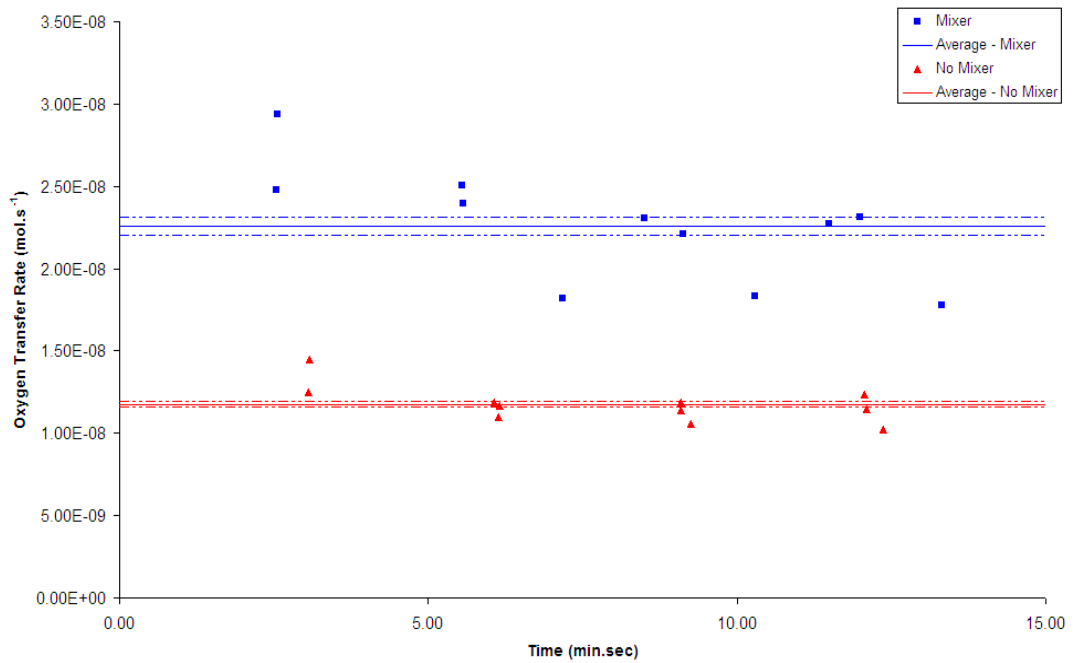


Figure 4.20 – Oxygen transfer rates in mixing and non-mixing oxygenators. Distilled water at 4 ml min^{-1} , 100% O_2 ventilation

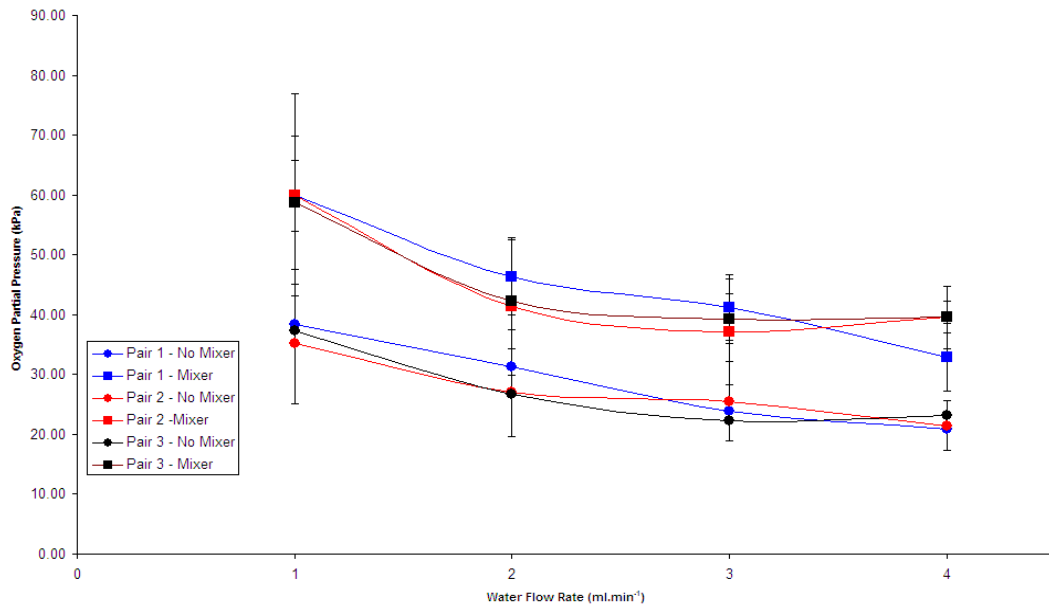


Figure 4.21 – Overall changes in P_{O_2} against water flow rate (Celgard 2500 oxygenators)

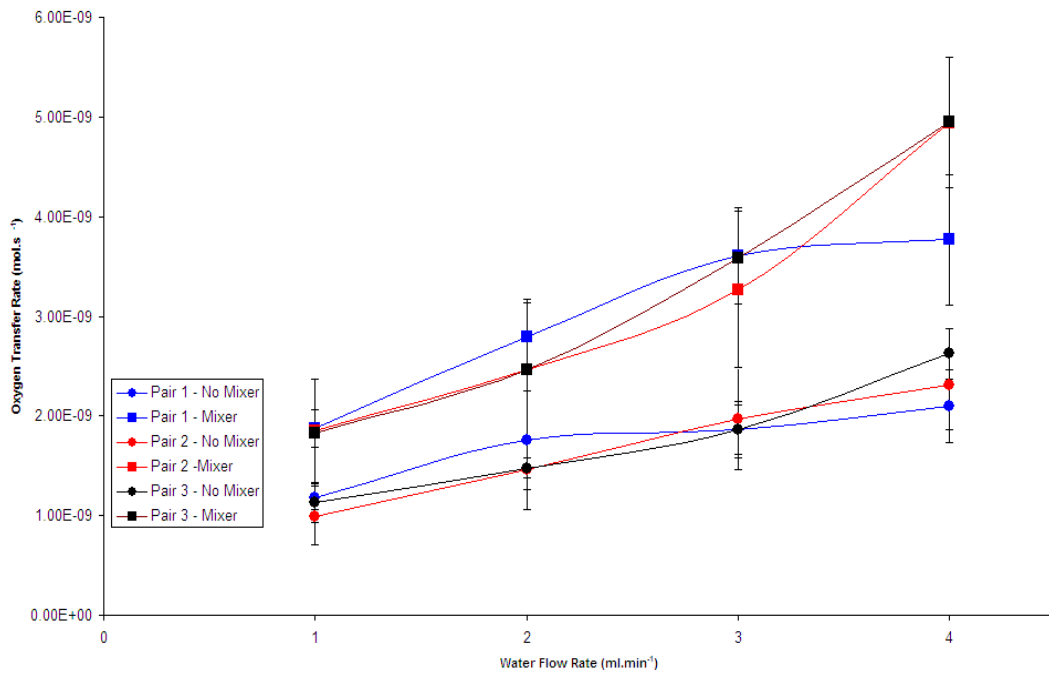


Figure 4.22 – O_2 transfer rates for three pairs of Celgard 2500 oxygenators

4.3 Discussion

The purpose of this current investigation is to ascertain if the inclusion of a helical static mixer in a tubular membrane oxygenator would have a beneficial effect on the oxygenation of blood. In the preliminary results reported, distilled water was used instead of deoxygenated blood. The oxygenators were constructed with the tube internal radius greatly increased compared to that of hollow fibres used in current clinical blood oxygenators. The increase in radius was to accommodate the commercially available helical static mixers. Experiments were conducted on individual tubular membranes.

Two material types were investigated for use as an oxygenating membrane. Tubes were constructed from PDMS and Celgard 2500. The oxygenation performance of these tubes was tested with a water flow rate of 2 ml min^{-1} and with air ventilation. Table 4.2 shows a comparison of the results shown in Figures 4.7 – 4.11.

Table 4.2 - Comparison of Materials

		PDMS	Celgard
Mixer	Inlet P _{O₂} (kPa)	4.54 ± 0.26	4.80 ± 0.36
	Outlet P _{O₂} (kPa)	9.47 ± 0.37	11.74 ± 0.32
	J _{O₂} (mol.s ⁻¹)	3.44x10 ⁻¹⁰ ± 1.85 x10 ⁻¹¹	4.98x10 ⁻¹⁰ ± 7.33 x10 ⁻¹¹
No Mixer	Outlet P _{O₂} (kPa)	7.12 ± 0.38	9.20 ± 0.36
	J _{O₂} (mol.s ⁻¹)	1.79x10 ⁻¹⁰ ± 2.67 x10 ⁻¹¹	2.86x10 ⁻¹⁰ ± 6.20 x10 ⁻¹¹

Considering these results, it is obvious that the Celgard 2500 membrane offers greater potential in oxygenation performance. Subsequent experiments were confined to oxygenators with Celgard 2500 tubes and using 100% O₂ as the ventilating gas.

Table 4.3 shows a comparison of the results shown in Figures 4.13 – 4.20.

Table 4.3 - Comparison of Water Flow Rates

		1 ml/min	2 ml/min	3 ml/min	4 ml/min
	Inlet P _{O₂} (kPa)	5.5 ± 0.9	5.8 ± 0.4	5.5 ± 0.9	5.8 ± 1.0
Mixer	Outlet P _{O₂} (kPa)	59.5 ± 0.7	43.3 ± 2.6	39.2 ± 2.0	37.3 ± 2.0
	J _{O₂} (mol.s ⁻¹)	8.92x10 ⁻⁹ ±	1.24x10 ⁻⁸ ±	1.71x10 ⁻⁸ ±	2.16x10 ⁻⁸ ±
	J _{O₂} (mol.s ⁻¹)	1.08x10 ⁻¹⁰	9.01x10 ⁻¹⁰	3.57x10 ⁻¹⁰	3.03x10 ⁻⁹
No Mixer	Outlet P _{O₂} (kPa)	37.0 ± 1.7	28.3 ± 2.6	23.9 ± 1.7	21.8 ± 1.2
	J _{O₂} (mol.s ⁻¹)	5.29x10 ⁻⁹ ±	7.55x10 ⁻⁹ ±	9.51x10 ⁻⁹ ±	1.14x10 ⁻⁸ ±
	J _{O₂} (mol.s ⁻¹)	4.78x10 ⁻¹⁰	8.01x10 ⁻¹⁰	9.09x10 ⁻¹⁰	6.06x10 ⁻¹⁰

Using a t-test to compare the flow rates, the differences in oxygen partial pressure and transfer rate are found to be statistically significant with all *p* values below 0.05.

Figure 4.21 takes the average values calculated for each fibre and shows the relationship between the outlet *P*_{O₂} and water flow rates. As mentioned above, the

partial pressures decrease as the flow rate is increased, leading to a downward trend in the relationship. This is observed in all three oxygenator pairs. The reason behind this trend is that the fluid residence time in the tube is reduced with increasing flow rate. Therefore the amount of time a volume of fluid is within the oxygenating region of the tube is reduced, leading to less oxygen entering that volume. Thus the outlet partial pressure decreases as the flow rate is increased.

The differences shown in Figure 4.21 between each oxygenator unit of a single type (i.e. between all mixing units and between all non-mixing units) are not statistically significant ($p \gg 0.05$).

From Figure 4.22, it is apparent that even if the outlet P_{O_2} decreases with increasing water flow rate, the oxygen transfer rate increases as it is dependent on the flow rate. In particular, at the highest flow rate, the mixing oxygenators of Pairs 2 and 3 have 89% and 114% increases in oxygen transfer over their non-mixing counterparts.

Figure 4.22 reveals several interesting details. The first of these is the shape of the curves calculated for Pair 1. In both the mixing and non-mixing cases, these curves do not follow the shapes Pairs 2 and 3 take. This is also true when one considers the shapes Pair 1 makes in Figure 4.21. The reason for this pair of membrane tubes having different values in partial pressure and oxygen transfer is related to the age of the material. Pairs 2 and 3, and the subsequent fibres constructed for the blood experiments described in Chapter 6 were made from material supplied by the manufacturer and used over a period of six months. Pair 1 was made from material

that had been kept in storage for an indeterminate period of time (>5 years), possibly resulting in the membrane degradation. The pore size may have become distended when compared with the fresh material, and would thus allow far more oxygen into the fibre. Conversely, as was noted during the water trials with Pair 1, the units made from the older membrane were prone to fluid leakage, furthering the possibility that the pore size of the material was enlarged.

There are additional points that can be made from these two Figures. That both lines for the mixing and non-mixing oxygenators lie close enough within the calculated errors would indicate that the construction is reproducible, and therefore any additional devices built using the same technique as described above in Chapter 4.1.1 could be expected to have a similar profile to those depicted above.

When the above data is considered collectively, several key points can be noted. The tubes constructed from Celgard 2500 membrane have better oxygenation properties than the thicker walled silicone rubber fibres. Obviously oxygenating the units with 100% oxygen is superior than air. Finally, the inclusion of the static mixing units appears to facilitate the oxygenation process within the fibre lumen. However, it must be stated that the purpose of the static mixer is not to ensure that the entire fluid becomes completely oxygenated; instead its function is to better distribute the available oxygen across the system.

The input conditions of these preliminary water experiments were taken to be used in conjunction with COMSOL Multiphysics⁹⁶ (formerly FEMLAB). Using the

practical data, it should be possible to accurately simulate the water experiments before attempting to simulate the behaviour of the fibres when bovine blood is used. Details of the water simulations can be found in Chapter 5.

Chapter 5 – Mathematical Simulations of Oxygenation of Water

In this chapter, the mathematical models based upon the experimental findings of the Celgard 2500 units in Chapter 4 are described fully. In Section 5.1, the boundary and initial conditions are detailed along with the model geometries and physio-chemical parameters. Section 5.2 discusses the development of the models, and the process by which the experimental work on the individual oxygenators were simulated. Section 5.3 contains the results of the mathematical models and in Section 5.4 these are discussed.

5.1 Boundary and initial conditions

5.1.1 Boundary conditions

In order to solve the governing equations, boundary conditions must be specified for the dependent variable, P_{O_2} . For the flow velocities, it is assumed that there is no flow at the solid boundary. Thus, $\bar{u} = 0$ at $r = R$, and at the surface of the mixing blade.

At both the inlet and outlet, it is assumed that the flow is parallel to the tube axis, i.e. $u_x = u_y = 0$. The axial flow, u_z , varies between 1 ml min^{-1} and 4 ml min^{-1} in 0.5 ml min^{-1} increments.

At the tube inlet, ($z = 0$), it is assumed that there are concentrations of dissolved and bound oxygen which satisfy the steady state equation $P_{O_2} = P_0$ and $C_{O_2} = C_0^i$. The values of P_0 are given in Table 5.1; the values of C_0 are determined by Equation (3.12) based upon the various values of P_0 . At the oxygenating membrane boundary, there is no flux of bound oxygen, but there is an influx of dissolved oxygen:

$$\frac{\partial C_{O_2}}{\partial r} = 0 \text{ on } r = R, \quad (5.1)$$

and recalling Equation (3.28),

$$\frac{\partial P_{O_2}}{\partial r} = \frac{Sh_w}{2R} (P_g - P_{O_2}) \text{ at } r = R. \quad (3.28)$$

The boundary conditions for the helical static mixer must also be defined. There is no oxygen flux through the blades:

$$\begin{aligned} n \cdot \nabla C_{O_2} &= 0 \\ n \cdot \nabla P_{O_2} &= 0 \end{aligned} \text{ on the mixer surfaces.}$$

5.1.2 Inlet conditions

The inlet oxygen partial pressure for the models will be the average inlet partial pressures measured experimentally.

Table 5.1 – Average inlet partial pressures for use in the mathematical models

Pair 1	No Mixer	Mixer
Flow Rate (ml min ⁻¹)	Pressure (kPa)	Pressure (kPa)
1.0	4.278	5.625
2.0	5.918	5.851
3.0	5.811	6.358
4.0	5.598	5.518
Pair 2		
Flow Rate (ml min ⁻¹)	Pressure (kPa)	Pressure (kPa)
1.0	6.545	6.398
2.0	5.798	5.705
3.0	6.558	5.545
4.0	4.705	3.719
Pair 3		
Flow Rate (ml min ⁻¹)	Pressure (kPa)	Pressure (kPa)
1.0	4.705	5.691
2.0	5.198	6.505
3.0	4.225	4.692
4.0	5.385	3.625

5.1.3 Model parameters

The following tables detail the constants used in the mathematical model.

Table 5.2 - Mathematical model dimensions

Parameter	Symbol	Value	Unit
Length of device	L	9×10^{-2}	m
Radius of device	R	1.2×10^{-3}	m
Membrane thickness	t_m	2.5×10^{-5}	m
Mixer blade radius	R_{blade}	2.39×10^{-3}	m
Mixer blade length	L_{blade}	2.39×10^{-3}	m

The mixer blade radius and length are taken from the physical dimensions of the mixer used in Chapter 4.

Table 5.3 - Convection-diffusion constants

Parameter	Symbol	Value	Unit
Gas Pressure	P_g	1.01×10^5	Pa
Celgard 2500 membrane porosity ⁸⁸		55%	
Diffusion of oxygen in membrane ⁹⁵	D_m	9.9×10^{-6}	$\text{m}^2 \text{s}^{-1}$
Solubility of oxygen in membrane ⁹⁵	α_m	1.54×10^{-9}	$\text{mol (STP) m}^{-3} \text{Pa}^{-1}$
Water			
Diffusion of oxygen in water ⁹⁵	D_{O_2}	3.24×10^{-9}	$\text{m}^2 \text{s}^{-1}$
Solubility of oxygen in water ⁹⁵	α_{O_2}	2.07×10^{-6}	$\text{mol (STP) m}^{-3} \text{Pa}^{-1}$
Gas transfer rate	G	3.01×10^{-8}	$\text{mol m}^{-2} \text{Pa}^{-1} \text{s}^{-1}$

The inlet flow rate shall range from 1 ml min^{-1} to 4 ml min^{-1} in 1 ml min^{-1} increments as done experimentally.

5.2 Materials and methodology

Using COMSOL Multiphysics⁹⁶, the equations described in Chapter 3, as well as the conditions detailed in Section 5.1, were evaluated.

The mathematical models were created to simulate the experiments conducted in the laboratory. To this end, the input conditions of the models were chosen to closely mimic the inlet conditions recorded experimentally, as shown in Table 5.1.

Initially, the Navier-Stokes equations were evaluated for each of the models, as there is a velocity component in Equation (3.21). The convection-diffusion reaction equations were then evaluated using the stored Navier-Stokes solutions. This stepwise approach is possible as the concentrations of oxygen do not enter the Navier-Stokes equations and thus the flow equations can be solved first.

Three models were created to simulate water flowing down an empty tube using the experimental initial conditions. The simulations were based upon one experimental run each. Once these three models had been developed, and the results analysed, the static mixer models were then created. Due to computational limitations, the exact nature of the static mixers could not be modelled. Instead of two units of twelve mixing elements used experimentally, the theoretical model simulated the mixer in blocks of three elements, up to a maximum of twelve.

All simulations of matching types (non-mixing; three blade mixer; six blade mixer; nine blade mixer; twelve blade mixer) had an identical number of finite elements comprising the model. This ensures that any differences between the simulations of one type are due to the input conditions, not due to differences in the model.

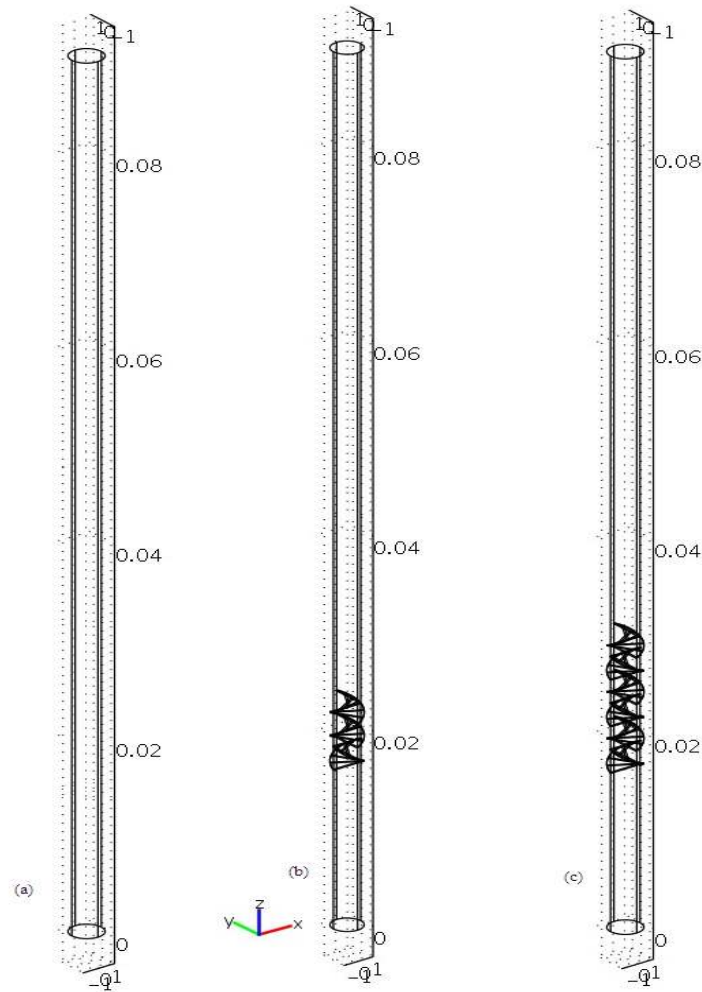


Figure 5.1 – COMSOL Multiphysics representation of (a) non-mixing unit, (b) three-blade mixing unit, and (c) six-blade mixing unit. Note: the mixing blades in (b) and (c) are not to scale; the tubes are set to 9 *cm* long and the blades are 2.39 *mm* long.

5.3 Results

5.3.1 Water flow in a three-dimensional non-mixing oxygenator

Figure 5.2 details the outlet oxygen partial pressure predicted by the mathematical model for the three oxygenators. Overall, as the flow rate increases, the partial pressure of oxygen within the system drops. This downward trend is similar to that observed experimentally (*see* Figure 4.21).

The change in oxygen transfer rate with flow rate is shown in Figure 5.3. The shape of the three curves matches that shown in Figure 4.22. As with Figure 5.2, any differences between the values recorded from the model are attributed to the non-identical initial conditions each device experienced.

A closer comparison of the individual units and their corresponding mathematical model is given below.

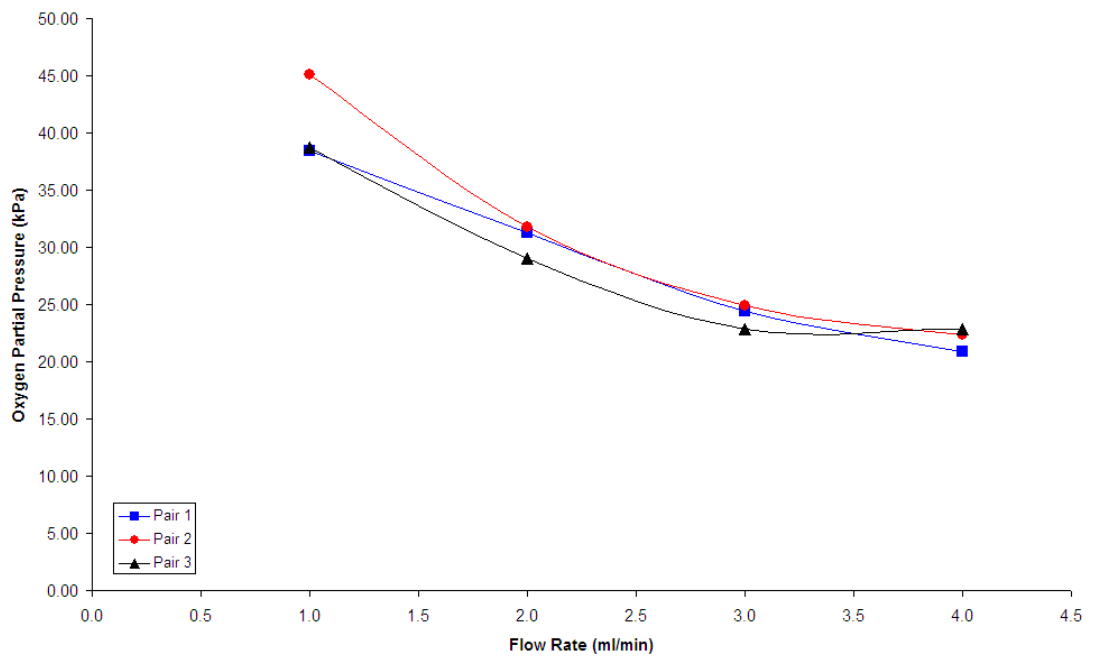


Figure 5.2 – Changes in P_{O_2} with water flow rate (non-mixing units)

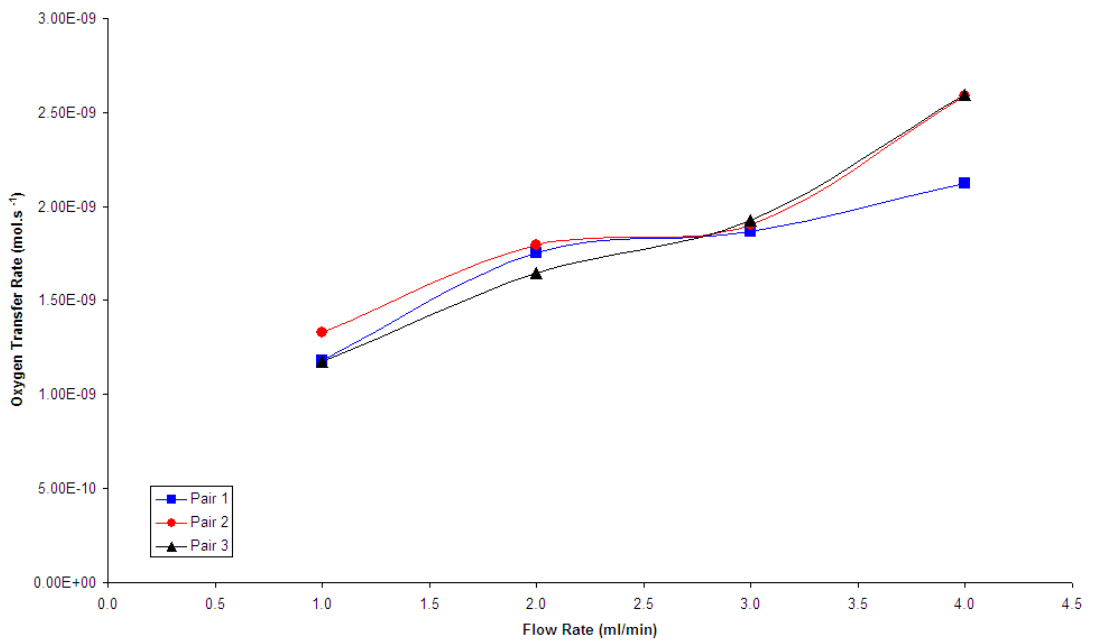


Figure 5.3 – Changes in J_{O_2} with water flow rate (non-mixing fibres)

5.3.1.1 Comparison between experimental and theoretical results

In these comparisons, the average experimental values will be used. It should be noted that the theoretical models have been solved time-independently and therefore represent the equilibrium state of the individual tubes. As such there may be discrepancies between the theory and practical outlet conditions.

Figures 5.3, 5.5 and 5.7 show the change in partial pressure for the non-mixing unit in Pairs 1, 2 and 3 respectively. As noted above, each oxygenator model has a similar downward trend in P_{O_2} with increasing flow rate similar to that seen in the experimental data.

Figures 5.4, 5.6 and 5.8 show the corresponding change in oxygen transfer rate for each of the empty devices.

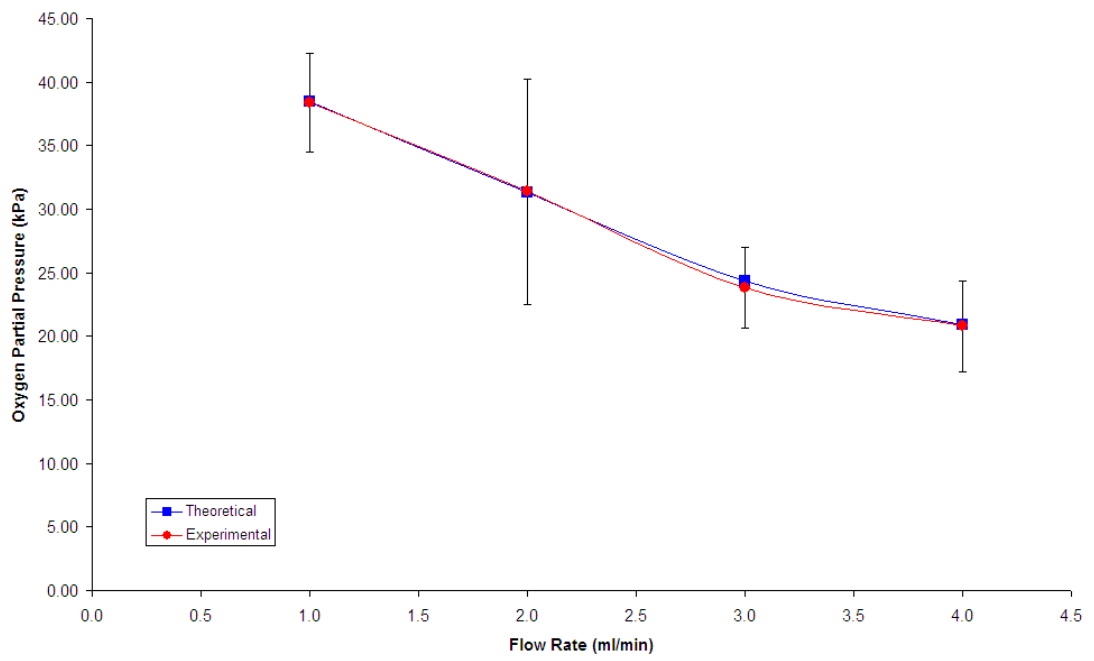


Figure 5.4 – Pair 1: Theoretical vs. experimental P_{O_2} with water flow rate

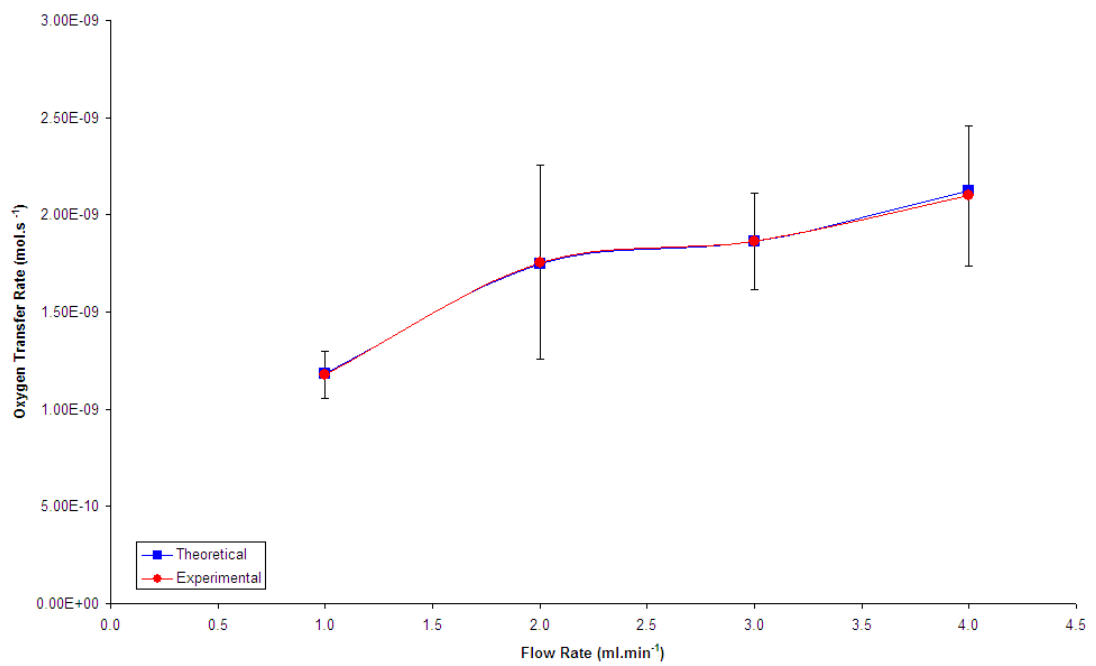


Figure 5.5 – Pair 1: Theoretical vs. experimental J_{O_2} with water flow rate

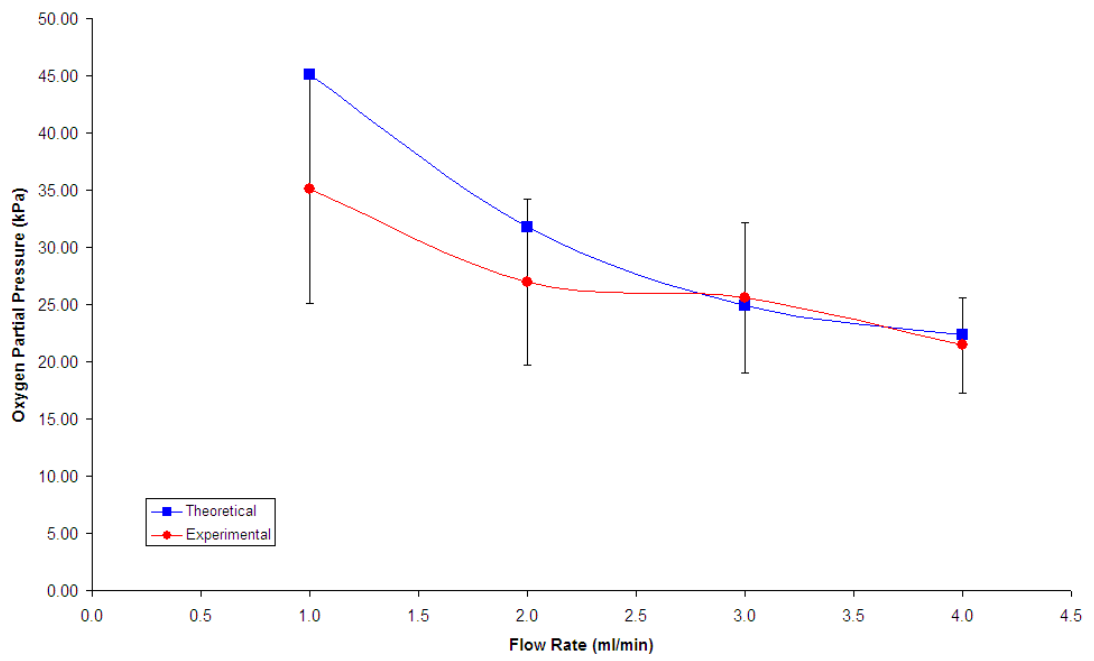


Figure 5.6 – Pair 2: Theoretical vs. experimental P_{O_2} with water flow rate

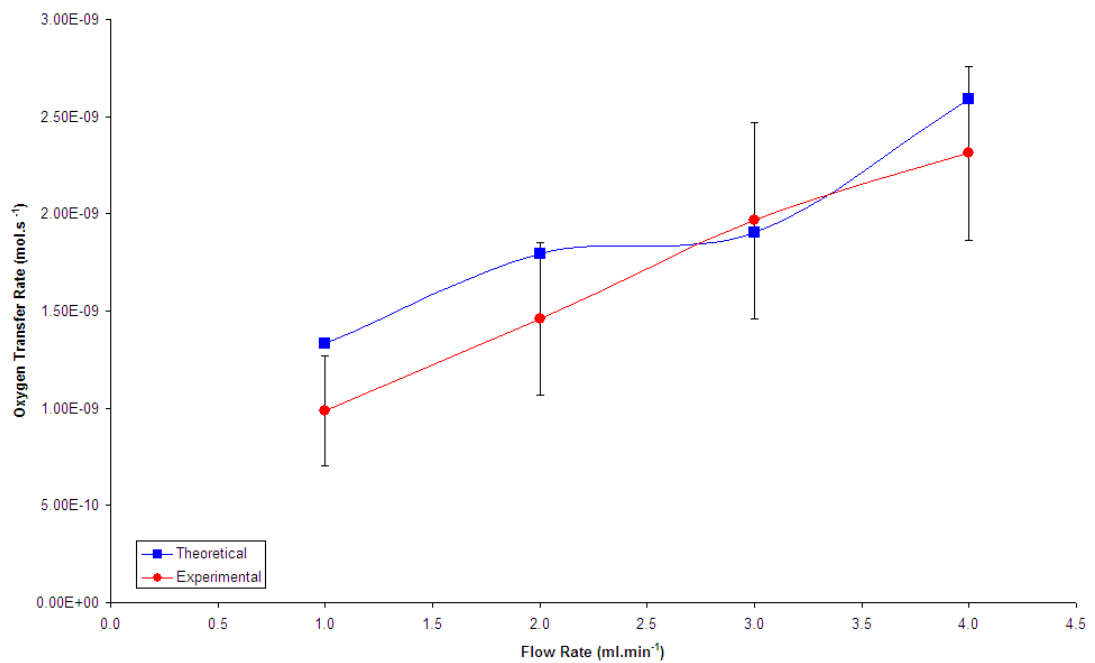


Figure 5.7 – Pair 2: Theoretical vs. experimental J_{O_2} with water flow rate

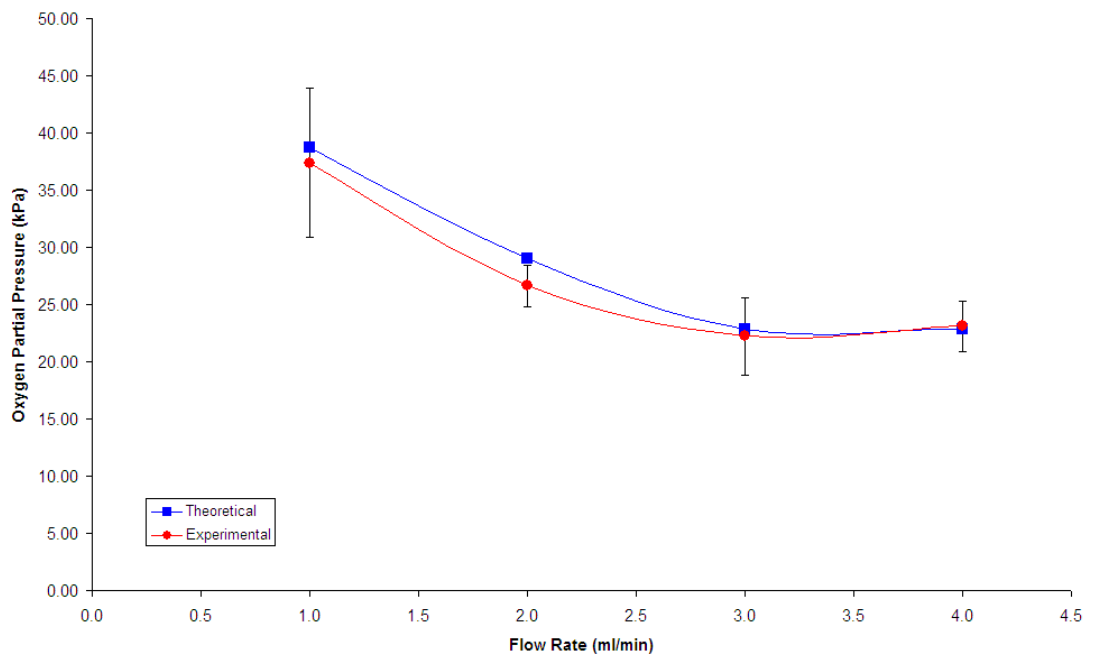


Figure 5.8 – Pair 3: Theoretical vs. experimental P_{O_2} with water flow rate

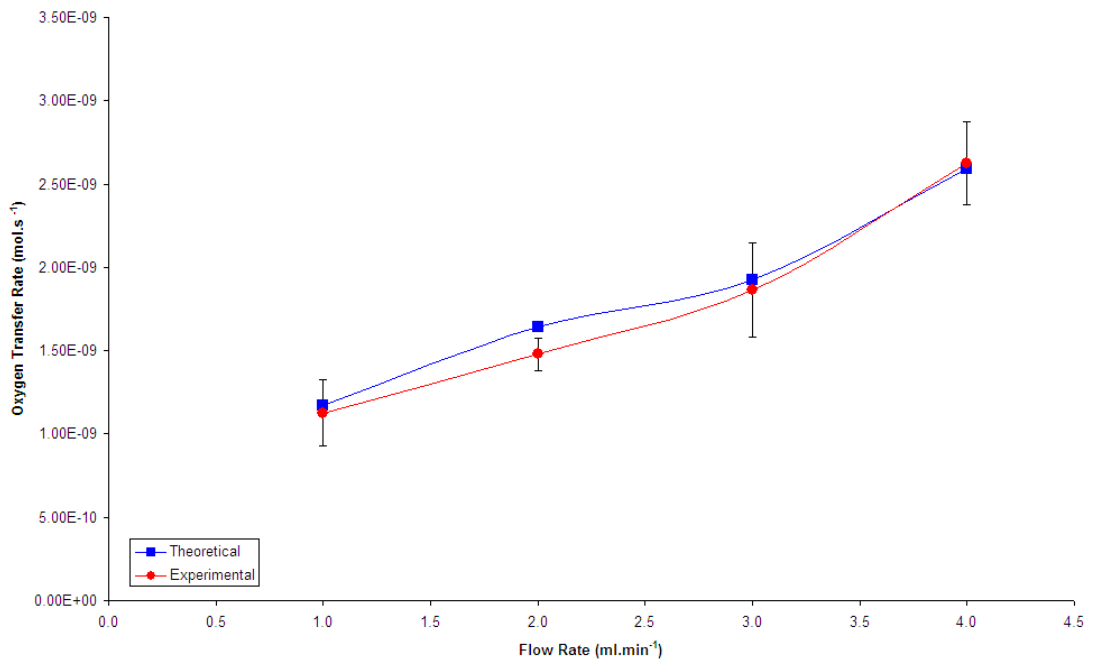


Figure 5.9 – Pair 3: Theoretical vs. experimental J_{O_2} with water flow rate

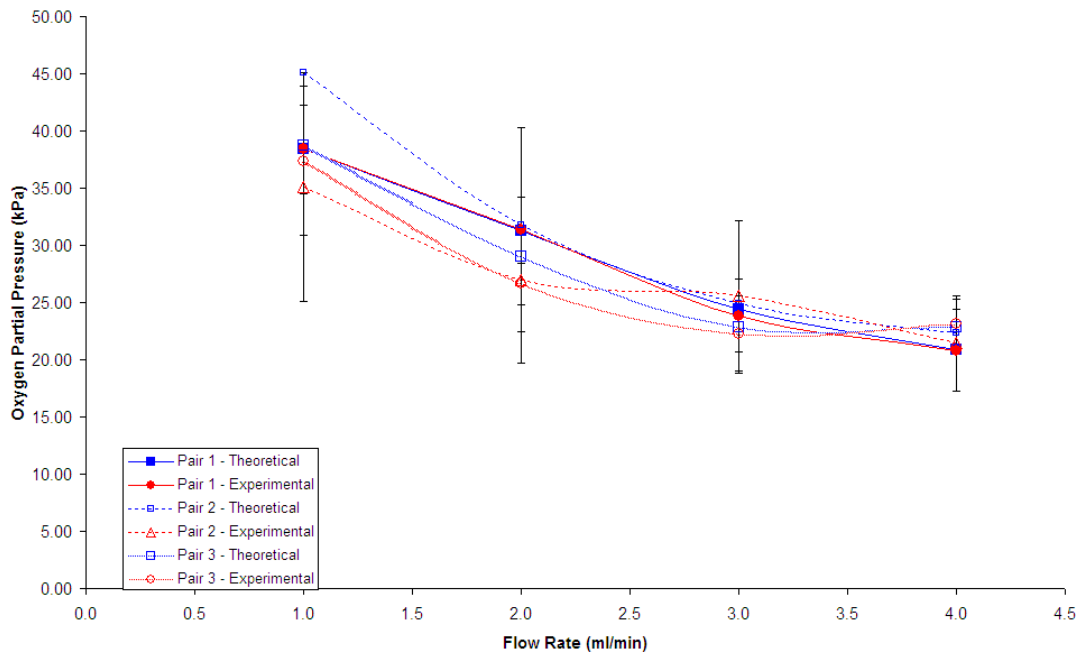


Figure 5.10 - Collection of theoretical and experimental findings for Pairs 1 to 3

5.3.2 Water flow in a three-dimensional mixing oxygenator

The static mixer within the fibre lumen was modelled in three-blade segments, due to computational limitations. The results for three- and six-blade mixers are presented below. The nine- and twelve-blade mixing simulations failed to return any results due to computational limitations.

Figure 5.11 shows the change in outlet P_{O_2} with increasing flow rate. As expected from experimental results, the partial pressure decreases.

Figure 5.12 indicates the corresponding oxygen transfer rate based upon the partial pressures shown in Figure 5.11. In keeping with experimental findings, each of the three simulations shows an increase in J_{O_2} with rising flow rate.

As previously mentioned with the non-mixing simulations, the differences in the mixing simulations may be attributed to differences in initial conditions, as these simulations were also based upon experimental data.

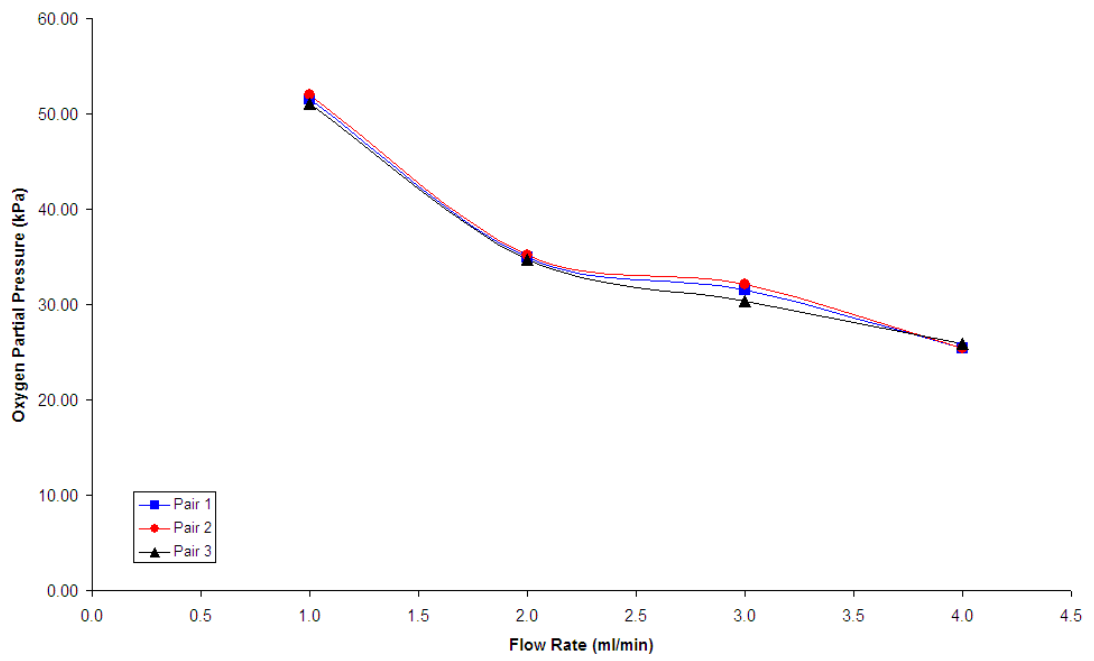


Figure 5.11 – Changes in outlet P_{O_2} with water flow rate (3 blade mixer)

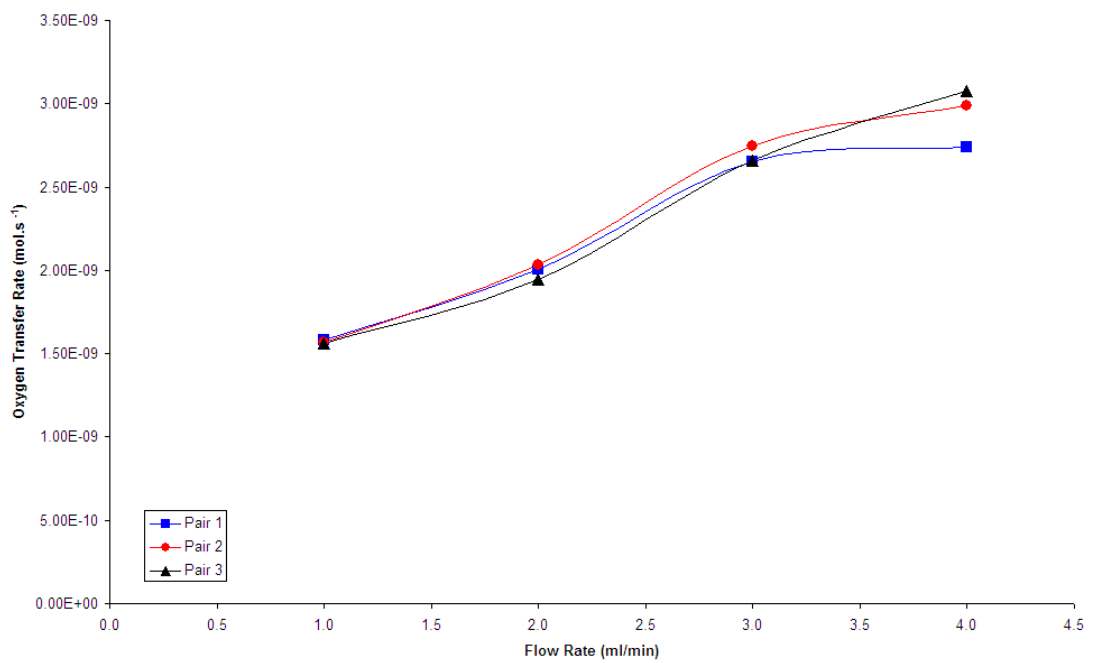


Figure 5.12 – Changes in J_{O_2} with water flow rate (3 blade mixer)

Figure 5.13 shows the change in outlet P_{O_2} with flow rate for the six-bladed static mixer. Once again, the overall downward trend is apparent. Presented in Figure 5.14 is the oxygen transfer for the six-blade mixer model. The lower flow rates appear to follow the pattern established by the experimental data; the oxygen transfer rises with increasing flow rates. However, there is a sharp decline after 3.5 ml min^{-1} is unexpected, mirroring the sharp drop in P_{O_2} at 4 ml min^{-1} seen in Figure 5.13.

As above, a comparison between the mathematical models and the experimental work they were based upon is presented below.

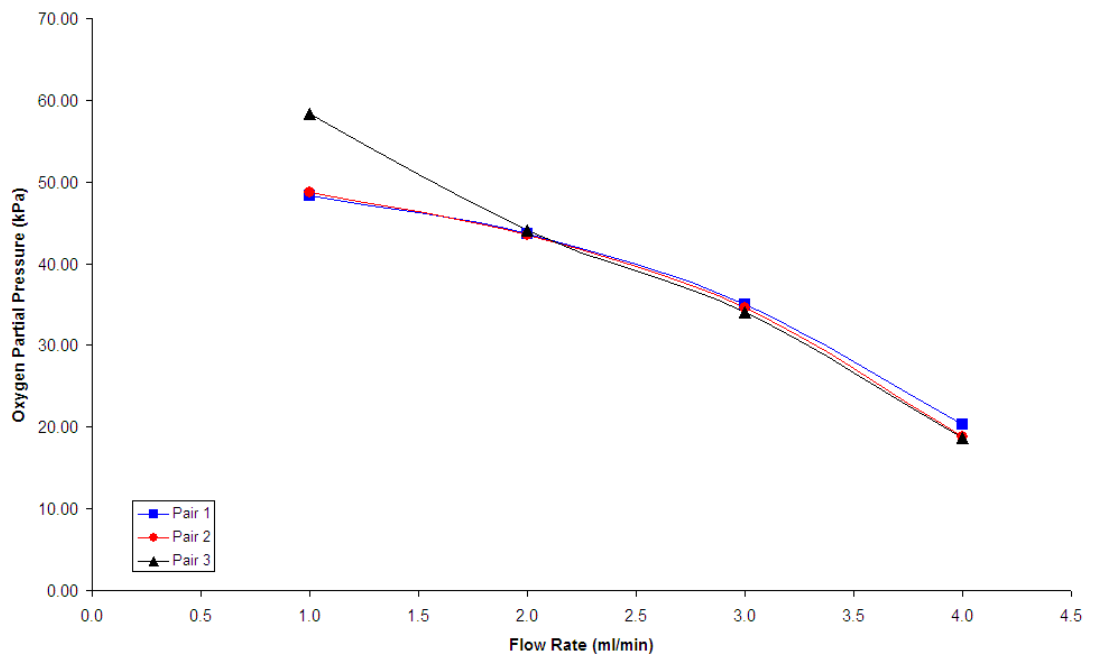


Figure 5.13 – Changes in absolute P_{O_2} with flow rate (6 blade mixer)

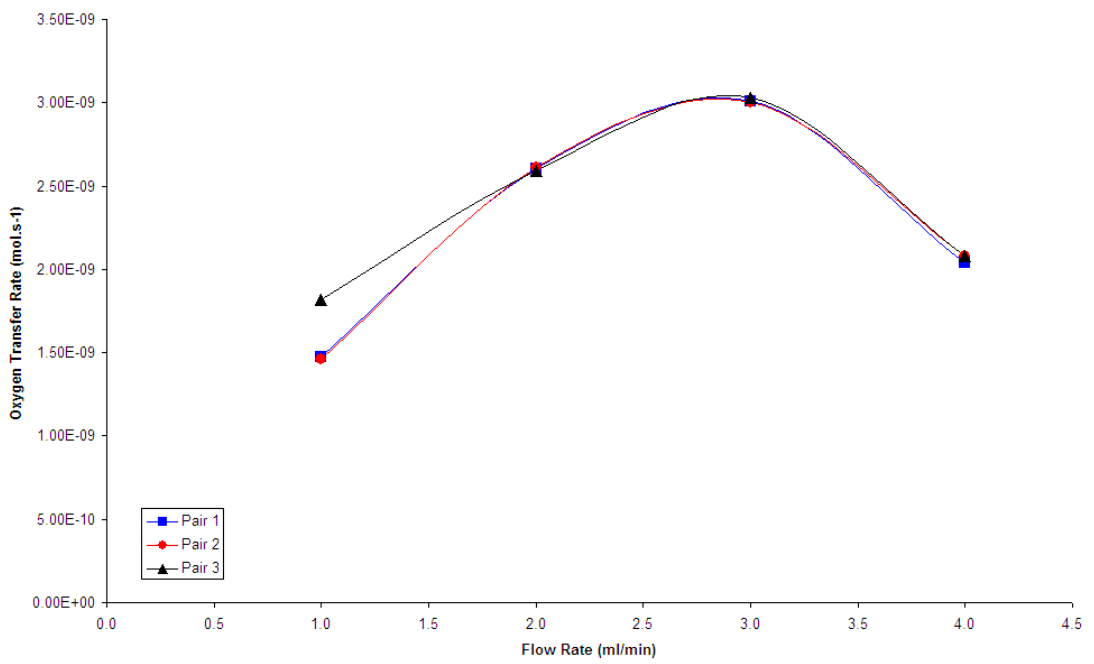


Figure 5.14 – Changes in J_{O_2} with flow rate (6-blade mixer)

5.3.2.1 Comparison between experimental and theoretical results

In each of the following figures, no values were returned for flow rates above 3 ml min^{-1} . At higher flow rates, the theoretical models returned unreliable results.

Figures 5.14, 5.16 and 5.18 show the change in partial pressure for the mixing fibre in Pairs 1, 2 and 3 respectively. The three- and six-bladed models are shown in the comparison in each figure. Both theoretical models have lower outlet levels of P_{O_2} than observed experimentally, but do follow the same approximate pattern.

Figures 5.15, 5.17 and 5.19 show the corresponding change in oxygen transfer rates for each of the mixing fibres.

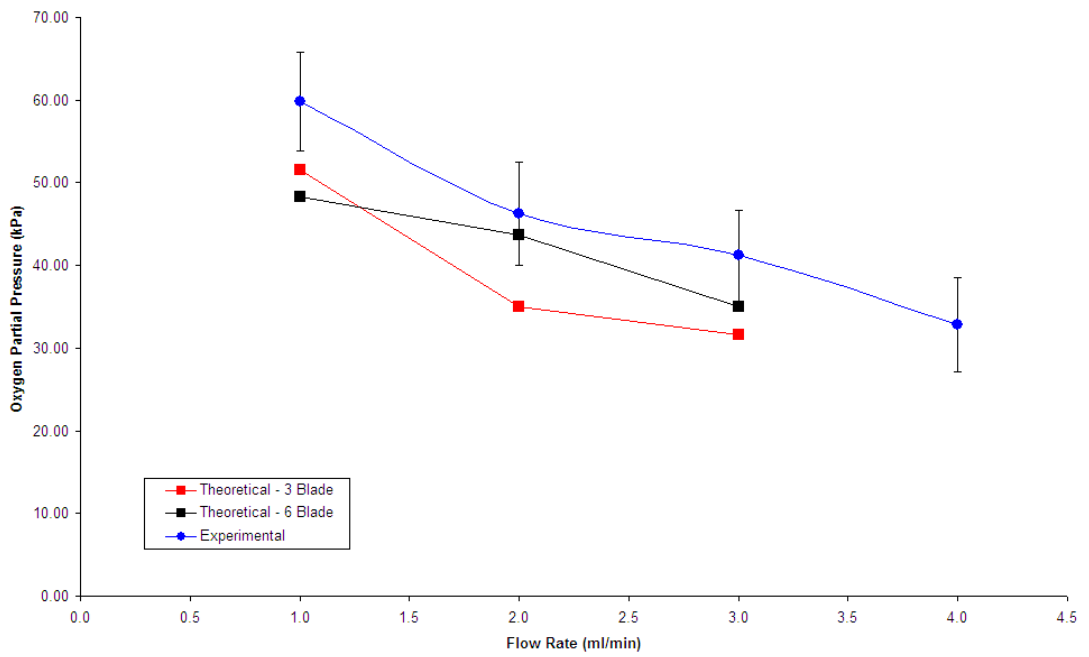


Figure 5.15 – Pair 1: Theoretical vs. experimental P_{O_2} with water flow rate (3- and 6-blade mixers)

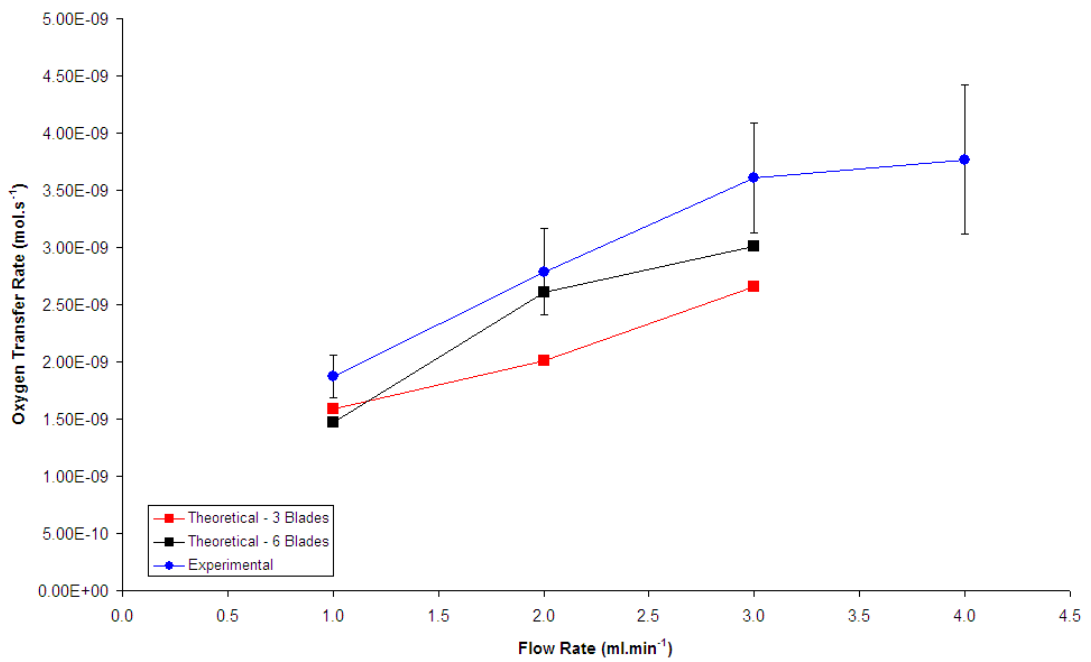


Figure 5.16 – Pair 1: Theoretical vs. experimental J_{O_2} with water flow rate (3- and 6-blade mixers)

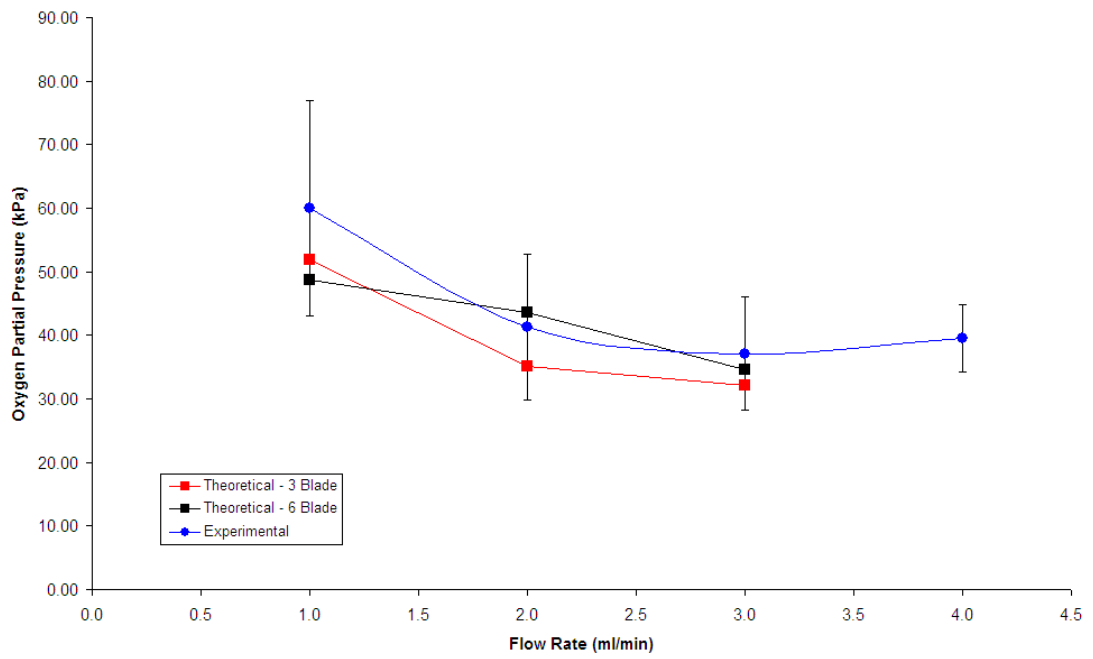


Figure 5.17 – Pair 2: Theoretical vs. experimental P_{O_2} with water flow rate (3- and 6-blade mixers)

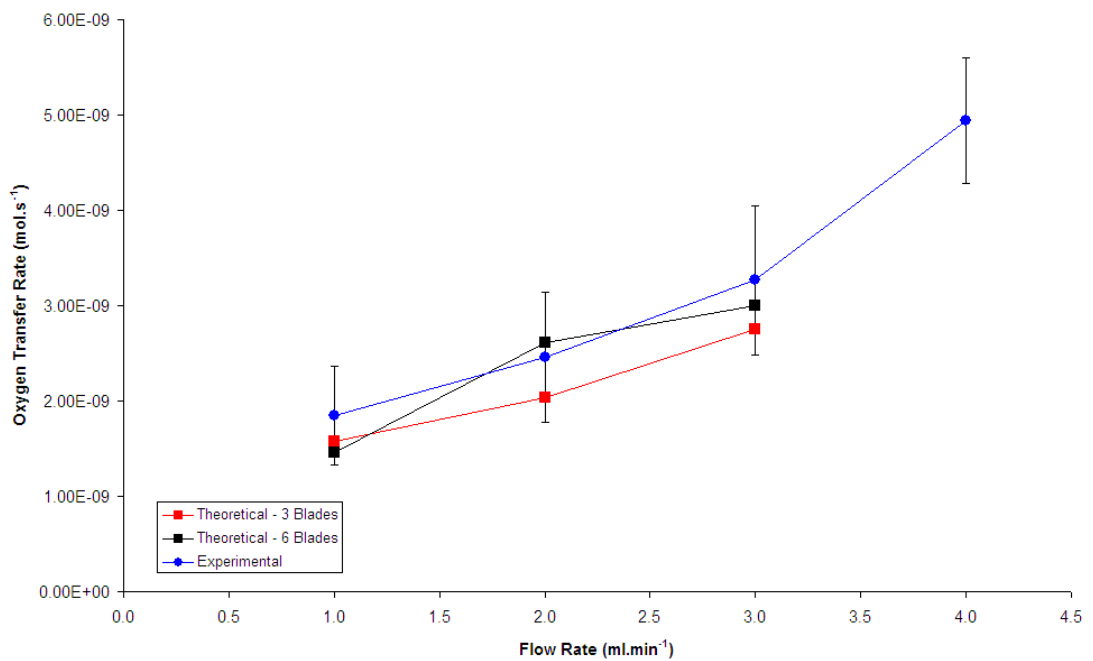


Figure 5.18 – Pair 2: Theoretical vs. experimental J_{O_2} with water flow rate (3- and 6-blade mixers)

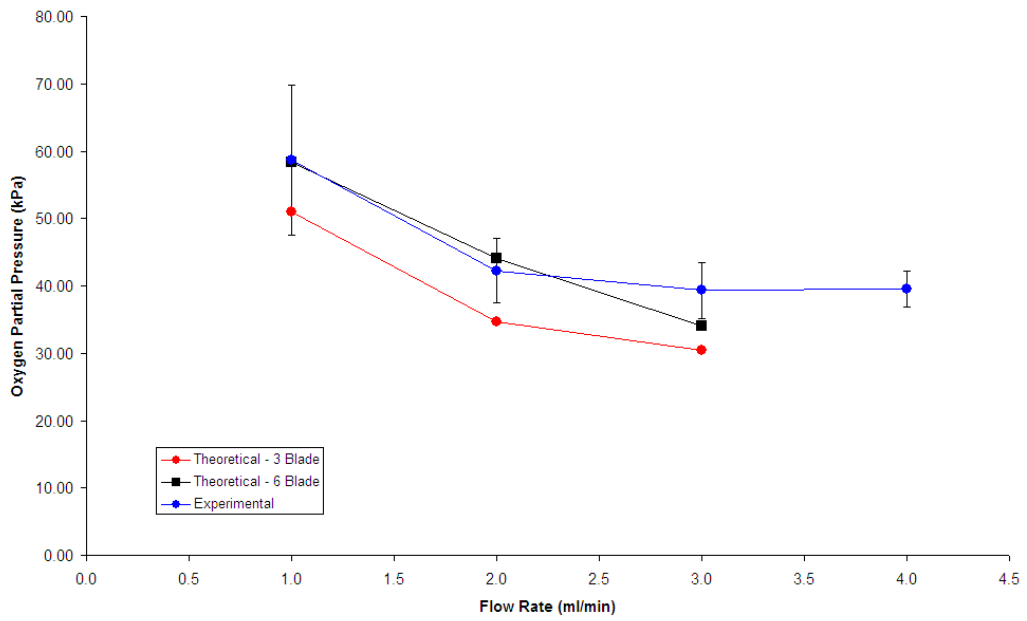


Figure 5.19 – Pair 3: Theoretical vs. experimental P_{O_2} with water flow rate (3- and 6-blade mixers)

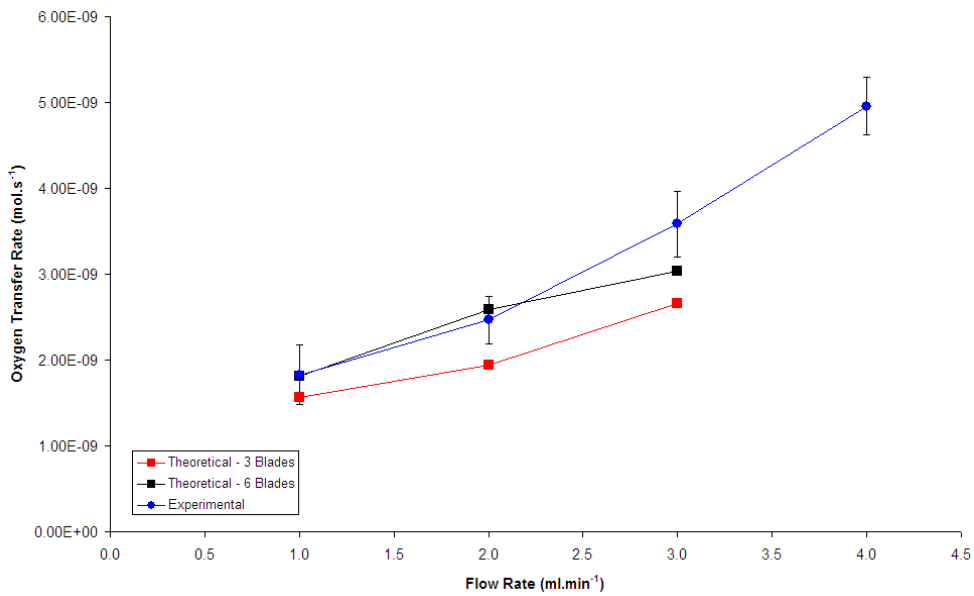


Figure 5.20 – Pair 3: Theoretical vs. experimental J_{O_2} with water flow rate (3- and 6-blade mixers)

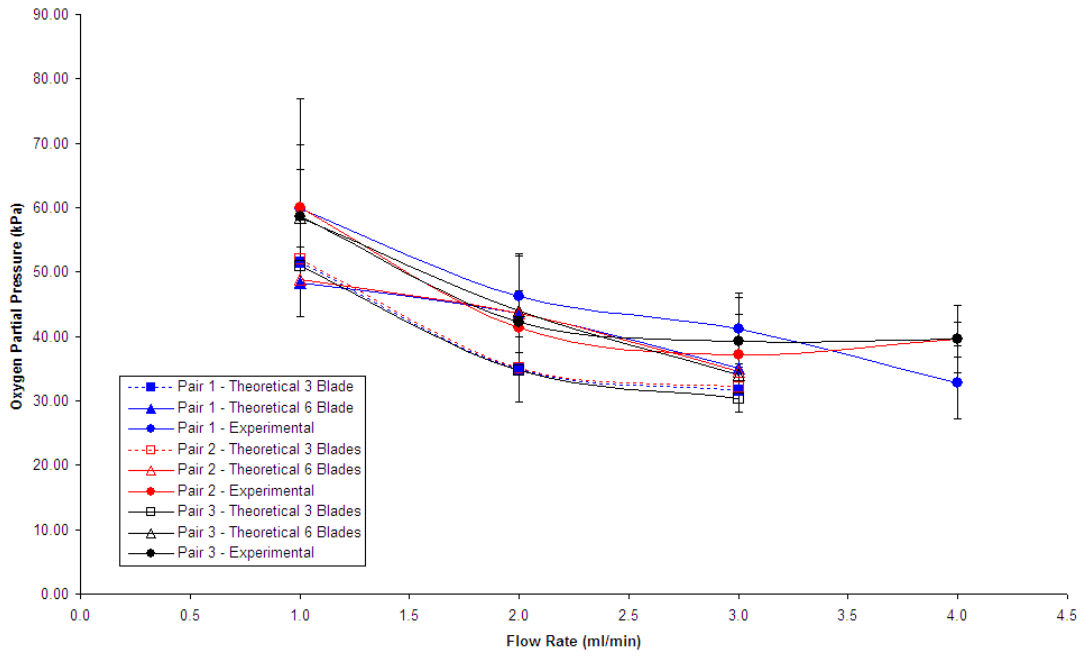


Figure 5.21 - Collection of theoretical and experimental findings for Pairs 1 to 3

5.4 Discussion

The purpose of creating a mathematical model is to confirm the laboratory findings and, ultimately, to shorten the length of time spent testing the device. With a model that can reliably reproduce experimental results, the amount of time spent testing in the laboratory can be reduced. In addition, the ease with which a mathematical model can be manipulated and altered allows for the testing and measuring of variables and geometries that may be difficult to achieve in practical terms. For example, when constructing the mixing devices, this study was limited to the size and shape of static mixers that were commercially available. In the simulations, the size of each mixing element could be altered; the dimensions of the mixer as a whole, or as individual blades, could be changed; even the distance over which each blade twisted was editable.

In this study, the main aims of the mathematical model were to verify the results found in Chapter 4. At the outset of the project, it was evident that computational power would be limited. To that end, a two-dimensional model was proposed. However, whilst creating a two-dimensional hollow fibre was not difficult, the geometry presented the problem of adequately designing the static mixer. Translating a solid three-dimensional, asymmetrical object into a two-dimensional one that allowed fluid to flow through it was considered to be too time-consuming.

Having dismissed the two-dimensional model, work began on the three-dimensional one. Creating the tubular membrane and the static mixer within COMSOL was uncomplicated as the chemical reaction engineering module⁹⁷ for the program comes with an inline laminar mixer design. However, this inline laminar mixer design must be scaled to the appropriate dimensions used in this study. To get the tube and mixer to the size necessary to simulate the Celgard 2500 fibres, all that was needed was to scale the preset model.

5.4.1 Non-mixing hollow fibre simulations

Initially, only the non-mixing tube was modelled. Basing one model on each of the experimental devices, the data in Figure 5.2 was gathered. The most important point to make about these results is that, even with the variations in initial conditions, the models generate reproducible solutions. This indicates that the models are reliable in their output.

Figure 5.3 shows the calculated oxygen transfer of the simulations. Due to the relationship between P_{O_2} and J_{O_2} , the variations in Figure 5.2 carry across into this figure. Importantly, the overall shape of each model is in keeping with what was observed experimentally; that is, as the flow rate was increased, the oxygen transfer rate rose. Of particular note is that Pair 1 does not follow the same shape as the other two fibres at a flow rate of 4 ml min^{-1} . At this flow rate, the oxygen transfer rate for Pair 1 takes the value $J_{O_2, \text{Pair 1}} = 2.12 \times 10^{-9} \text{ mol s}^{-1}$, whereas for the other two

units $J_{O_2,Pair2} = J_{O_2,Pair3} = 2.59 \times 10^{-9} \text{ mol.s}^{-1}$. This is a 22% decrease in oxygen transfer rate. As had been discussed in the previous chapter, Pair 1 was not constructed from the same batch of material as Pairs 2 and 3, giving rise to a possible explanation for any experimental differences.

Concentrating solely on Pair 1, Figure 5.4 shows a comparison between the data presented in Figure 5.2 and Figure 4.21. The theoretical model matches the experimental findings almost exactly. All of the flow rates simulated fall well within the error limits calculated for the physical fibre. Overall, Figure 5.4 shows a promising comparison, although the condition of the physical fibre must be kept in mind. As stated in Chapter 4.3, the fibres in Pair 1 were constructed from material that was of an indeterminate age and may have suffered degradation. This would give rise to the possibility of pore size increasing as the material degrades, which would allow the fluid within to reach an equilibrium state far sooner than younger material, but could also have adverse effects such as leakage and structural instabilities.

Figure 5.5 shows the corresponding oxygen transfer rate comparison. As expected based upon the partial pressures found in Figure 5.4, the theoretical and experimental data are very similar in nature.

In Figure 5.6 is the comparison for Pair 2. The visual agreement between theory and practice is not as close as that found for the previous oxygenator. The partial pressures predicted by the model are higher at lower flow rates than those observed.

The difference is greatest at 1 ml min^{-1} , where the model is 28% higher. At 3 ml min^{-1} , the two data sets converge and give good agreement. Recalling Figure 5.2, it can be noted that even within the simulations, the solutions for Pair 2 are higher initially than the other two devices, whereas from Figure 4.21 the practical Pair 2 fibre lies well within the error limits of the other units. One possible explanation for the discrepancy is that the model is solving for the steady-state values, which the fibre did not reach in the laboratory environment. Figure 5.7 shows the oxygen transfer rate comparison for Pair 2. From the previous figure, the higher transfer predicted by the model is expected. However, it can be seen that after the first point at 1 ml min^{-1} , the theoretical transfer is within the error bars of the practical experiment, indicating that the model is within the limits of the ideal practical conditions. Referring to Figure 5.3, it is evident that the oxygen transfer rate of Pair 2 follows that of Pair 3 very closely. Above this flow rate, the theoretical oxygen transfer matches the experimental values, suggesting that at the higher flow rates the oxygen transfer rate observed in the laboratory was at optimum levels.

Figure 5.8 depicts the partial pressure comparison for the third device. As with the results shown in Figure 5.6, for flow rates lower than 3 ml min^{-1} , the theoretical values are higher than the experimental ones. Above this flow rate, the simulation begins to match the observed values. However, unlike the previous model, the lowest flow rate has reasonable agreement with the practical limits. Despite this difference, the overall trend is the same, with partial pressure decreasing with increasing flow rate.

Figure 5.9 illustrates the oxygen transfer rate comparison for Pair 3. Given the information shown in Figure 5.8, the disparity in transfer values at lower flow rates is expected.

5.4.2 Mixing hollow fibre simulations

Having modelled the water flow through a non-mixing tubular membrane to a level of reasonable accuracy, attention was turned to creating a model that would allow reproduction of the mixing device results. In order to build this geometry, the standard COMSOL laminar static mixer was tailored to be of the necessary scale before being inserted in a representation of a oxygenating unit. The properties of the membrane in this model were identical to those used in the non-mixing case; the mixer was designed to be a solid object, through which no flow or oxygen transfer rate could occur.

The position of the first blade relative to the inlet was the same as that experimentally, approximately 160 *mm* from the inlet. As before, the experimental conditions dictated the initial conditions of the model in an attempt to better simulate what had already been observed. Due to the computational limits, the mixing units were constructed in blocks of three individual blades up to a maximum of twelve. As can be seen from Chapter 5.3.2, the results for the nine- and twelve-blade mixers are not included in the figures. They have been omitted because these simulations had large instabilities presenting themselves even at the lowest flow rate. There are

instabilities present in the three- and six-blade mixers, and these will be discussed in detail below.

Figure 5.11 shows that the partial pressure results from the three-blade mixing simulations are reproducible, even with the changing inlet conditions between models. The downward trend with increasing flow rate is also present, indicating that regardless of the numerical values generated and without the need for an in depth comparison, the simulations are similar to the experimental findings.

In Figure 5.12, the increasing oxygen transfer rate with increasing flow rate can be clearly seen. The purpose of this figure and Figure 5.11 is to show that the mathematical models give reproducible results, and to that end, they succeed. It can be noted that several of the values for the fibres coincide, indicating that the different initial conditions seem to matter little at the outlet.

Figure 5.13 shows the partial pressures predicted by the six-blade mixing models. Considering a flow rate of 1 ml min^{-1} , Pair 3 appears to be approximately 20% higher in partial pressure than either of the other fibres. However, as the flow rate increases, this deviation vanishes to bring Pair 3 back into line with the other models. Recalling Figure 4.21, it has already been noted that the decreasing partial pressure at higher flow rates is greatly reduced. Roughly comparing the experimental results and the six-blade models, it would appear that the simulations are having some difficulty resolving realistic values at the higher flow rates.

This difficulty is more evident in Figure 5.14. The behaviour noted in Figure 5.13 at higher flow rates is carried over when the oxygen transfer is calculated. Looking specifically at 4 ml min^{-1} , the simulations return an oxygen transfer far below that expected based upon the experimental transfer behaviours.

Having reviewed both the three- and six-blade mixer simulations, and noted the difficulty both models have at higher flow rates, these values were discounted in further analysis. In each figure, the line becomes broken above 3 ml min^{-1} to show the values, but because of their unreliability they will not be commented upon.

Another general comment about the comparison figures is that the simulated partial pressures are lower than the experimental results. The reason for this is self evident; the simulations are not modelling exactly the same situation as that found in the laboratory. In the physical mixing devices, there are twenty-four individual mixing blades present; the models have been limited to three and six blades. This reduction in element number results in a reduction in the amount of mixing the fluid undergoes as it travels through the tube, and therefore will reduce the effectiveness of the mixer. However, it is expected that the mixing models will still show an increase in partial pressures and oxygen transfer over the non-mixing fibres.

From Figure 5.15, it can be seen that despite having a smaller number of mixing elements, the mathematical models generate the same pattern as the physical data. The three-blade model follows the experimental shape closer than the six-blade simulation. As mentioned above, the outlet values for both models are lower than

that of the physical testing; this can be attributed to the lower number of elements. At 2 ml min^{-1} , there is only a 6% difference in the partial pressure measured and simulated.

Figure 5.16 shows the corresponding oxygen transfer rate values. As expected, the six-blade mixing fibre lies close to the physical data, with the three-blade mixer falling at lower transfer values, but both following the same trend.

Figure 5.17 displays some interesting characteristics. Firstly, all of the data points for both the three- and six-blade mixers fall within the experimental error lines, indicating that the simulated results are already in agreement with the practical ones. At 2 ml min^{-1} , the six-blade model even gives a higher partial pressure than that measured. This would indicate that at this flow rate, some of the mixing blades used in the laboratory were redundant. Alternatively, the experimental values may be reduced due to leakage past the mixing blades at the membrane boundary if the manufacturing process was less than ideal.

In Figure 5.18, the oxygen transfer comparison for Pair 2 can be seen. Unsurprisingly, the three-blade mixing model follows the rising trend observed experimentally. As with the partial pressure in the previous figure, despite only having one-eighth the number of blades the physical fibre contained, the three-blade model remains within the error limits, arguing that the full twenty-four may not be needed to achieve the same level of mixing. The results of the six-blade mixer add to this point, with each of the points above the first lying very close to the experimental

results. At 2 ml min^{-1} , the oxygen transfer simulated with the six-blade model is higher than that seen experimentally.

Figure 5.19 indicates the partial pressure comparisons of the theoretical and experimental results for the mixing fibre in Pair 3. Concentrating on the three-blade mixer first of all, there is better matching between theory and experiment than in the previous units. The gradient of the downward slope between 1 ml min^{-1} and 2 ml min^{-1} is exactly the same for both theory and practical data sets. This shows that even the three-blade mixer is capable of simulating the experimental data approximately. Or, at the very least, giving a rough estimate of what the practical value could be and also how this value changes with flow rate. Beyond 2 ml min^{-1} , the three-blade mixing model falls below the error limits, suggesting that more blades are required at the higher flow rates to maintain the same level of fluid mixing.

For the six-blade model in Figure 5.19, there is almost perfect agreement with the physical situation at certain flow rates. At 1 ml min^{-1} , for example, there is only a 1% difference in values between the theory and experimental partial pressures. As with Pair 2, as the flow rate increases to 2 ml min^{-1} , the theory overtakes the practical values, indicating that there are sufficient blades in the six-blade mixer to achieve the same results as the experimental twenty-four bladed mixer. As the flow rate is increased further, this agreement begins to diverge as the six-blade model approaches the flow rate at which it becomes numerically unstable.

Finally, in Figure 5.20 the oxygen transfer for Pair 3 can be seen. The three-blade mixer is able to follow the same shape as the experimental data for the entire data set, although the only time that any of the values are within error limits is at the slowest flow rate.

Considering all of the simulations, it can be said with some certainty that using COMSOL Multiphysics, the experimental results can be reproduced with some degree, with 50% of the simulated points falling within a standard normal deviate. When concentrating on the non-mixing tubes alone, for the first fibre, there is an almost perfect correlation between theory and experiment. This agreement is not carried across to the other fibres at low flow rates, but does appear once the fluid is moving at 3 ml min^{-1} or faster. Given that the simulations are thought to be solving for the optimum conditions, it would appear that the physical Pair 1 non-mixing fibre reaches this stage more readily than the other fibres. However, as has been mentioned earlier, Pair 1 was made from a different batch of material to the other two units, and may have suffered some degradation in the material. If this is the case, and the pore size, for example, has increased, then the physical fibre will accept in the influx of oxygen more readily than the more robust material. That said, despite possibly being more efficient at oxygen transfer, the older material may also be more liable to suffer fluid leakage during the oxygenation process, and as such would not make for a suitable material. This may go some way to explaining why there is such good correlation between the theory and practical values for Pair 1, but not for the other devices.

The values generated for Pair 1 in the mixing units are also evidence that this material may not be suitable for use in any oxygenation device. For the mixing devices simulated for Pairs 2 and 3, there is a definite indication that for certain flow rates, only six mixing blades may be needed to achieve the level of mixing observed experimentally. For the theoretical Pair 1, whilst the oxygen transfer rate and partial pressure values of both the three- and six-blade mixers approached that obtained experimentally, neither model was able to gain the same agreement that Pairs 2 and 3 were, especially with the six-blade mixers.

On a general note, there is a definite increase between from the three-blade model to the six-blade one, which lends further support to the idea that both models fail to match the experimental data exactly due to having too few elements. It is believed that if it were possible, perhaps in a future study, to increase the number of mixing elements within the simulations, the lines of theory and experiment would converge. In Pairs 2 and 3, this did occur for the six-blade mixer at the lower flow rates, but as was mentioned at the start of this discussion, as the flow rate increased, the models became more unstable. Perhaps if these simulations were repeated on a more powerful computer, then there would be agreement from the six-blade mixer for all of the tested flow rates.

Another point to be made is that it would not be challenging to alter the non-mixing model hollow fibre to simulate a different material. As long as the material properties are known, then the models can be adjusted to simulate it. Based upon the findings of this chapter, it is believed that a theoretical model has been developed

that can, to some degree of accuracy, model water flow through an oxygenating fibre, both with and without a helical static mixer. Of the 36 simulations conducted in this study, 50% returned values within standard normal deviate of the experimental results.

If another future study were to use a different material, then time could be saved on preliminary water testing by simply amending certain aspects of the model already developed.

Chapter 6 – Blood Experiments

This chapter details the experiments conducted using Celgard 2500 tubes with bovine blood. As with the distilled water experiments previously, the results described in this chapter provide the initial conditions for the subsequent mathematical modelling, discussed in Chapter 7. In Section 6.1, the experimental procedure is described. Section 6.2 contains the results gathered and these will be discussed in Section 6.3.

6.1 Materials and methodology

The tubes used in this experiment were all constructed from Celgard 2500. Twelve new oxygenating pairs, six with static mixers and six without, were created for the blood trials. The material was from the same batch that Pairs 2 and 3 were made from as detailed in Chapter 4. The static mixers in these experiments were coated with Sigmacote®⁹⁸ in order to prevent blood clots forming on the mixer blades. Bovine blood was obtained from a local abattoir. It was obtained from a local abattoir, anti-coagulated with 2 mg.ml^{-1} dipotassium EDTA and used within 48 hours of collection. Before use in the experiments, the blood was filtered with a Medtronic Paediatric Arterial filter⁹⁹, (pore size $30\mu\text{m}$).

The blood was heated to 37°C and the oxygen levels were raised to physiological venous levels. At this stage, a blood sample was taken to record the haematocrit,

using a Hawksley Micro Haematocrit Centrifuge¹⁰⁰. The experimental setup was the same as that used in the preliminary water trials. In addition to the setup detailed in Section 4.1.2, a Radiometer OSM-2 Haemoximeter was used to measure the oxygen saturation and haemoglobin concentration of the blood. The oxygenator was ventilated with 100% O_2 , at a flow rate of 30 ml min^{-1} .

As testing was performed on single tubes, blood flow rates remained at low levels. The blood flow rates was varied between 1 ml min^{-1} and 4 ml min^{-1} in 1 ml min^{-1} increments.

Measurements were taken both before and after the oxygenator in order to determine inlet and outlet P_{O_2} , O_2 saturation and haemoglobin concentration.

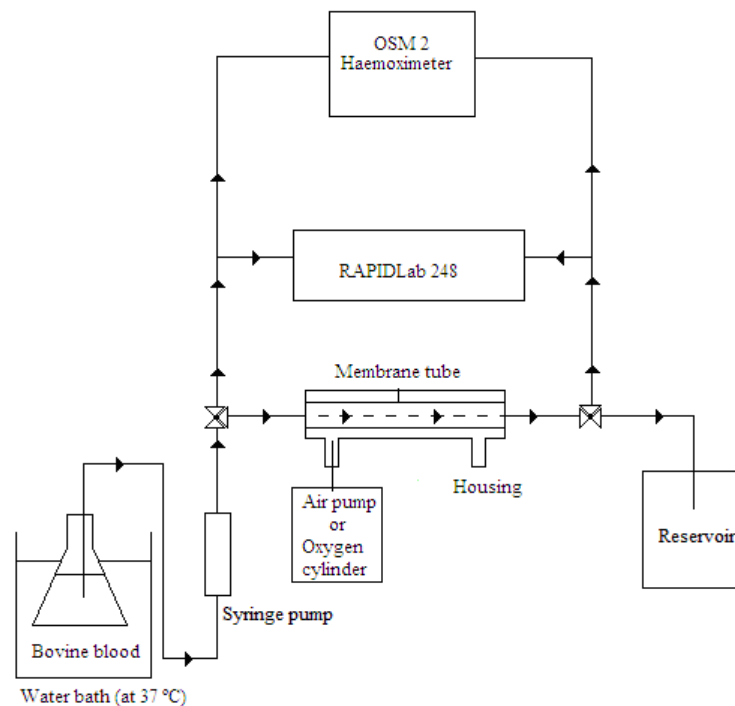


Figure 6.1 - Experimental Setup

6.2 Results

The twelve oxygenators, six with helical static mixers and six without, were separated into six device pairs. Each pair contained one of each oxygenator configuration. Both tubes in a pair were tested with the same batch of bovine blood.

The haematocrit of the blood used in the procedures was measured. All haematocrit values are given as the average \pm one standard deviation, with the sample set size as 6. The values measured are recorded in Table 6.1.

Table 6.1 - Haematocrit values measured before procedure

	Haematocrit (%)			
	1 ml/min	2 ml/min	3 ml/min	4 ml/min
Mixer	38.6 \pm 2.32	38.8 \pm 2.72	38.0 \pm 1.90	40.5 \pm 2.03
No Mixer	39.0 \pm 3.12	39.1 \pm 2.74	39.4 \pm 4.33	39.9 \pm 3.19

The inlet fractional saturation was measured at the start of each test. The blood was brought to as close to physiological levels as possible. All fractional saturation values are given as the average \pm one standard deviation, with the sample set size as 6. For a flow rate of 1 ml min^{-1} , the S was measured as $71.9\% \pm 5.6\%$ for the mixing tubular membranes and $72.4\% \pm 3.2\%$ for the non-mixing devices. At 2 ml min^{-1} , the mixing tubes had an S of $72.2\% \pm 5.2\%$ and the non-mixing devices $72.5\% \pm 3.6\%$. The 3 ml min^{-1} tests had initial S of $72.6\% \pm 3.8\%$ and $70.5\% \pm 6.1\%$ for mixing and non-mixing devices respectively. At 4 ml min^{-1} , the inlet S for the mixing tubes was

found to be $71.5\% \pm 3.1\%$ and for the non-mixing cases it was $72.0\% \pm 2.4\%$. Whilst the majority of these values are higher than normal physiological venous return levels ($S = 70.7\%$), it was felt that they were close enough to allow experimentation to continue.

Using Equation (3.30), including dissolved oxygen as well as bound, the oxygen transfer for each fibre was calculated. The values for the solubility of oxygen in blood, $\alpha_{O_2} = 9.98 \times 10^{-6} \text{ mol.m}^{-3}.\text{Pa}^{-1}$ and the maximum O_2 binding capacity, $\beta_{O_2} = 5.98 \times 10^{-2} \text{ mol.kg}^{-1}$.

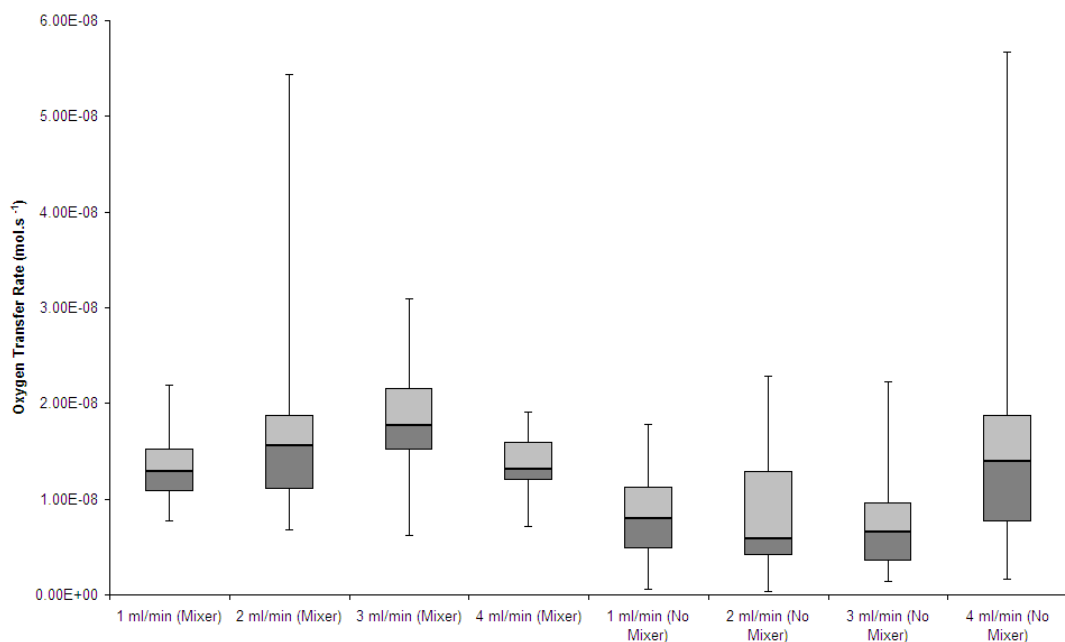


Figure 6.2 - Boxplot showing scattering in results recorded in bovine blood

Figure 6.2 shows the scattering of the values calculated for the oxygen transfer. For the individual flow rates, the comparison between mixing and non-mixing units is

shown in Figures 6.3 to 6.6. In all figures, the mixing results are indicated in blue and the non-mixing fibres as red. The average values for both mixing and non-mixing cases are also shown as a solid line in their respective colours; the broken lines represent a single standard deviation in the average.

In Figure 6.7, the average values of oxygen transfer for each fibre are shown against the flow rates tested. The individual data points shown in this figure are those that fall within one standard deviation of the average, to give some context of the results.

Figure 6.8 and Figure 6.9 show the absolute and relative values of the fractional saturation measured at the outlet for each oxygenator.

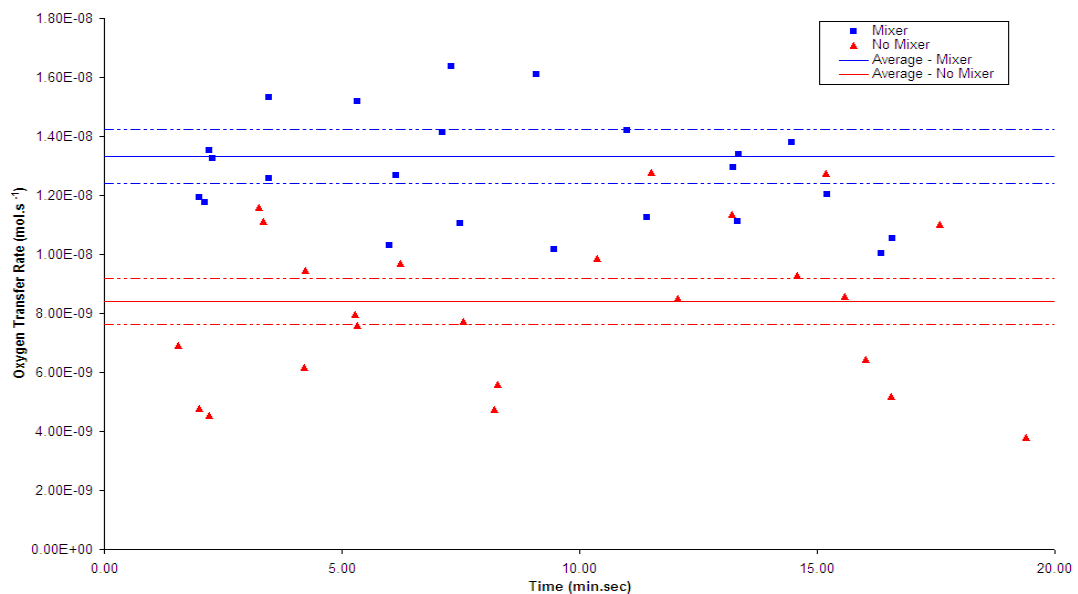


Figure 6.3 – O₂ transfer rate for Celgard 2500 oxygenators – bovine blood at 1 ml min⁻¹ and 100% O₂ ventilation

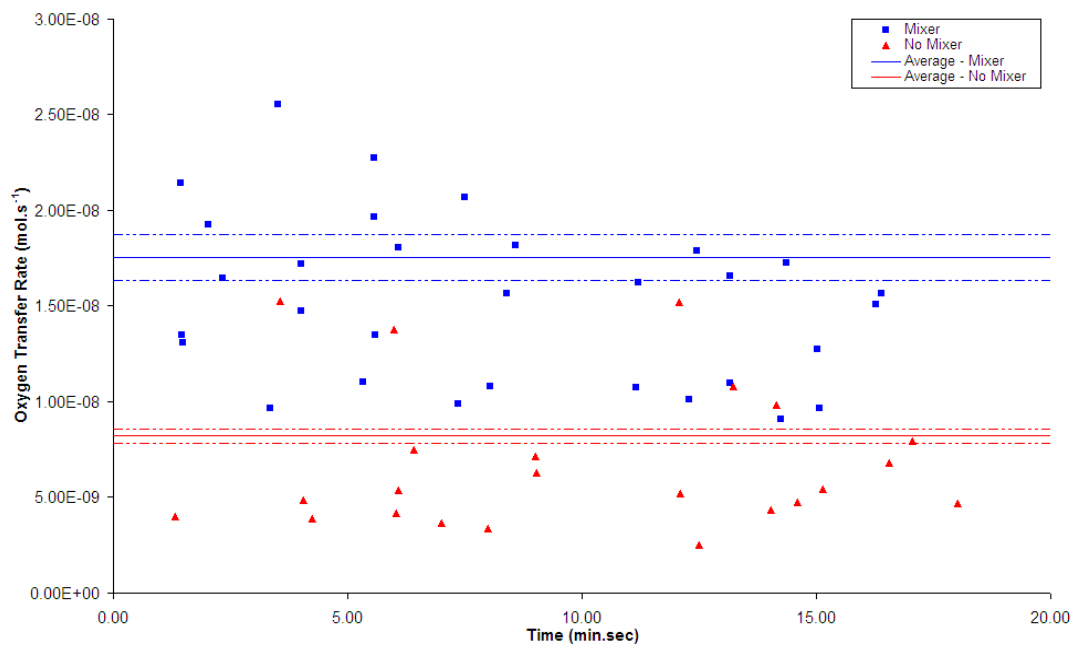


Figure 6.4 – O₂ transfer rate for Celgard 2500 oxygenators – bovine blood at 2 ml min⁻¹ and 100% O₂ ventilation

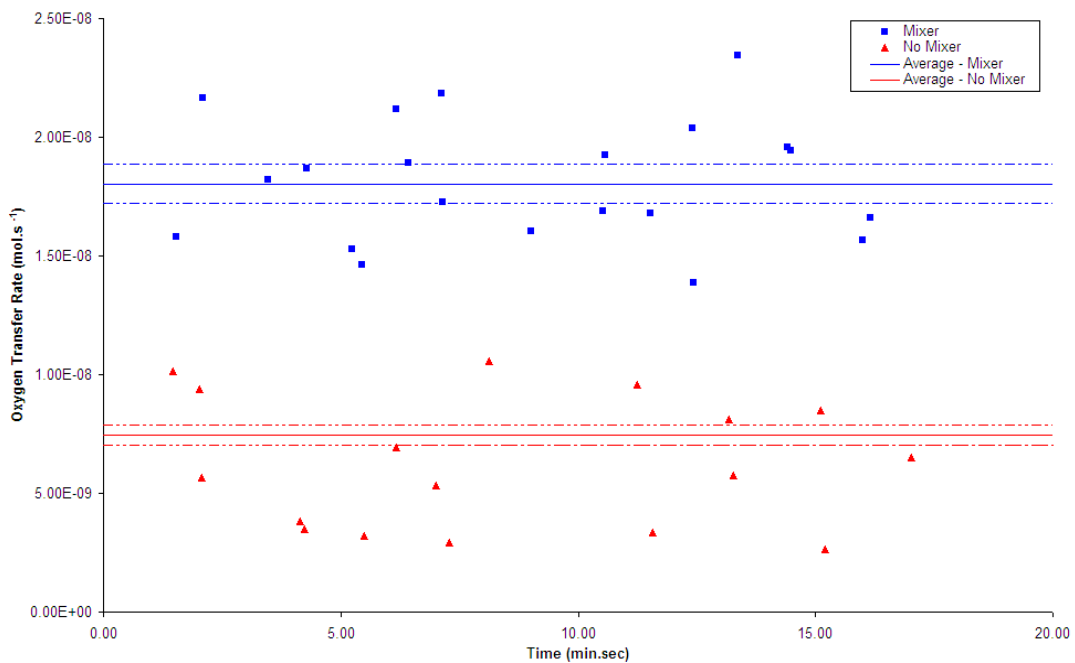


Figure 6.5 – O₂ transfer rate for Celgard 2500 oxygenators – bovine blood at 3 ml min⁻¹ and 100% O₂ ventilation

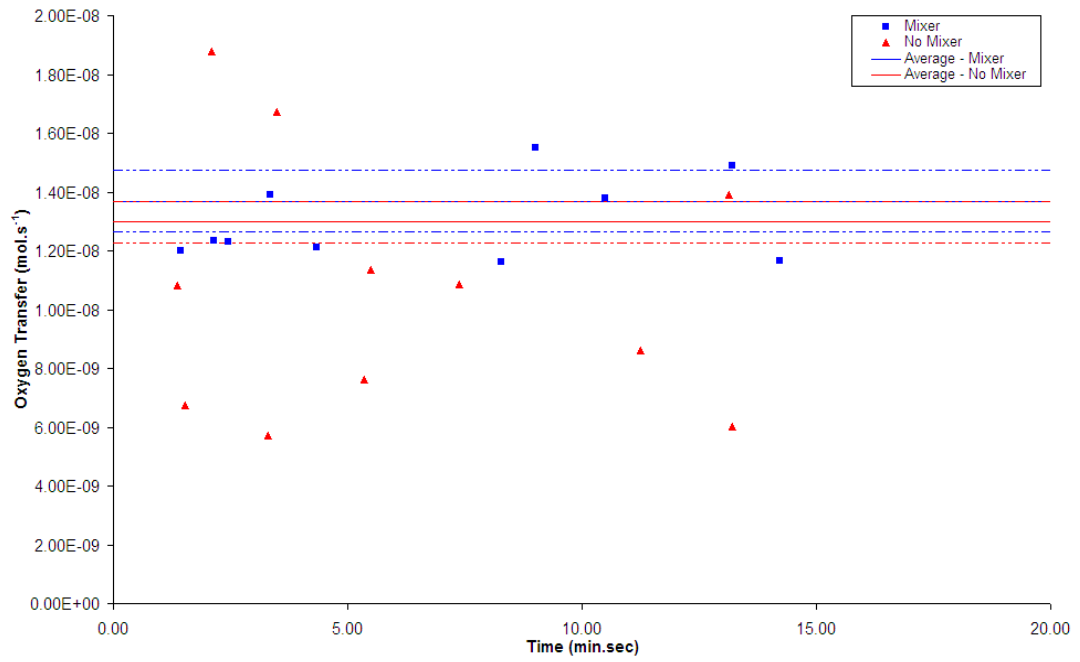


Figure 6.6 – O₂ transfer rate for Celgard 2500 oxygenators – bovine blood at 4 ml min⁻¹ and 100% O₂ ventilation

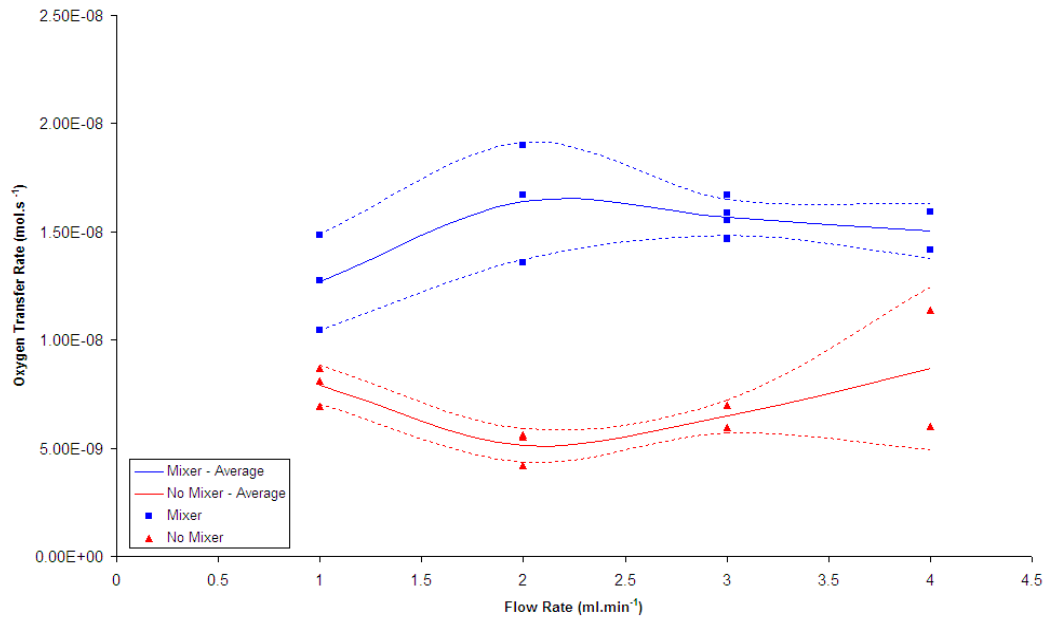


Figure 6.7 – Average O₂ transfer rates as a function of blood flow in Celgard 2500 oxygenators – bovine blood and 100% O₂ ventilation

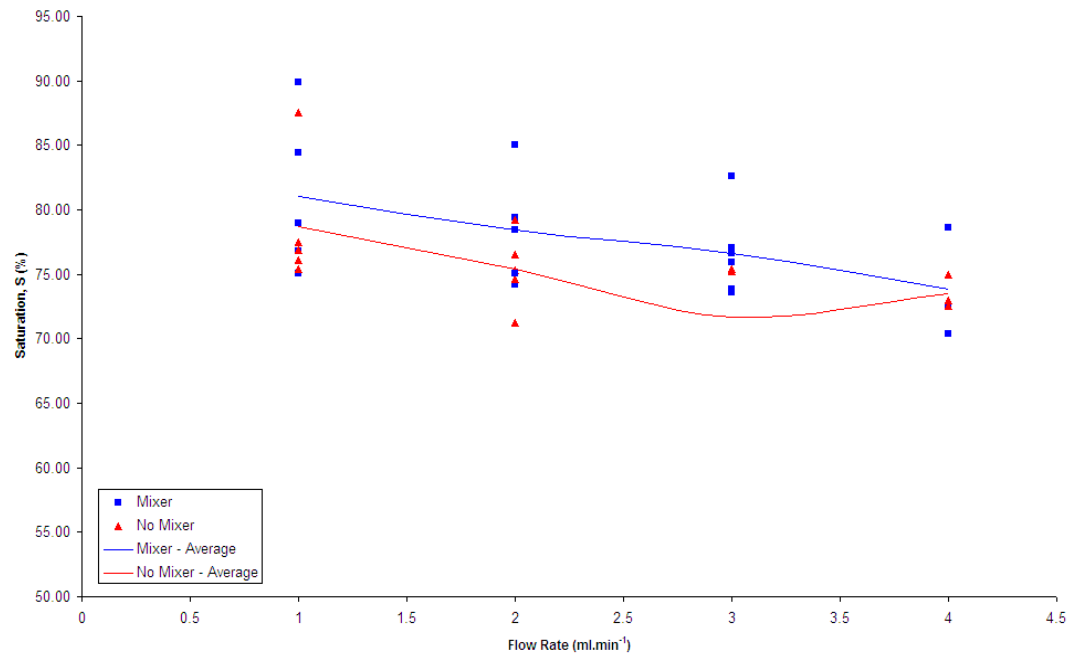


Figure 6.8 - Outlet O₂ saturation with varying blood flow rate in Celgard 2500 oxygenators – bovine blood and 100% O₂ ventilation

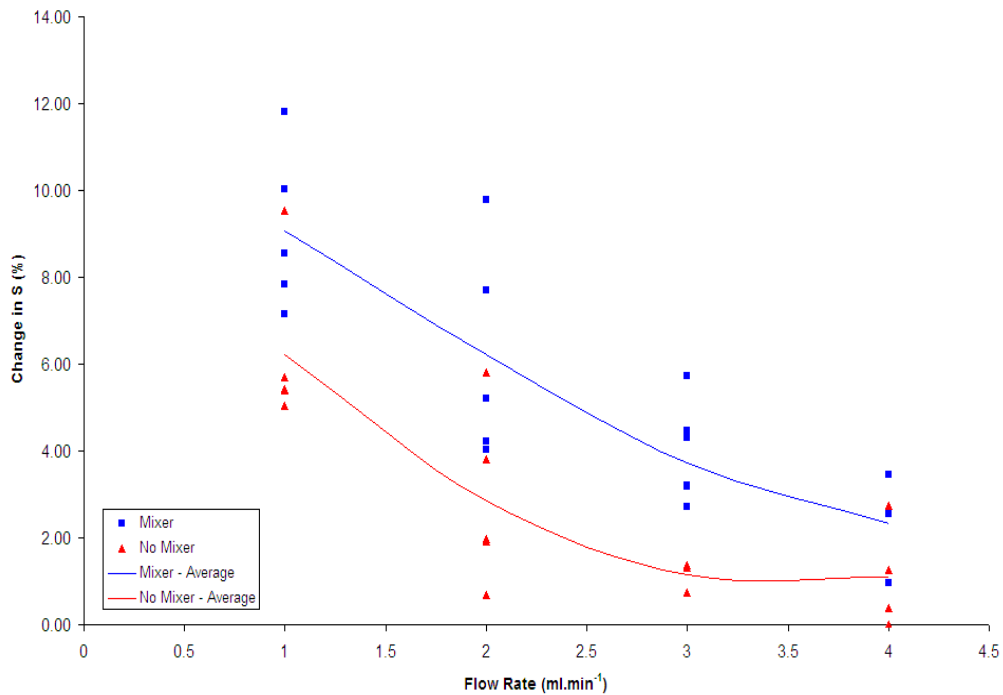


Figure 6.9 – Increase in S across devices with blood flow rate in Celgard 2500 oxygenators – bovine blood and 100% O₂ ventilation

6.3 Discussion

The aim of this study is to ascertain if the inclusion of a helical static mixer within a hollow fibre lumen is beneficial to the oxygen transfer of the system. Having already performed preliminary trials using distilled water and found the results to be promising, the logical progression was to conduct the experiments again using blood.

In the preliminary water trials, detailed in Chapter 4, it was found that the oxygenators containing a static mixer were at least two-thirds more efficient at gas transfer than the non-mixing configuration. Unlike water, blood contains

haemoglobin, which has a great affinity for binding oxygen molecules. It was initially expected that the differences caused by the inclusion of the helical static mixer seen in the water trials would carry across into the blood study, but that the oxygen transfer of both types of fibre would be increased due to oxygen binding to haemoglobin.

The mixing blades were coated with Sigmacote® to prevent clot formation around the mixers. After each tubular membrane had been tested, it was washed through with 0.9% saline before being used again. This wash was intended to remove any blood that remained within the tube, either on the walls or on the blades of the mixer.

Table 6.2 - Oxygen Transfer Rate for mixing and non-mixing units at varying blood flow rates (values shown as Mean \pm SD)

		1 ml/min	2 ml/min	3 ml/min	4 ml/min
Mixer	J_{O_2} (mol.s ⁻¹)	1.33x10 ⁻⁸ \pm	1.75x10 ⁻⁸ \pm	1.80x10 ⁻⁸ \pm	1.37x10 ⁻⁸ \pm
		3.41x10 ⁻⁹	9.94x10 ⁻⁹	5.32x10 ⁻⁹	3.20x10 ⁻⁹
No		8.41x10 ⁻⁹ \pm	8.20x10 ⁻⁹ \pm	7.45x10 ⁻⁹ \pm	1.67x10 ⁻⁸ \pm
Mixer	J_{O_2} (mol.s ⁻¹)	4.38x10 ⁻⁹	5.83x10 ⁻⁹	4.86x10 ⁻⁹	1.33x10 ⁻⁸

Comparing the findings in Table 6.2, the units with helical static mixers produce significantly higher oxygen transfer rates than those without except at a flow rate of

4 *ml/min*. For each of the other flow rates, $p \gg 0.05$, indicating that the inclusion of the mixer produces a significant benefit to the oxygenation process; however at a flow rate of 4 *ml/min*, the difference between the two configurations is not statistically significant, indicating that the mixer does not have any affect on the oxygenation.

The oxygen transfer rates found in bovine blood can be compared with those previously mentioned for the water trials to illustrate the effect haemoglobin has on oxygen transfer. Table 6.3 clearly shows that the oxygen transfer rate in blood is higher than in water, indicating that the presence of haemoglobin enhances the O₂ uptake.

Table 6.3 - Comparison of oxygen transfer rates between bovine blood and distilled water

Flow Rate (<i>ml</i> <i>min</i> ⁻¹)	Blood transfer rate (mol.s ⁻¹)		Water transfer rate (mol.s ⁻¹)	
	Mixing	Non-mixing	Mixing	Non-mixing
1	1.33x10 ⁻⁸ ±	8.41x10 ⁻⁹ ±	8.92x10 ⁻⁹ ±	5.29x10 ⁻⁹ ±
	3.41x10 ⁻⁹	4.38x10 ⁻⁹	1.08x10 ⁻¹⁰	4.78x10 ⁻¹⁰

2	$1.75 \times 10^{-8} \pm$	$8.20 \times 10^{-9} \pm$	$1.24 \times 10^{-8} \pm$	$7.55 \times 10^{-9} \pm$
	9.94×10^{-9}	5.83×10^{-9}	9.01×10^{-10}	8.01×10^{-10}
3	$1.80 \times 10^{-8} \pm$	$7.45 \times 10^{-9} \pm$	$1.71 \times 10^{-8} \pm$	$9.51 \times 10^{-9} \pm$
	5.32×10^{-9}	4.86×10^{-9}	3.57×10^{-10}	9.09×10^{-10}
4	$1.37 \times 10^{-8} \pm$	$1.67 \times 10^{-8} \pm$	$2.16 \times 10^{-8} \pm$	$1.14 \times 10^{-8} \pm$
	3.20×10^{-9}	1.33×10^{-8}	3.03×10^{-9}	6.06×10^{-10}

Figure 6.7 shows the average O₂ saturation plotted against the blood flow rates tested. It details the information stated in the explanation of the previous group of figures; that at all blood flow rates, the tubular membrane with static mixer included has higher oxygen transfer than the non-mixing counterparts. This is especially true at a blood flow rate of 2 ml min^{-1} , where there is the largest difference between the device types.

Figure 6.8 depicts the O₂ saturation measured at the outlet of each oxygenator. The solid line shows the average value for each fibre type. Evident from the average lines, the fibres with static mixers tend to have a higher outlet O₂ saturation, indicating that more of the blood contained within the sample has been oxygenated. As the blood flow rate increases, for both types of unit, the O₂ saturation decreases, although greatly. This may be due to the blood spending less time within the tube lumen as the blood flow rate increases, resulting in the haemoglobin being unable to bind oxygen at the same rate it does at lower flow rates.

Another point to note from Figure 6.8 is that for all oxygenators, the blood does not reach full oxygen saturation. This could be achieved by increasing the residence time either by reducing the blood flow rate to below 1 ml min^{-1} or by increasing the tube length.

Figure 6.9 illustrates the relative fractional saturation across the devices. When one considers the increase of O_2 saturation in each device type, the mixing units appear to have the greater rise. This would indicate that despite the absolute values being similar for both mixing and non-mixing cases, the mixing devices are better at increasing the O_2 saturation across the length of the device.

Plotting the residence time on top of the data shown in Figure 6.9, it can be shown that there is a strong correlation between the residence time and the O_2 saturations achieved by the non-mixing tubes.

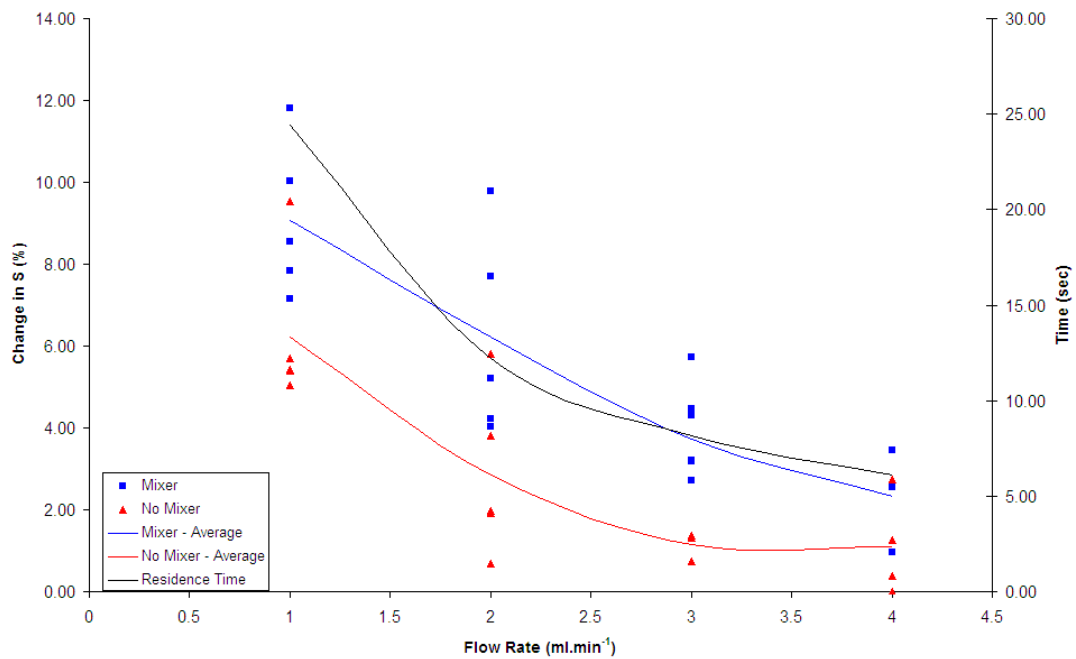


Figure 6.10 - Residence time shown on Figure 6.8

Both the residence time and the average O₂ saturation of the non-mixing oxygenators share a similar profile. This suggests that there is a relationship between the two. This would make sense, as the longer the blood remains within the oxygenating tube, the more likely the O₂ saturation is to increase as dissolved oxygen has more time to bind to the haemoglobin. The average O₂ saturation for the mixing tubes does not follow the residence time profile as closely due to the effect the mixer has on the O₂ saturation value. As seen in Figure 6.9, the mixing devices are able to attain higher relative O₂ saturation levels than the non-mixing case, suggesting that the relationship between the mixing units and the residence time may not be as obvious as that for the non-mixing configuration.

Unlike the water trials detailed previously, the bovine blood experiments do not appear to have a constant increase in oxygen transfer. In the water study, there was a clear correlation between the water flow rate and the oxygen transfer; in the figures shown in this chapter, that correlation is not evident. Considering the non-mixing device only, when the blood flow rate is increased, the oxygen transfer appears to drop before climbing again as the blood flow rate is raised further.

This can also be seen in the mixing devices, but in a different form. As the blood flow rate is increased above 2 ml min^{-1} , the oxygen transfer begins to drop, although not greatly.

Of the six tubular membrane pairs, 58% suffered some form of leak (three mixing tubes and four non-mixing ones). The majority of these leaks occurred on the final testing run – from the seven fibres that experienced leaking, four occurred after three tests. Five of the leaks occurred at a flow rate of 3 ml min^{-1} or higher. Any results gathered during the run when the leak occurred was discarded, although data from previous tests was kept. Based upon this information, it would be reasonable to assume that the construction method used in these trials is not suitable for prolonged periods of testing.

Considering all of the data discussed above, it is possible to state that the inclusion of a helical static mixer within the tube lumen greatly assists oxygen transfer. The increases in oxygen transfer noted previously in Chapter 4 were observed in the blood trials. It is evident that at all blood flow rates tested, the oxygenators with the

static mixer included were able to produce higher oxygen transfer rates than those without. The smallest difference observed was still a 81% increase when the mixer was used, indicating that this configuration is beneficial to the oxygenation process. At a flow rate of 3 ml min^{-1} , the oxygen transfer of the mixing tubes were noted to be 241% higher than the non-mixing ones. The static mixer is thought to be aiding the oxygenation process by transporting deoxygenated blood from the central region of the lumen to the walls where it becomes oxygenated. This does not occur in the non-mixing tube and as such, only the blood flowing at the membrane walls becomes oxygenated. Diffusion is the only mechanism that the blood in the non-mixing unit becomes oxygenated, relying solely on the diffusivity of oxygen within the blood; with the introduction of the static mixer, convective oxygenation is allowed to happen, making the mixing devices better at the transfer of oxygen than the non-mixing units.

As noted above, there are several factors that need to be addressed in any future work based upon this study. The first of these would be the construction method. Given that over half of the devices tested, of both types, were destroyed during the experiments, this may be indicative of a problem in the manufacturing of the fibres. It stands to reason that if work were to continue, then different manufacturing methods should be investigated. Another factor limiting the study is the residence time of the blood within the tube, not allowing the blood to become fully saturated at any point. This can be rectified by either increasing the fibre length or reducing the blood flow rate. Alternatively, the oxygenators could be constructed with an array of parallel connected membrane tubes.

Overall, the mixing oxygenators have been shown to be better at oxygen transfer than the non-mixing devices. As before with the water trials, the data gathered in this study will form the basis for a mathematical model described in Chapter 7.

Chapter 7 – Blood Simulations

This chapter discusses the mathematical modelling based upon the experimental results found in Chapter 6. The model used in this chapter is a modified version of that detailed in Chapter 5, reworked to simulate blood instead of distilled water. In Section 7.1, the boundary and initial conditions are described, along with a note of the major constant terms. Section 7.2 describes the methodology of the models. Section 7.3 contains the results and Section 7.4 is a discussion of this model.

7.1 Boundary and initial conditions

7.1.1 Boundary conditions

The boundary conditions for the blood simulations are exactly the same as those for the water model.

7.1.2 Inlet conditions

The inlet oxygen partial pressure for the models will be the average inlet partial pressures measured experimentally. For flow rates that were not examined experimentally, the inlet value for the flow rate immediately preceding it will be used.

Table 7.1 - Convection-diffusion constants

Blood			
Diffusion of oxygen in blood ⁶⁸	D_{O_2}	1.191×10^{-9}	$m^2 s^{-1}$
Solubility of oxygen in blood ⁸¹	α_{O_2}	9.98×10^{-6}	$mol (STP) m^{-3} Pa^{-1}$

The parameters used in the blood simulations are the same as those listed in

Table 5.1, and are therefore not repeated.

The fluid velocity shall range from $1 ml min^{-1}$ to $4 ml min^{-1}$ in $1 ml min^{-1}$ increments.

7.2 Materials and methodology

Using COMSOL Multiphysics, the equations described in Chapter 3, as well as the conditions detailed in Section 7.1, were evaluated.

The mathematical models were created to simulate the experiments conducted in the laboratory. To this end, the input conditions of the models were chosen to closely mimic the inlet conditions recorded experimentally.

The non-mixing, three- and six blade models were modified from Chapter 5 to include a reaction equation to simulate the removal of oxygen from the system as it binds to haemoglobin. Recalling Equation (3.21):

$$D \left(\frac{\partial^2 P_{O_2}}{\partial x^2} + \frac{\partial^2 P_{O_2}}{\partial y^2} \right) = u_z \frac{\partial P_{O_2}}{\partial z} \left(1 + \frac{\beta_{O_2} C_{Hb}}{\alpha_{O_2}} \frac{\partial S}{\partial P_{O_2}} \right), \quad (3.21)$$

the binding reaction is defined as:

$$\left(1 + \frac{\beta_{O_2} C_{Hb}}{\alpha_{O_2}} \frac{\partial S}{\partial P_{O_2}}\right). \quad (7.1)$$

For simplification, $\frac{\beta_{O_2} C_{Hb}}{\alpha_{O_2}} \frac{\partial S}{\partial P_{O_2}}$ can be redefined as φ , thus making Equation (3.21),

$$D \left(\frac{\partial^2 P_{O_2}}{\partial x^2} + \frac{\partial^2 P_{O_2}}{\partial y^2} \right) = u_z \frac{\partial P_{O_2}}{\partial z} (1 + \varphi). \quad (7.2)$$

The experimental initial conditions were used as the initial conditions for the simulations. As the non-mixing, three- and six-blade models had already been developed, each pair was solved for in sequential order, i.e. non-mixing Pair 4 followed by mixing Pair 4; non-mixing Pair 5 followed by mixing Pair 5 etc.

As a result of computational limitations, the three-dimensional models were unable to resolve the oxygen uptake by the blood. In an attempt to remove some of the computational strain, a two-dimensional, axial symmetric model was investigated again. Previously, in the water simulations detailed in Chapter 5, the two-dimensional model had only been able to give an approximate indication of the experimental values for the non-mixing tube and unable to reproduce the mixing devices. However, an approximate model would be adequate for this study, and a solution to the mixing problem was conceived.

Based upon the three-dimensional mixing simulations, the average radial velocity for each flow rate around the six-blade mixer can be calculated. Using this velocity in the two-dimensional models, the effect of the mixer could be simulated without having to alter the fibre geometry from that of the tube.

Despite the modifications to the model, the simulations remained unable to resolve the oxygen transfer into blood. Further investigation revealed the mathematical model was struggling to calculate ϕ close to the fibre wall at the experimental value for the haemoglobin concentration.

Further amendments to the model were made. In order to find exactly where the simulation was experiencing difficulty, the value of ϕ was decreased. This was done by reducing the haemoglobin concentration in the system to very low levels ($C_{Hb} \approx 1.40 \times 10^{-4} \text{ kg m}^{-3} - 1.40 \times 10^{-1} \text{ kg m}^{-3}$). This change allowed the model to be solved, as effectively the fluid in the simulation became plasma with a small number of red blood cells.

7.3 Results

The three-dimensional models for both the mixing and non-mixing cases were unable to provide solutions. The cause of this was determined to be the inclusion of haemoglobin in the models; even lowering the levels of haemoglobin present did not relieve this problem.

A two-dimensional, axially symmetric model was therefore created. This simulated both the non-mixing and the mixing configurations. Given the relative accuracy of the water simulations, both mixing (specifically the six-blade mixer) and non-mixing, the values obtained for the radial velocities in those models were taken from the three-dimensional mixing models for the various flow rates and used in the two-dimensional model to attempt to simulate the effects of a mixer in the tube.

As part of the investigation into the model's instability, the value of φ was adjusted by varying the haemoglobin concentration.

Modelling a non-mixing device, the O₂ saturation for each haemoglobin concentration was measured at various points up the device length. Figure 7.1 shows the O₂ saturation measured solely across the device outlet and Figure 7.2 shows the O₂ saturation measured solely across the device outlet and Figure 7.2 shows the O₂ saturation at three equidistant points on the device length, taken across the tube's radius (3cm, 6cm, and the outlet at 9cm).

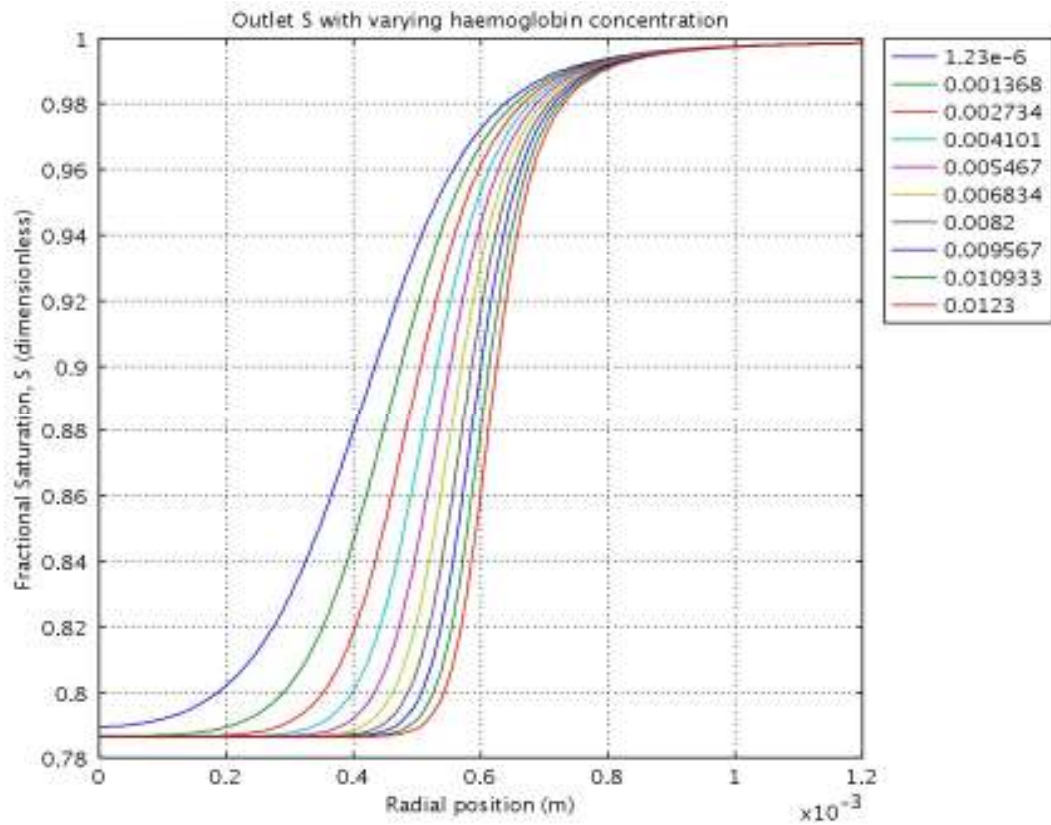


Figure 7.1 – O₂ Saturation, S, measured at the outlet of a non-mixing oxygenator. The legend shows the varying levels of haemoglobin concentration ($kg\ m^{-3}$).

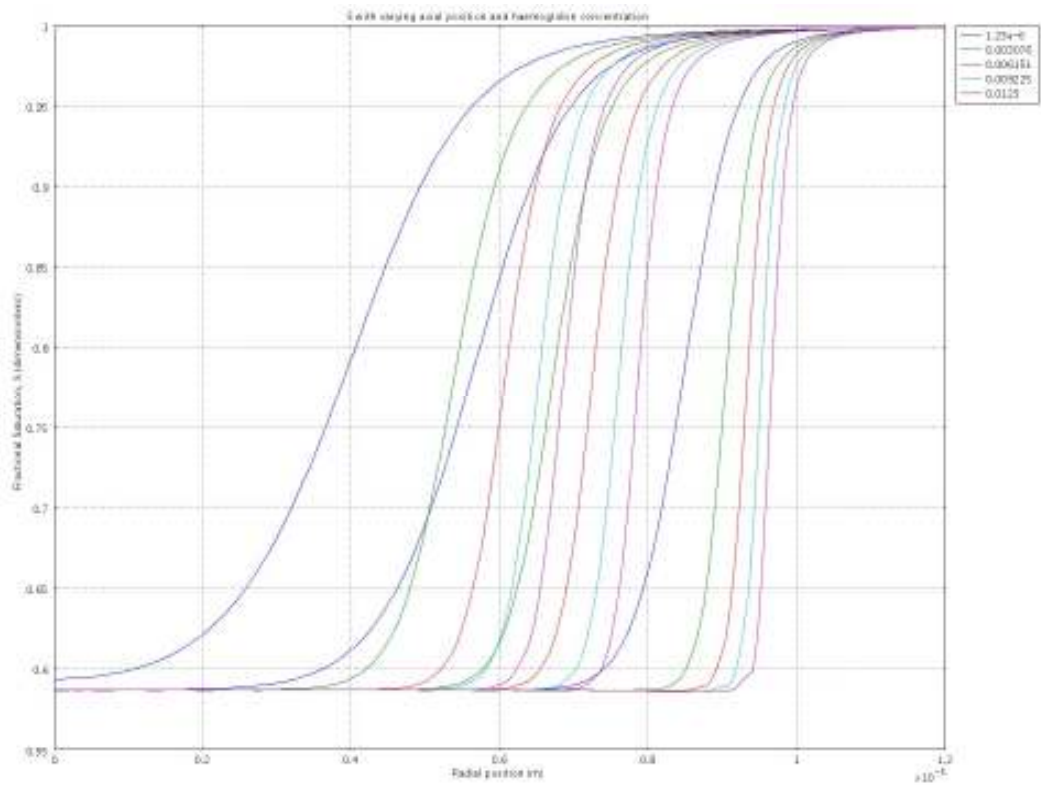


Figure 7.2 – O₂ Saturation, S, measured at different axial positions along a non-mixing oxygenator. The legend shows the varying levels of haemoglobin concentration ($kg\ m^{-3}$).

In Figure 7.3, the radial P_{O_2} profile at the outlet of a non-mixing oxygenator is shown. Figure 7.4 details this varying with device length. The axial positions are the same as those for Figure 7.2.

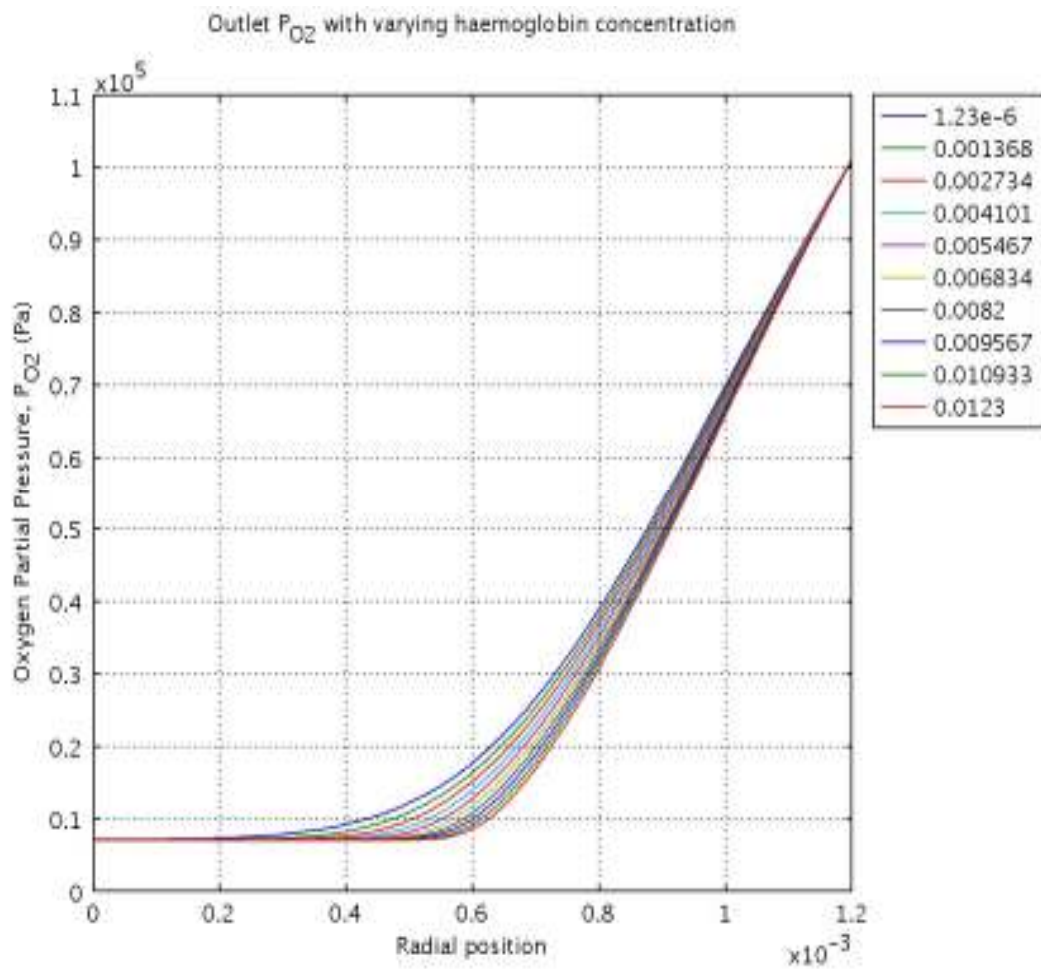


Figure 7.3 – Radial profile of P_{O_2} at the non-mixing device outlet. The legend shows the varying levels of haemoglobin concentration ($kg\ m^{-3}$).

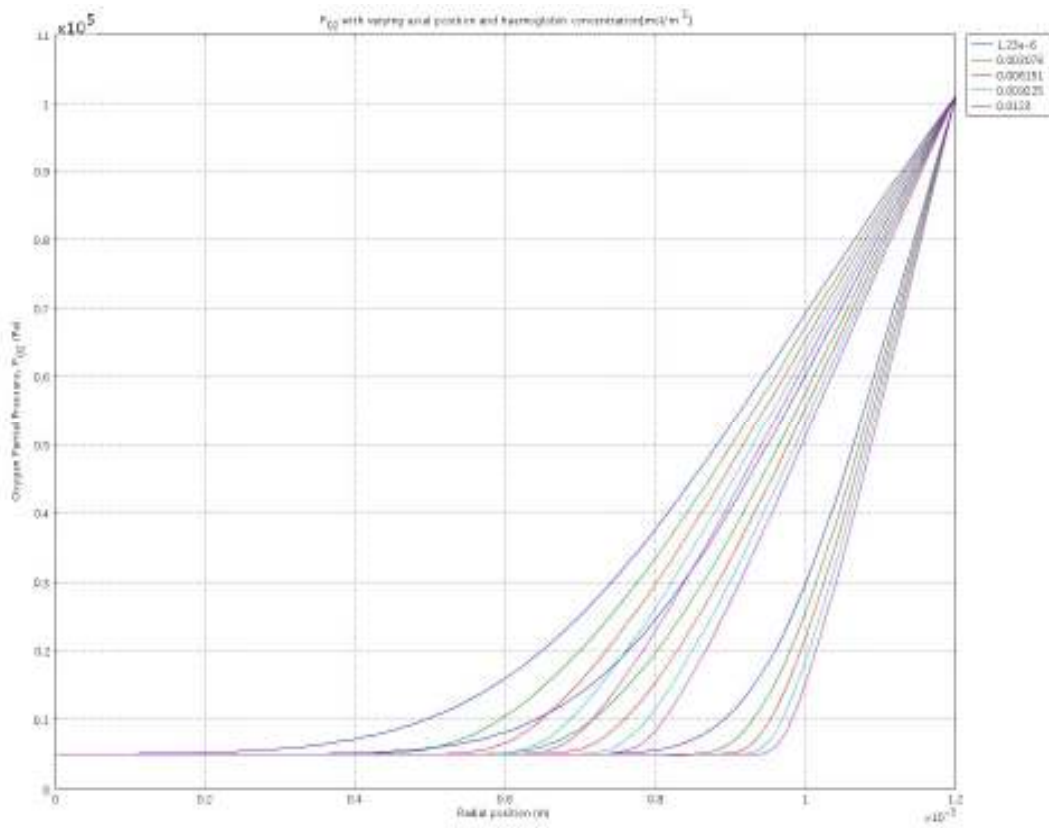


Figure 7.4 – Radial profile of P_{O_2} measured at different axial positions along non-mixing device. The legend shows the varying levels of haemoglobin concentration ($kg\ m^{-3}$).

Figure 7.5 depicts the effect of varying haemoglobin has on ϕ at the outlet of the non-mixing unit and Figure 7.6 shows this effect along the device length.

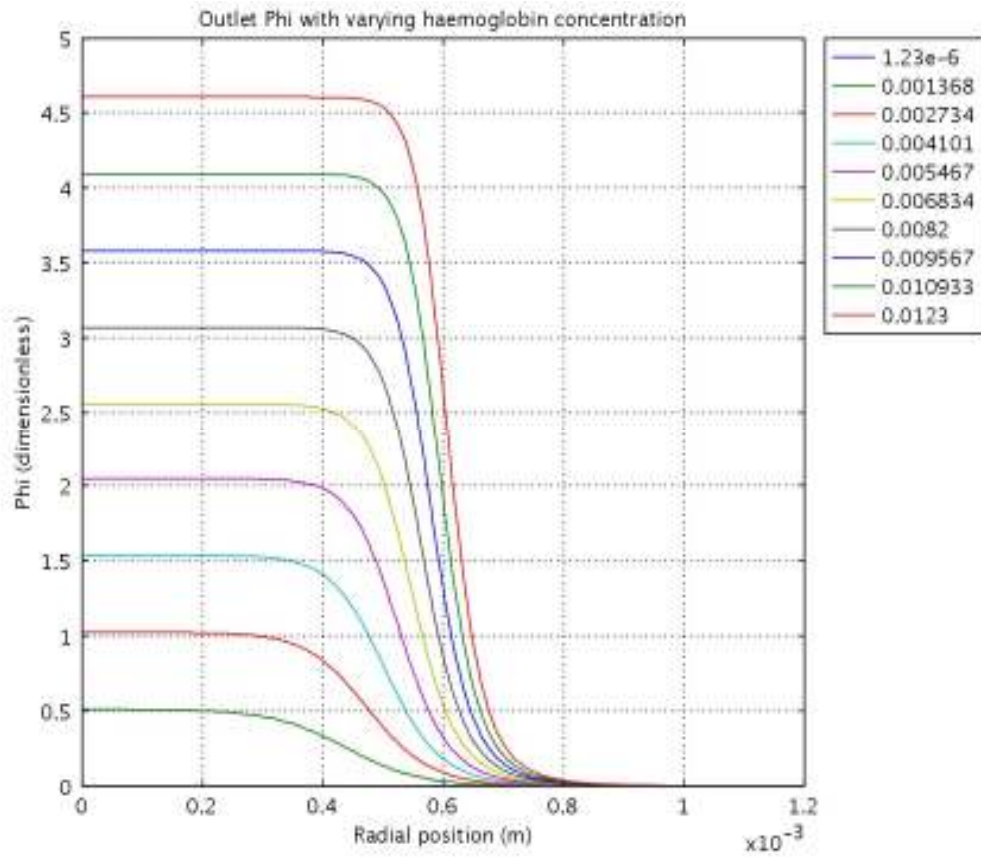


Figure 7.5 - φ predicted at non-mixing device outlet. The legend shows the varying levels of haemoglobin concentration ($kg\ m^{-3}$).

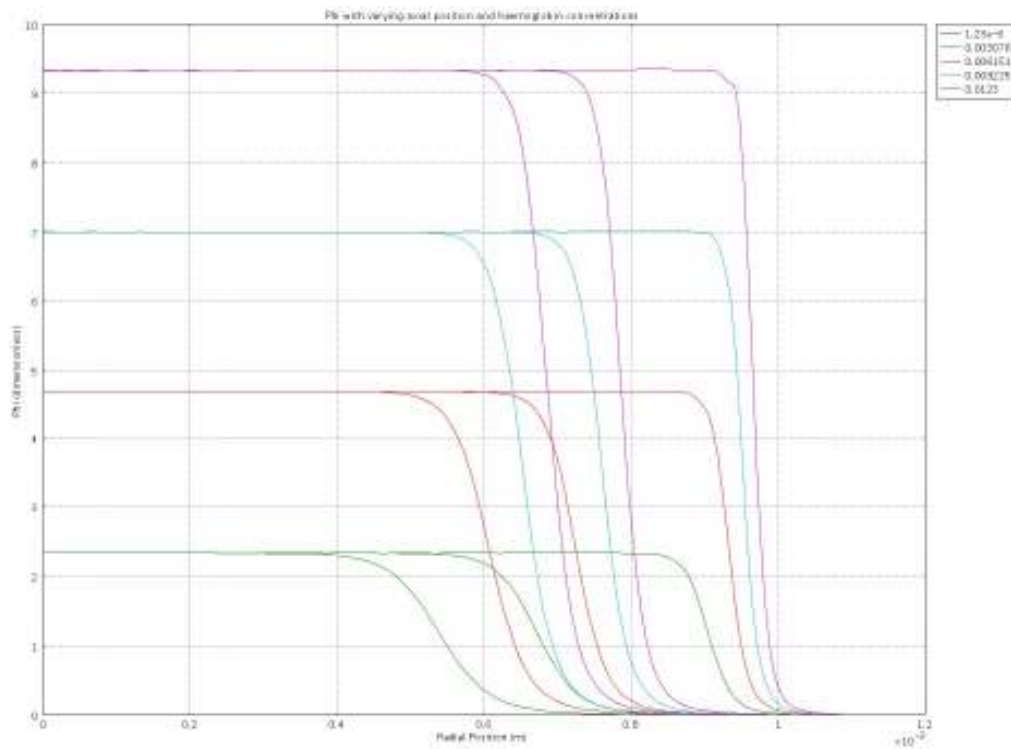


Figure 7.6 - ϕ predicted at different axial positions along the non-mixing device.

The legend shows the varying levels of haemoglobin concentration ($kg\ m^{-3}$).

Using the different values of haemoglobin concentration in Equation (3.19), along with the O_2 saturations calculated for those values, the concentration of bound oxygen was calculated. The C_b calculated for two pairs, non-mixing and mixing, is shown in Figure 7.7 and Figure 7.8.

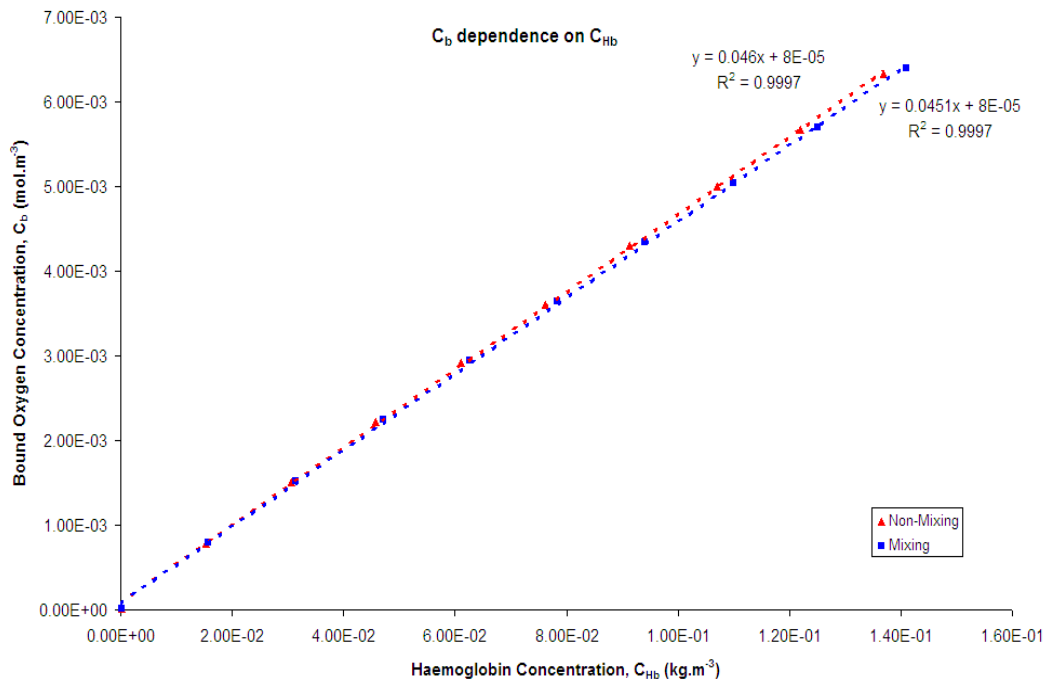


Figure 7.7 – C_b dependence on C_{Hb} : Example One

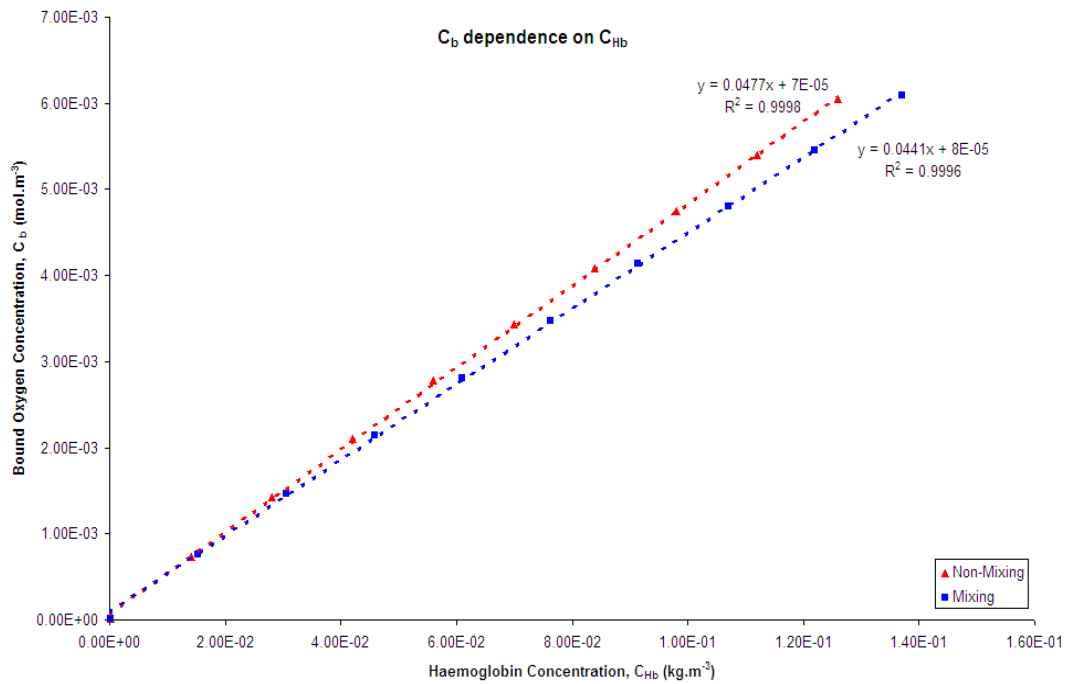


Figure 7.8 – C_b dependence on C_{Hb} : Example Two

7.4 Discussion

Initially, the reasoning behind the creation of the mathematical model is the same as described in Chapter 5; to reduce the amount of time spent in the laboratory. In this portion of the study, it was hoped that the mathematical model would be able to simulate the results presented in Chapter 6 with a similar degree of accuracy as the water simulations in Chapter 5. As stated previously, it was apparent early in the study that computational power would be limited and may become a factor in the creation of a suitably accurate model.

The models used in Chapter 5 were amended to better reflect the removal of oxygen from the system by binding to haemoglobin. However, none of the simulations ran to completion; all failed to return results. This was believed to be as a result of insufficient computational power.

In order to investigate the problem further, a two-dimensional model was devised. The limitation with working in only two-dimensions was the difficulty in creating an effective static mixer. However, when the two-dimensional model was originally conceived, there had been no work conducted on the three-dimensional simulations. Based upon the work carried out previously discussed, the average radial velocity from the three-dimensional six-blade mixing model was taken and used in the two-dimensional model to simulate the effect, although not the physical geometry, of the static mixer.

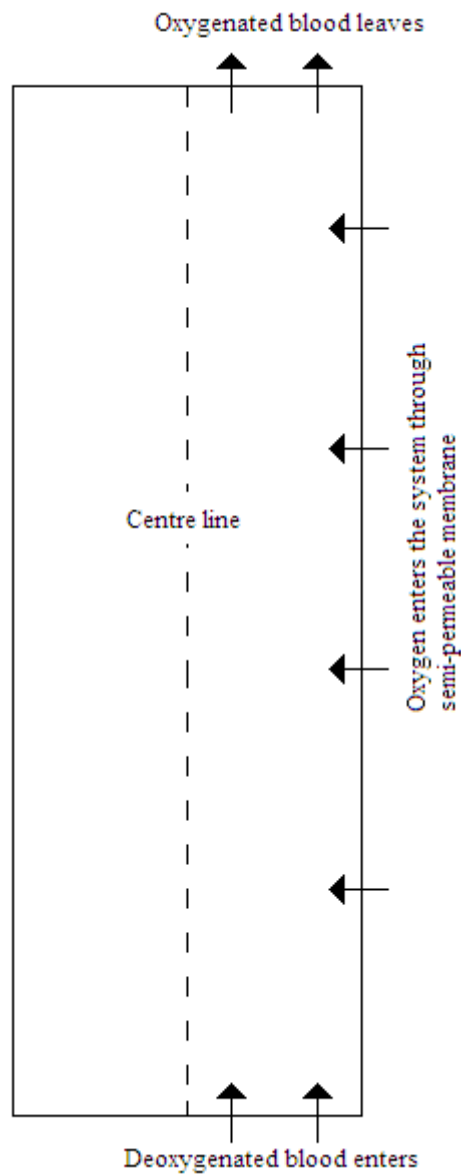


Figure 7.9 – The mixing and non-mixing two-dimensional models shared a geometry shape. To simulate the effect of the mixer within the fibre, the mixing model had radial velocity, whereas the non-mixing model did not.

All of the figures presented in Section 7.3 were taken from the two-dimensional models. Figure 7.1 shows the O_2 saturation of a two-dimensional non-mixing tube at

the outlet for varying values of the haemoglobin concentration. The blue line, furthest to the left of the graph, represents the fractional saturation form when $C_{Hb} = 1.23 \times 10^{-6} \text{ kg.m}^{-3}$. When the haemoglobin concentration is increased, the line shifts towards the right. The reason behind this shift is that oxygen molecules are getting bound to haemoglobin more readily when there is more haemoglobin present; this means that oxygen molecules are more likely to encounter a haemoglobin molecule before diffusing into the fibre lumen. As such, one would expect the region of diffuse oxygen to become increasingly smaller as the haemoglobin concentration rises.

An indication of the source of the instabilities in the models can be seen in Figure 7.2. Examining the line furthest the right, taken at 3 cm along the device length, the highest haemoglobin concentration for the first sample point, noise can be detected at the bottom of the curve, where it turns to an almost vertical line. This noise is indicative of the trouble the software has computing the ϕ factor. COMSOL is unable to resolve $\frac{\partial S}{\partial P}$ as the gradient becomes larger, which it evidently does as the haemoglobin concentration is increased. As some values of C_{Hb} did solve, the continued failure of the simulations is believed to be solely a computational one.

Figure 7.3 shows the oxygen partial pressure measured at the outlet for the various haemoglobin concentrations. As with the O_2 saturation in Figure 7.1, the line representing the lowest haemoglobin concentration is the one furthest to the left. As the haemoglobin concentration increases, the line shifts towards the right. As before,

this represents the dissolved oxygen molecules not infiltrating far into the tube lumen before they bind to a haemoglobin molecule.

Figure 7.4 depicts the oxygen partial pressure at the sample points along the device length. Like the groups of data shown in Figure 7.2, the group furthest to the right shows the oxygen partial pressured simulated at the sample point closest to the inlet. As the sample point moves further along the device length, the oxygen diffuses further into the lumen.

Figure 7.5 describes the dependence φ has upon the haemoglobin concentration. As the haemoglobin concentration rises, φ increases. Experimentally when $C_{Hb} \approx 140 \text{ kg.m}^{-3}$, then $\varphi \approx 70$. Figure 7.5 shows that there is a central region in the fibre lumen where φ is high. When this figure is compared with Figure 7.1, the turn in the fractional saturation curve closest to the fibre wall (radial position of approximately $0.8 \times 10^{-3} \text{ m}$) corresponds to the first turn in φ . Again, the next turn in S , at approximately $0.5 \times 10^{-3} \text{ m}$, matches with another turn in φ . As $\frac{\partial S}{\partial P}$ changes, φ increases accordingly; therefore if the haemoglobin concentration increases, the gradient of the curves in Figure 7.1 steeper, the more computational power will be required to resolve the model.

Figure 7.6 shows φ at the same axial sample points. On closer examination of the red curve representing the highest haemoglobin concentration, the line furthest to the right (closest to the inlet) does not have a completely smooth second turn unlike what

was seen only at the inlet. It is believed that as the haemoglobin concentration is increased, this instability also increases; at experimental values, the model is unable to adequately resolve this problem.

The data presented in Figure 7.7 and Figure 7.8 is based upon the two-dimensional simulations of two fibre pairs. The figures show how the bound oxygen concentration varies with increasing haemoglobin concentrations. As can be seen, the variance is linear; using the equations in the figures, substituting in the experimental values for the haemoglobin concentrations (Figure 7.7: non-mixing = 137 kg.m^{-3} ; mixing = 141 kg.m^{-3} . Figure 7.8: non-mixing = 126 kg.m^{-3} ; mixing = 137 kg.m^{-3}), then the bound oxygen concentrations calculated fall within $\pm 1.3\%$ of the experimental values. As the experimental values can be predicted via extrapolation of the data gathered from the two-dimensional models, it could be argued that although the simulations do not model the experimental results, they can be used to predict the approximate values as long as certain information is already known, chiefly the haemoglobin concentration.

Many of the problems arising when trying to simulate oxygen transfer to blood can be attributed to insufficient computing power. As the models can be resolved at low levels of haemoglobin, and therefore low values of $\frac{\partial S}{\partial P}$, but develop instabilities as these values increase, it is believed there is nothing wrong with the models themselves, just with the computational power of the resources available. With a

more powerful computer, it is thought that the three-dimensional models will be resolved.

It is regrettable that after simulating the water experiments, COMSOL Multiphysics was unable to solve the blood simulations. An alternate solution to this problem, rather than using a more powerful computer system, would be to investigate the use of a different software package.

Chapter 8 – A Comparison of Findings

This chapter brings together all of the evidence presented in the previous chapters and compares the findings. Section 8.1 looks at the distilled water experiments and simulations and compares the findings. In Section 8.2, the blood experimentation and simulations are discussed. Section 8.3 will consider the effect the helical static mixer has on oxygen transfer. Section 8.4 discusses the limitations of the study.

8.1 Comparison of water experiments

The purpose of this current investigation is to ascertain if the inclusion of a helical static mixer in a hollow fibre would have a beneficial effect on the oxygenation of blood. In the preliminary results reported, distilled water was used instead of deoxygenated blood. This chapter will consider only the Celgard 2500 fibres ventilated with 100% oxygen.

8.1.1 Practical

The experimental findings for distilled water are presented in Table 8.1 and Table 8.2.

Table 8.1 - Water Experimental Results (O_2 Partial Pressure) with values = mean \pm SD

<u>Flow Rate ($ml\ min^{-1}$)</u>	Outlet P_{O_2} (kPa)		
	<u>Non-mixing Fibres</u>	<u>Mixing Fibres</u>	<u>Difference (%)</u>
1	37.0 \pm 1.7	59.5 \pm 0.7	61
2	28.3 \pm 2.6	43.3 \pm 2.6	53
3	23.9 \pm 1.7	39.2 \pm 2.0	64
4	21.8 \pm 1.2	37.3 \pm 2.0	71

Considering the results in Table 8.1, it is clear that as the flow rate increases the oxygen partial pressure in both fibre types decreases. This is as a result of the time a specific volume spends within the fibre has decreased at the faster flow rates and is to be expected. Thus, the faster the flow rate, the lower the outlet partial pressure for a given inlet P_{O_2} .

Another point raised by Table 8.1 is the difference between the two configurations of oxygenator. At each of the four flow rates tested, the mixing fibres had higher outlet oxygen partial pressure compared to their non-mixing counterparts. At a flow rate of $2\ ml\ min^{-1}$, the difference between the two fibres is the lowest observed, suggesting that there may be some limiting factor at this flow rate in the mixing fibres. However, this difference may also be attributed to experimental error.

Despite the respective outlet partial pressures decreasing overall, the final column in Table 8.1 shows that the drop in non-mixing fibre is larger than that observed in the mixing fibres. Thus, the mixer appears to assist the fibre in keeping the partial pressure higher than it ordinarily would be at varying flow rates.

Table 8.2 - Water Experimental Results (Oxygen Transfer) with values = mean \pm SD

<u>Flow Rate ($ml\ min^{-1}$)</u>	O₂ transfer rate ($mol\ s^{-1}$)		
	<u>Non-mixing Fibres</u>	<u>Mixing Fibres</u>	<u>Difference (%)</u>
1	5.29x10 ⁻⁹ \pm 4.78x10 ⁻¹⁰	8.92x10 ⁻⁹ \pm 1.08x10 ⁻¹⁰	69
2	7.55x10 ⁻⁹ \pm 8.01x10 ⁻¹⁰	1.24x10 ⁻⁸ \pm 9.01x10 ⁻¹⁰	64
3	9.51x10 ⁻⁹ \pm 9.09x10 ⁻¹⁰	1.71x10 ⁻⁸ \pm 3.57x10 ⁻¹⁰	80
4	1.14x10 ⁻⁸ \pm 6.06x10 ⁻¹⁰	2.16x10 ⁻⁸ \pm 3.03x10 ⁻⁹	89

Table 8.2 is concerned with the calculated oxygen transfer, based upon the results in Table 8.1. It is expected that the mixing fibres will achieve higher oxygen transfer than the non-mixing ones, given that the oxygen partial pressures were consistently higher, and this is confirmed in the values presented above.

As the flow rate increases, the oxygen transfer for both fibres also increases. Recalling Equation (3.31), the reason for this increase is that the oxygen transfer rate is proportional to ΔP_{O_2} and the fluid flow rate. Although residence time will decrease with higher fluid flow rate, more fluid at low P_{O_2} is transported to the region near the tube wall where a higher P_{O_2} driving force is being maintained, leading to a higher oxygen transfer rate with increasing fluid flow rate.

Considering the evidence presented above, the inclusion of a helical static mixer has a beneficial effect on oxygen transfer. Even though the fluid used in this preliminary study was only distilled water and not blood, it was believed that the benefits of the static mixer would be carried across when testing with bovine blood. This will be discussed further below.

8.1.2 Theory

The mathematical models used the inlet conditions recorded experimentally. Three three-dimensional models were created to simulate the results presented above: a simple hollow fibre; a three-bladed mixer; a six-bladed mixer. The boundary, initial and inlet conditions were all tailored to meet those present in the laboratory environment.

Considering the non-mixing fibre models first, it can be stated that the experimental conditions were successfully reproduced theoretically. Concentrating on the oxygen

partial pressure figures presented in Chapter 5, the mathematical models all follow the same trend as the experimental results – all outlet partial pressures decrease as the flow rate is increased. The corresponding oxygen transfer figures show again that the experimental results can be reproduced, as the oxygen transfer modelled theoretically increases as the flow rate rises, and the majority of the data points generated fall within experimental limits.

Considering the theoretical three-blade mixer models, the outlet partial pressure figures show the familiar decrease with increasing flow rate. However, the theoretical model does not match the experimental results as closely as the hollow fibres did because the model is not simulating exactly the laboratory experiment. Practically, two units of twelve blade elements were placed inside the lumen of each fibre; in this model, only three blade elements have been modelled. Despite this departure from reality, the model is encouraging in the sense that the partial pressure values are not too dissimilar to the experimental ones. Any difference between experimental and theory can be attributed to the low number of blades in the mathematical model. The oxygen transfer for the three-blade mixers were also lower than those measured experimentally; the trend of the figures show that overall the same behaviour was modelled, and again any difference between reality and simulation is generally believed to be due to the difference in the number of blades modelled.

When the mixing model was altered to represent six blade elements, both the outlet partial pressures and the oxygen transfer began to match the experimental values

closer than the three-blade mixer. The most surprising aspect of the six-blade figures is the distinct similarity between the model and the experimentally measured values. The implication of this similarity is only apparent when considering the mathematical model as a device-optimisation tool; there are times in the simulations where the theoretical partial pressure and oxygen transfers match or surpass the practical values, indicating that although twenty-four blade elements used in the laboratory, there may be a degree of redundancy in the practical fibres. The theoretical models have proven to be relatively accurate when compared to the experimental findings, giving confidence to any device alteration based upon the mathematical results.

8.2 Comparison of blood experiments

Having completed the preliminary water experimentation, and having confidence in the mathematical models' ability to reproduce the findings, the follow-up work used bovine blood.

8.2.1 Practical

Table 8.3 shows the experimental oxygen transfer results.

Table 8.3 – Bovine Blood Experimental Results (Oxygen Transfer) with values = mean \pm SD

Flow Rate ($ml\ min^{-1}$)	Blood oxygen transfer rate ($mol.s^{-1}$)		
	Mixing	Non-mixing	Difference (%)
1	$1.33 \times 10^{-8} \pm 3.41 \times 10^{-9}$	$8.41 \times 10^{-9} \pm 4.38 \times 10^{-9}$	158
2	$1.75 \times 10^{-8} \pm 9.94 \times 10^{-9}$	$8.20 \times 10^{-9} \pm 5.83 \times 10^{-9}$	214
3	$1.80 \times 10^{-8} \pm 5.32 \times 10^{-9}$	$7.45 \times 10^{-9} \pm 4.86 \times 10^{-9}$	242
4	$1.37 \times 10^{-8} \pm 3.20 \times 10^{-9}$	$1.67 \times 10^{-8} \pm 1.33 \times 10^{-8}$	82

From Table 8.3 it is clear that the fibres with static mixer have a distinct advantage over the hollow fibres. Before, in the water experiments, whilst the mixing devices achieved higher oxygen transfer than the non-mixing units, the difference was not as large as with the bovine blood at certain flow rates. The reason for this is that the oxygen can exist within the blood in both a bound state and a dissolved one, unlike in the water where there is no haemoglobin present to actively bind to the oxygen.

The most important point to note from Table 8.3 is the difference between the non-mixing and mixing fibres. The mixing fibres are all substantially higher in oxygen transfer than the non-mixing ones, except at the highest flow rate. At flow rates of 2 ml min^{-1} and 3 ml min^{-1} , the mixing fibres attain over triple the non-mixing oxygen transfer for the same flow rates. Clearly at these flow rates, the blood behaves in such a fashion to allow for greater oxygen transfer; at the same flow rates, the non-mixing fibre oxygen transfer has actually reduced from that of the lower flow rate, which was not expected.

The mixers were each coated with a siliconising solution to prevent thrombosis formation on the blades. Encouragingly, after testing no thrombi were observed.

8.2.2 Theory

As stated in Chapter 7, the three-dimensional simulations based upon the blood experiments were unable to be completed due to the limitations of the resources available.

Axisymmetric models were constructed in an attempt to resolve this issue. Despite only being able to simulate very low levels of haemoglobin, the two-dimensional models were able to produce results that can be compared with the experimental findings. An approximation of the experimental bound oxygen concentrations could be extrapolated using the equation of the trend line generated by the mathematical model.

8.3 Evaluation of static mixer

The aim of this study is to ascertain if the inclusion of a helical static mixer within the fibre lumen is beneficial to oxygen transfer. From the experimental results, both in distilled water and bovine blood, it can clearly be seen that the static mixer facilitates the oxygen transfer.

At all of the flow rates tested, the fibres with the static mixer included were able to produce higher oxygen transfer rates than those without. The purpose of the static mixer is not to increase the oxygen within the tube; it is there to aid the transport of the blood from the central region where diffusing oxygen will not reach to the fibre walls where the oxygen is entering the system. However, as deoxygenated blood is moved from the centre region to the membrane boundary, the local oxygen partial pressure in the blood is reduced, increasing the driving force from the gas side, which in turn increases the concentration of oxygen entering the system. Thus, the oxygen transfer for the mixing fibres is considerably higher at all of the flow rates than the non-mixing fibres as the hollow oxygenators are reliant upon the diffusion process only for oxygenation, whereas the static mixer introduces convective processes as well, increasing the amount of blood available in the wall region to bind oxygen.

Overall, this study has shown that fibres with static mixers included in their design have higher oxygen transfer than those without. Through the use of mathematical

modelling, any device using this design could be tested rigorously before practical work was undertaken.

8.4 Limitations of the study

8.4.1 Practical limitations

During this study, a great deal of time was spent investigating different materials to construct the fibres from. As stated in Chapter 4, initially silicone rubber was used. Once the results had been analysed and the oxygen transfer calculated, this material was deemed unsuitable.

Once Celgard 2500 had been selected as the material to be used, another of the limitations in this study was the method of construction of the hollow fibres. Manual construction of the individual fibres and placing the mixers inside was a very time consuming process. Another problem with the construction method was the propensity for the thin-walled material to tear when putting the mixer in place. Unfortunately, tears were not always obvious, and subsequently some fibres were sealed within the test casing and had fluid flowing through them before the structural instabilities became evident. This meant having to rebuild another fibre to replace the torn one, limiting the amount of time spent testing.

Once the practical aspect of this study was completed, it was discovered that the fibre length was a limiting factor in the oxygenation process. None of the fibres tested, non-mixing or mixing, achieved 100% saturation. The reason for this is believed to be that the fibres were not of sufficient length to allow enough oxygen into the

system. Whilst it has been shown that the static mixer greatly enhances the oxygen transfer, in a future study the fibres will need to be longer in order to increase the blood residence time, and hence outlet O₂ saturation, for a given fluid flow rate. Alternatively, a parallel array of oxygenating tubes could be considered in order to increase the residence time.

Another limitation was the fluid flow rates that were selected for testing. If the fluid flow rate was sufficiently reduced, then 100% saturation could be achieved; however, the flow rates that were chosen were done so to allow sampling of the fluid at the oxygenator outlet to occur over a practical timescale.

As the membrane tubes were manually constructed, there remains the possibility that the contact between the static mixer and the membrane wall was imperfect. In this event, there would be channels forming between the mixing blades and the membrane wall, reducing the oxygen transfer in these regions.

A final issue that was raised at the end of the study was the subject of haemolysis. It is unknown if the static mixer damages the red blood cells as they pass the blades and therefore no comment can be made on the long-term usage of the mixing fibre configuration.

These comprise a list of the major practical limitations of the project.

8.4.2 Theoretical limitations

The majority of the problems experienced in the theoretical aspect of this study can be attributed to insufficient computing power. The most obvious case is the inability to simulate the bovine blood experiments after so accurately simulating the water trials. The major difference between the two models was the inclusion of the reaction term when the model was adapted to simulate blood; the computer used was able to solve the two-dimensional blood problem for very low levels of haemoglobin, implying that it is not the introduction of the haemoglobin that is the problem, just that a more powerful computer is needed.

The same can be said for the water trials' inability to solve for mixers comprised of any more than six blades. If more computational power was available, then perhaps more blades could have been modelled. However, having discussed the six-blade mixing model previously, modelling more blades may only be an exercise in device optimisation.

A final limitation in the theoretical aspect of this study is the limited resources available. Any further work to this report must certainly investigate the use of a more powerful computer system or an alternative software package.

8.5 Conclusions

The aim of this project has been to investigate a method of improving the oxygen transfer in a prototype membrane oxygenator. This was done by inserting a commercially available helical static mixer in custom made hollow fibres. The majority of the study was taken up with trying to find a suitable material to construct the fibres from and then building them.

The study found that when a helical static mixer is included in the fibre design, the oxygen transfer in bovine blood is greatly enhanced. This was found to be most obvious at a flow rate of 3 ml min^{-1} , at which a hollow fibre with no mixer was found to have an oxygen transfer of $7.45 \times 10^{-9} \pm 4.86 \times 10^{-9} \text{ mol.s}^{-1}$. When the fibre with mixer was tested, this transfer was observed to have increased to $1.80 \times 10^{-8} \pm 5.32 \times 10^{-9} \text{ mol.s}^{-1}$, which is a 242% rise in favour of the mixing fibre. Other flow rates were also tested, and at each the mixing fibre was found to have higher oxygen transfer, leading to the conclusion that the helical static mixer has a beneficial effect on oxygen transfer within bovine blood.

During the study, a series of two- and three-dimensional mathematical models were created to simulate the oxygen transfer within the device. When the fluid being reproduced was distilled water, the theoretical findings had good correlation with the experimental results. This indicated that the model was accurate in its design and implementation. However, when simulating bovine blood, the models were unable

to cope with the inclusion of haemoglobin, resulting in the breakdown of the numerical code. Despite this setback, work was undertaken to create an axisymmetric model which could simulate the experimental data at low levels of haemoglobin; the findings of this model was that the experimental conditions could be extrapolated from the model, suggesting that the theoretical reproduction was able to model reality in an abstract fashion.

8.6 Future work

There are a number of logical continuations to this study. Firstly, an alternative method of device construction would need to be investigated; the majority of the units used in this study failed due to leakage. This problem would need to be addressed before any further work could continue. As the membranes were constructed manually, there remains the possibility that the static mixers inserted into the tubes did not fit perfectly, leading to the formation of channels between the blades and the membrane wall, removing the convective aspect of the oxygenation process.

Another way that this study could be improved upon would be to investigate the residency time of the blood within the fibre. At no point in the course of this trial did the blood become wholly saturated, indicating that the blood was not within the fibre for long enough. Increasing the residence time would ensure that the blood would become fully saturated. This could be tackled by either increasing the fibre length or by reducing the flow rate. This could be investigated by the development of a theoretical model that was able to simulate blood flow and the oxygen transfer to it.

Finally, whilst it is apparent that the helical static mixer had a beneficial effect on the oxygen transfer to the blood, the effect the mixer had upon the blood itself was not studied. A priority for any future work should be to investigate possible haemolysis arising from red blood cells interacting with the leading edges of mixing blade

elements in addition to any microscopic thrombus formation on the blades of the static mixer. Further research would also be required into the inflammatory response this configuration of device would have upon the immune system.

References

¹ Bronchi, Bronchial Tree and Lungs, *National Cancer Institute*, (2011), Available at <http://training.seer.cancer.gov/anatomy/respiratory/passages/bronchi.html> [Accessed 23 March 2011]

² Brain JD, Exchanging Oxygen and Carbon Dioxide, *The Merck Manuals Online Medical Library*, (August 2006), Available at: <http://www.merck.com/mmhe/sec04/ch038/ch038d.html> [Accessed 11 May 2010]

³ UK coronary heart disease statistics 2009-10, (2010), *British Heart Foundation*, Available at: <http://www.bhf.org.uk> [Accessed August 2010]

⁴ Klien AA, Webb ST, Tsui S, Sudarshan C, Shapiro L, Densem C, (2009), Transcatheter Aortic Valve Insertion of Emerging New Technology, *British Journal of Anaesthesia*, **103** (6): 792 – 799

⁵ Machin D, Allsager C, (2006), Principles of cardiopulmonary bypass, *Continuing Education in Anaesthesia, Critical Care & Pain*, **6** (5): 176 – 181.

⁶ Dewey TM, Mack MJ, (2008), Myocardial Revascularization without Cardiopulmonary Bypass, *Cardiac Surgery in the Adult (3rd Edition)*, New York, McGraw-Hill: 633 – 654

⁷ Shekar PS, (2006), On-Pump and Off-Pump Coronary Artery Bypass Grafting, *Circulation*, 113: e51 – e52

⁸ Drummond M, Braile DM, Lima-Oliveria APM, Camim AS, Oyama RSK, Sandoval GH, (2005), Technological Evolution of Membrane Oxygenator, *Brazilian Journal of Cardiovascular Surgery*, **20** (4): 432 – 437

⁹ Remadi JP, Marticho P, Butoi I, Rakotoarivelo Z, Trojette F, Benamar A, Beloucif S, Foure D, Poulain HJ, (2004), Clinical experience with the mini-extracorporeal circulation system: an evolution or revolution?, *Annals of Thoracic Surgery*, **77**: 2172 – 2175

¹⁰ Brix-Christensen V, (2001), The systemic inflammatory response after cardiac surgery with cardiopulmonary bypass in children, *Acta Anaesthesiol Scand*, **45**: 671 – 679

¹¹ Vidal Melo MF, (2004), Clinical respiratory physiology of the neonate and infant with congenital heart disease, *International Anaesthesia Clinics*, **42**: 29 – 43

¹² SORIN Eos Oxygenator datasheet, Available at <http://www.sorin.com/product/eos> [Accessed August 2011]

¹³ Kukielka GL, Smith CW, Manning A, Youker KA, Michael LH, Entman ML, (1995), Induction of interleukin-6 synthesis in the myocardium. Potential role in postperfusion inflammatory injury, *Circulation*, **92**: 1866 – 1875

¹⁴ Fromes Y, Gaillard D, Ponzio O, Chauffert M, Gerhardt MF, Deleuze P, Bical OM, (2001), Reduction of the inflammatory response following coronary bypass grafting with total minimal extracorporeal circulation, *European Journal of Cardio-Thoracic Surgery*, **22**: 527 – 533

¹⁵ Hooke R, (1667), An account of an experiment made by R Hooke of preserving animals alive by blowing air through their lungs with bellows, *Philosophical Transactions of the Royal Society*, **2**: 539 – 540.

¹⁶ Baskett TF, (2004), Robert Hooke and the origins of artificial respiration, *Resuscitation*, **60**: 125 – 127.

¹⁷ LeGallois JJC, (1812), Experiments on the Principles of Life (Expériences sur le principe de la vie). Notamment sur Celui des Mouvements du Coeur, et Sur le Siège de ce Principe; Suivies du rapport fait a' la première classe de l'Institt sur celles relatives aux mouvements du Coeur. Paris: D'Hautel.

¹⁸ Lim MW, (2006), The history of extracorporeal oxygenators, *Anaesthesia*, **61**: 984 – 995.

¹⁹ Stammers AH, (1997), Historical Aspects of Cardiopulmonary Bypass: From Antiquity to Acceptance, *Journal of Cardiothoracic and Vascular Anaesthesia*, **11** (3): 266 – 274.

²⁰ von Schröder W, (1882), Über die Bildungstätte des Harnstoffs, *Archiv Fur Experimentelle Pathologie und Pharmakologie*, **15**: 364 – 402.

²¹ von Frey M, Gruber M, (1885), Ein respirations-apparat fur isolirte organe, *Arch Physiol* **9**: 519 – 532

²² Hooker DR, (1910), A Study of the isolated kidney: the influence of pulse pressure upon renal function, *The American Journal of Physiology*, **27**: 24 – 44.

²³ Hooker DR, (1915), The perfusion of the mammalian medulla: The effect of calcium and of potassium on the respiratory and cardiac centers, *American Journal of Physiology*, **38**: 200 – 208.

²⁴ Probert WR, Melrose DG, (1960), An early Russian heart-lung machine, *British Medical Journal*, **1**: 1047 – 1048.

²⁵ Konstantinov IE, Alexi-Meskishvili VV, (2000), Sergei S. Brukhonenko: The Development of the First Heart-Lung Machine for Total Body Perfusion, *Annals of Thoracic Surgery*, **69**: 962 – 966.

-
- ²⁶ Brukhonenko SS, (1928), Artificial circulation of the whole body of a dog with arrested heart, *Trudi Nauchnogo Khimiko-Pharm Inst*, **20**: 44 – 72.
- ²⁷ Gibbon JH Jr, (1970), The development of the heart-lung apparatus, *Rev Surg*, **27**(4): 231 – 244.
- ²⁸ Fou AA, (1997), The First 20 Years of the Heart-Lung Machine, *Texas Heart Institute Journal*, **24** (1): 1 – 8.
- ²⁹ Bjork VO, Sternlieb JJ, Davenport C, (1985), From the spinning disc to the membrane oxygenator for open-heart surgery, *Scandinavian Journal of Thoracic and Cardiovascular Surgery*, **19**: 207 – 216.
- ³⁰ Gibbon JH Jr, (1939), An oxygenator with large surface area to volume ratio, *Journal of Laboratory and Clinical Medicine*, **24**: 1192 – 1198.
- ³¹ Hanna BD, Lioy F, (1979), Evaluation of a screen oxygenator suitable for small animal organ perfusion, *American Journal of Physiology*, **237** (2): H269 – H274.
- ³² Gibbon JH, (1937), Artificial maintenance of the circulation during experimental occlusion of the pulmonary artery, *Archives of Surgery*, **34**: 1107 – 1108

³³ Miller BJ, (2003), Laboratory work preceding the first clinical application of cardiopulmonary bypass, *Annals of Thoracic Surgery*, **76**: 2203 – 2209

³⁴ Gibbon JH, (1978), The development of the heart-lung apparatus, *American Journal of Surgery*, **135**: 608-19.

³⁵ Kirklin JW, Donald DE, Harshbager HG, Hetzel PS, Patrick RT, Swan HJC, Wood EH, (1956), Studies in extracorporeal circulation. I. Applicability of Gibbon-type pump-oxygenator to human intracardiac surgery: 40 cases, *Annals of surgery*, **144**: 2 – 8.

³⁶ Hurt R, (1967), The technique and scope of open-heart surgery, *Postgraduate Medical Journal*, **43**: 668 – 674.

³⁷ Wegner JA, (1997), Oxygenator Anatomy and Function, *Journal of Cardiothoracic and Vascular Anaesthesia*, **11** (3): 275 – 281

³⁸ Cooley DA, (1999), C. Walton Lillehei, the “Father of Open Heart Surgery”, *Circulation*, **100**: 1364 – 1365

³⁹ Clowes GHA, Hopkins AL, Kolobow T, (1955), Oxygen diffusion through plastic films, *Transactions – American Society of Artificial Internal Organs*, **1**: 23 – 24

⁴⁰ Kolff WJ, Baltzer R, (1955), The artificial coil lung, *Transactions – American Society for Artificial Internal Organs*, **1**: 39–42

⁴¹ Dutton RC, Mathe FW, Lipps BJ, Rudy LW, Severinghaus JW, Edmunds LH, (1971), Development and Evaluation of a New Hollow Fibre Membrane Oxygenator, *Transactions – American Society of Artificial Internal Organs*, **17**: 331 – 336

⁴² Kolff WJ, Berk HT, (1944), Artificial kidney: dialyzer with great area, *Acta Medica Scandinavica*, **117**: 121 – 134.

⁴³ Clowes GHA, Hopkins AL, (1956), Further studies with plastic films and their use in oxygenating blood, *American Society of Artificial Internal Organs*, **2** (1): 6 – 12.

⁴⁴ Burns N, Melrose D, (1971), An Improved Silicone Membrane, *Mechanical Devices for Cardiopulmonary Assistance*, **6**: 58 – 71

⁴⁵ Haworth WS, (1976), Materials for Membrane Oxygenation, *Physiological and Clinical Aspects of Oxygenator Design*, Dawids SG, Engell HC (Eds.), (Elsevier Scientific Publishing Company), pp 293 – 298

⁴⁶ Burns N, (1969), Production of a silicone rubber film for the membrane lung, *Biomedical Engineering*, **4**: 356 – 359

⁴⁷ Burns N, Melrose D, (1971), An Improved Silicone Membrane, *Adv. Cardiol.*, **6**: 58 – 71

⁴⁸ Lightfoot EN, (1968), Low-Order Approximation for Membrane Blood Oxygenators, *Journal of American Institute of Chemical Engineers*, 669 – 670

⁴⁹ Seghaye MC, (2003), The clinical implications of the systemic inflammatory reaction related to cardiac operations in children, *Cardiology in the Young*, **13**: 228 – 239

⁵⁰ Chugani HT, (1998), Biological basis of emotions: brain systems and brain development, *Paediatrics*, **102**: 1225 – 1229

⁵¹ Bestic M, Reed MD, (2005), The ontogeny of human kidney development: influence on neonatal diuretic therapy, *NeoReviews*, **6**: e363 – e368

⁵² Eberhart RC, Curtis RM, (1973), The effects of solid and hollow fibre screens on gas exchange in membrane oxygenators, *Transactions – American Society of Artificial Organs*, **19**: 66 – 71

⁵³ Gaylor JDS, (1988), Membrane oxygenators: current developments in design and application, *Journal of Biomedical Engineering*, **10**: 541 – 547

-
- ⁵⁴ Beretta M, Borghi AL, Fumero R, (1982), Cross flow capillaries oxygenators, *3rd International Conference on Mechanics in Medicine and Biology*, Compiègne, 187 – 188
- ⁵⁵ Robb, WC, (1968), Thin silicone membranes, *Materials in Biomedical Engineering*, Annals of the New York Academy of Sciences, **146** (1): 119 – 137
- ⁵⁶ Montoya JP, Shanley CJ, Merz SI, Bartlett RH, (1992), Plasma leakage through microporous membranes – role of phospholipids, *American Society of Artificial Internal Organs*, **38** (3): M399 – M405
- ⁵⁷ Lee JK, Kung HH, Mockros LF, (2008), Microchannel Technologies for Artificial Lungs (1): Theory, *American Society of Artificial Internal Organs*, **54** (4): 372 – 382
- ⁵⁸ Kung MC, Lee JK, Kung HH, Mockros LF, (2008), Microchannel Technologies for Artificial Lungs (2): Screen-Filled Wide Rectangular Channels, *American Society of Artificial Internal Organs*, **54** (4): 383 – 389
- ⁵⁹ Lee JK, Kung MC, Kung HH, Mockros LF, (2008), Microchannel Technologies for Artificial Lungs (3): Open Rectangular Channels, *American Society of Artificial Internal Organs*, **54** (4): 390 – 395
- ⁶⁰ Dorson W Jr., Baker E, Hull H, (1968), A shell and tube oxygenator, *Transactions – American Society of Artificial Internal Organs*, **14**: 242 – 249

⁶¹ Drinker PA, (1963), Progress in membrane oxygenator designs, *Anaesthesiology*, **37**: 242 – 260

⁶² Bellhouse BJ, (1989), The influence of vortex mixing on the performance of artificial organs, *Blood Flow in Artificial Organs and Cardiovascular Prostheses*, Oxford, Oxford Science Publications: 175 – 183

⁶³ Pierce EC II, Dibelius WR, (1968), The membrane lung: studies with a new high permeability co-polymer membrane, *Transactions – American Society of Artificial Internal Organs*, **14**: 220 – 226

⁶⁴ Kolobow T, Bowman RL, (1963), Construction and evaluation of an alveolar membrane artificial heart-lung, *Transactions – American Society of Artificial Internal Organs*, **9**: 238 – 243

⁶⁵ Drinker PA, Bartlett RH, Bailer RM, Noyes BS Jr., (1969), Augmentation of membrane gas transfer by induced secondary flows, *Surgery*, **66**: 775 – 781

⁶⁶ Bellhouse BJ, Bellhouse FH, Curl CM, MacMillan TI, Gunning AJ, Spratt EH, MacMurray SB, Nelems JM, (1973), A high efficiency membrane oxygenator and pulsatile pumping system, and its applications to animal trials, *Transactions – American Society of Artificial Internal Organs*, **19**: 72 – 79

⁶⁷ Spratt EH, Melrose D, Bellhouse B, Badolato A, Thompson R, (1981), Evaluation of a membrane oxygenator for clinical cardiopulmonary bypass, *Transactions – American Society of Artificial Internal Organs*, **27**: 285 – 288

⁶⁸ Colton CK, (1976), Fundamentals of gas transport in blood, *Artificial lungs for acute respiratory failure theory and practice*, Zapol WM, Qvist J (Eds.), (Academic Press), pp 3 – 40

⁶⁹ Armeniades CD, Johnson WC, Raphael T, Arthur D. Little Inc (1965), Mixing device, *United States Patent Office No. 3,286,992*

⁷⁰ Mixing and Reaction Technology: Oil, Gas and Refinery, (2011), Available at http://www.sulzerchemtech.com/desktopdefault.aspx/tabid-1061/4835_read-8682/ [Accessed August 2011]

⁷¹ Arons IJ, (2008), The Disposable “Motionless Mixer”, [online], Available at: <http://adlittlechronicles.blogspot.com/2008/07/disposable-motionless-mixer.html> [Accessed July 2010]

⁷² Najarian S, Bellhouse BJ, (1995), Enhanced microfiltration of bovine blood using a tubular membrane with a screw-threaded insert and oscillatory flow, *Journal of Membrane Science* **112**: 249 – 261

-
- ⁷³ Dong Sung K, In Hwan L, Tai Hun K, Dong-Woo C, (2003), A barrier embedded Kenics micromixer, *Journal of Micromechanics and Microengineering*, **14**: 1294 – 1301
- ⁷⁴ Kumar V, Shirke V, Nigam KDP, (2007), Performance of Kenics static mixer over a wide range of Reynolds number, *Chemical Engineering Journal*, **139**: 284 – 295
- ⁷⁵ Weissman MH, Mockros LF, (1967), Oxygen transfer to blood flowing in round tubes, *Journal of the Engineering Mechanics Division*, **93**(6): 225 – 244
- ⁷⁶ Weissman MH, Mockros LF, (1969) Oxygen and carbon dioxide transfer in membrane oxygenators, *Medical and Biological Engineering*, **7**: 169 – 184
- ⁷⁷ Dindorf JA, Lightfoot EN, Solen KA, (1971), Prediction of blood oxygenation rates, *Chemical Engineering Progress Symposium Series*, **114**(67): 75 – 87
- ⁷⁸ Colton CK, Drake RF, (1971), Effect of boundary conditions on oxygen transport to blood flowing in a tube, *Chemical Engineering Progress Symposium Series*, **114**(67): 88 – 95
- ⁷⁹ Spaeth EE, (1973), Blood oxygenation in extracorporeal devices: theoretical considerations, *CRC Critical Reviews in Bioengineering*, **1**: 383 – 417

⁸⁰ Jayaraman G, Lautier A, Jarry G, Bui-Mong-Hung, Laurent D, (1981), Numerical scheme for modelling oxygen transfer in tubular oxygenators, *Medical and Biological Engineering and Computing*, **19**: 524 – 534

⁸¹ Mayes PJD, (1985), An application of the method of lines in biological mass transfer, *Biotechnology Progress*, **1**(4): 269 – 272

⁸² Vaslef SN, Mockros LF, Cook KE, Leonard RJ, Sung JC, Anderson RW, (1994), Computer-assisted design of an implantable, intrathoracic artificial lung, *Artificial Organs*, **18**(11): 813 – 817

⁸³ Catapano G, Hornscheidt R, Wodetzki A, Baurmeister U, (2004), Turbulent flow technique for the estimation of oxygen diffusive permeability of membranes for the oxygenation of blood and other cell suspensions, *Journal of Membrane Science*, **230**: 131 – 139

⁸⁴ Vaslef SN, Mockros LF, Anderson RW, Leonard RJ, (1994), Use of a mathematical model to predict oxygen transfer rates in hollow fibres membrane oxygenators, *American Society of Artificial Internal Organs*, **40**: 990 – 996

⁸⁵ Baker DA, Holte JE, Patankar SV, (1991), Computationally two-dimensional finite-difference model for hollow-fibre blood-gas exchange devices, *Medical and Biological Engineering and Computing*, **29**: 482 – 488

⁸⁶ Dorrington KL, (1989), *Anaesthetic and Extracorporeal Gas Transfer* (Clarendon Pr), pp203-238

⁸⁷ Margaria R, (1963), A mathematical treatment of the blood dissociation curve for oxygen, *Clinical Chemistry*, **9**(6): 745 – 762

⁸⁸ Celgard 2500 datasheet, *Celgard*, (May 2009), Available at: http://www.celgard.net/documents/2500_Data_Sheet_2009-05_20004.pdf [Accessed 04 February 2010]

⁸⁹ Series 120 Disposable Mixing Elements, *Nordson EFD*, (2010), Available at: http://www.nordson.com/en-us/divisions/efd/products/tah/static-mixers/Documents/mixers_120.pdf [Accessed 16 February 2009]

⁹⁰ Female Luer Connectors , *Altec*, (June 2010), Available at: <http://www.altecweb.com/home.asp?cat=Subcategory13100> [Accessed March 2010]

⁹¹ Silicone rubber compound, *RS Components*, Available at: <http://uk.rs-online.com/web/search/searchBrowseAction.html?method=getProduct&R=0692542>
[Accessed March 2010]

⁹² Araldite® epoxy adhesive, *RS Components*, Available at: <http://uk.rs-online.com/web/search/searchBrowseAction.html?method=getProduct&R=3149653>
[Accessed April 2010]

⁹³ Ritchie AC, Bowry K, Fisher AC, Gaylor JDS, (1996), A novel automated method for the determination of membrane permeability in gas-liquid transfer applications, *Journal of Membrane Science*, **121** (2): 169 – 174

⁹⁴ Lewis ME, (2006), Dissolved Oxygen (version 2.1), *U.S. Geological Survey Techniques of Water-Resources Investigations*, Book 9, Chap. A6., section 6.2
Available at: http://water.usgs.gov/owq/FieldManual/Chapter6/6.2_contents.html
[Accessed February 2010]

⁹⁵ Campbell Ritchie A, (1996), Performance characterisation of membrane oxygenators, *PhD Thesis*, University of Strathclyde

⁹⁶ COMSOL Multiphysics, *COMSOL Inc*, (2010), Available at: <http://www.comsol.com> [Accessed July 2010]

⁹⁷ Chemical Reaction Engineering Module for COMSOL Multiphysics, *COMSOL Inc*, (2010), Available at: <http://www.comsol.com/products/chemical-reaction-engineering> [Accessed July 2010]

⁹⁸ Sigmacote® Silicone Solution, Sigma-Aldrich (2010), Available at: http://www.sigmaaldrich.com/catalog/ProductDetail.do?D7=0&N5=SEARCH_CONCAT_PNO|BRAND_KEY&N4=SL2|SIGMA&N25=0&QS=ON&F=SPEC [Accessed September 2010]

⁹⁹ Medtronic AFFINITY Paediatric Arterial Filter, Medtronic (2008), Available at: <http://www.medtronic.com/affinitypedfilter> [Accessed September 2010]

¹⁰⁰ Hawksley HaematoSpin 1400, Hawksley Medical and Laboratory Equipment, Available at: http://www.hawksley.co.uk/centrifuges/03a_centrifuges/03a02_1400_i.shtml [Accessed May 2011]